UNIVERSITEIT VAN PRETORIA
UNIVERSITY OF PRETORIA
YUNIBESITHI YA PRETORIA

OPTIMISATION OF ADAPTIVE LOCALISATION TECHNIQUES FOR COGNITIVE RADIO

by

Robin Rajan Thomas

Submitted in partial fulfilment of the requirements for the degree

Master of Engineering (Electronic Engineering)

in the

Department of Electrical, Electronic and Computer Engineering
Faculty of Engineering, Built Environment and Information Technology
UNIVERSITY OF PRETORIA

April 2012

SUMMARY

OPTIMISATION OF ADAPTIVE LOCALISATION TECHNIQUES FOR COGNITIVE RADIO

by

Robin Rajan Thomas

Supervisor(s):	Prof. Dr. B. T. Maharaj
Department:	Electrical, Electronic and Computer Engineering
University:	University of Pretoria
Degree:	Master of Engineering (Electronic Engineering)
Keywords:	bandwidth efficiency, cognitive radio, least squares estimation, location awareness, maximum-likelihood estimation, multiband positioning, single-input-multiple-output, time-of-arrival.

Spectrum, environment and location awareness are key characteristics of cognitive radio (CR). Knowledge of a user's location as well as the surrounding environment type may enhance various CR tasks, such as spectrum sensing, dynamic channel allocation and interference management. This dissertation deals with the optimisation of adaptive localisation techniques for CR. The first part entails the development and evaluation of an efficient bandwidth determination (BD) model, which is a key component of the cognitive positioning system. This bandwidth efficiency is achieved using the Cramer-Rao lower bound derivations for a single-input-multiple-output (SIMO) antenna scheme. The performances of the single-input-single-output (SISO) and SIMO BD models are compared using three different generalised environmental models, viz. rural, urban and suburban areas. In the case of all three scenarios, the results reveal a marked improvement in the bandwidth efficiency for a SIMO antenna positioning scheme, especially for the 1×3 urban case, where a 62% root mean square error (RMSE) improvement over the SISO system is observed.

The second part of the dissertation involves the presentation of a multiband time-of-arrival (TOA) positioning technique for CR. The RMSE positional accuracy is evaluated using a fixed and dynamic bandwidth availability model. In the case of the fixed bandwidth availability model, the multiband TOA positioning model is initially evaluated using the two-step maximum-likelihood (TSML) location estimation algorithm for a scenario where line-of-sight represents the dominant signal path. Thereafter, a more realistic dynamic bandwidth availability model has been proposed, which is based on data obtained from an ultra-high frequency spectrum occupancy measurement campaign. The RMSE performance is then verified using the non-linear least squares, linear least squares and TSML location estimation techniques, using five different bandwidths. The proposed multiband positioning model performs well in poor signal-to-noise ratio conditions (-10 dB to 0 dB) when compared to a single band TOA system. These results indicate the advantage of opportunistic TOA location estimation in a CR environment.

OPSOMMING

OPTIMERING VAN AANPASBARE LOKALISERINGSTEGNIEKE VIR KOGNITIEWE RADIO

deur

Robin Rajan Thomas

Studieleier(s):	Prof. Dr. B. T. Maharaj
Departement:	Elektriese, Elektroniese en Rekenaar-Ingenieurswese
Universiteit:	Universiteit van Pretoria
Graad:	Magister in Ingenieurswese (Elektroniese Ingenieurswese)
Sleutelwoorde:	bandwydtedoeltreffendheid, kognitiewe radio, kleinste kwadrate skatting, plekbewustheid, maksimum waarskynlikheidskatting, multiband-posisionering, enkel-inset-verskeie-uitsette, tyd van aankoms.

Spektrum, omgewing en plekbewustheid is die sleuteleienskappe van kognitiewe radio (KR). Kennis van ’n KR-gebruiker se posisie asook omliggende omgewingtipe kan verskeie KR-take soos spektrumwaarneming, dinamiese kanaaltoekenning en inmenging verbeter. Die onderwerp van hierdie verhandeling is die optimering van aanpasbare lokalisering-tegnieke vir KR. Die eerste deel is die ontwikkeling en evaluering van ’n effektiewe bandwydtebepalingmodel (BB-model) wat ’n belangrike komponent van die kognitiewe posisioneringsisteem (KPS) is. Hierdie bandwydtedoeltreffendheid word bereik deur gebruik te maak van die ondergrensafleidings vir ’n enkel-inset-verskeie-uitsette- (EIVU) antennaskema. Die vertonings van die enkel-inset-enkel-uitset- (EIEO) en EIVU-BB-modelle word vergelyk in drie verskillende omgewingsmodelle, die plattelandse, stedelike en voorstedelike modelle. In al drie gevalle, toon die resultate ’n merkbare verbetering in die bandwydtedoeltreffendheid vir ’n EIVU-antennaplasingskema, veral in die stedelike geval, waar ’n 62% wortel-gemiddelde-kwadraat foutverbetering (RMSE) oor die EIEO-stelsel vir die 1×3 geval waargeneem word.

Die tweede deel van die verhandeling behels die aanbieding van ’n multiband-tyd-van-aankomsposisioneringstegniek (TVA-posisioneringstegniek) vir KR. Die RMSE se posisionele akkuraatheid word geëvalueer met behulp van ’n vaste en dinamiese bandwydtebeskikbaarheidsmodel. In die geval van die vaste bandwydtebeskikbaarheidsmodel, is die multiband-TVA-posisioneringsmodel aanvanklik geëvalueer met behulp van die tweestap-maksimumwaarskynlikheid-(TSMW) plekskattingalgoritme vir ’n situasie waar lyn van sig die dominante seinpad verteenwoordig. Vervolgens is ’n meer realistiese dinamiese bandwydtebeskikbaarheidsmodel voorgestel wat gebaseer is op uitslae wat verkry is van ’n ultra-hoë-frekwensie spektrumbesettingmetingveldtog. Die werkverrigting van die RMSE word dan geverifieer deur gebruik te maak van die nie-lineêre kleinste-kwadrate-, lineêre minste-kwadrate- en TSMW-plekskattingtegnieke deur gebruik te maak van vyf verskillende bande. Die voorgestelde multiband-posisioneringmodel presteer goed in swak geraasverhoudingtoestande (-10 dB tot 0 dB) wanneer dit vergelyk word met ’n enkelband-TVA-stelsel. Hierdie uitslae dui op die voordeel van opportunistiese TVA-plekskatting in ’n KR-omgewing.

I wish to dedicate this thesis to Almighty God, for the countless blessings during the course of my studies and for being an ever-present pillar of strength throughout my life. This work is also dedicated to my loving family, including my Achan, Amma and sister, who have motivated me every step of the way.

Acknowledgments

I would like to extend my humble and sincerest gratitude to:

- My parents and sister for their patience and support.
- My supervisor, Prof. B.T. Maharaj, for all the invaluable guidance, advice as well as experience gained during the course of my post-graduate study.
- My mentors, Prof. Raymond Knopp and Dr. Bassem Zayen, for the research internship opportunity at Eurecom, as well their valuable assistance and feedback with regard to my Masters research.
- The Sentech Chair in Broadband Wireless Multimedia Communications at the University of Pretoria and the National Research Foundation for their financial support during the course my post-graduate studies.
- The Independent Communications Authority of South Africa for their financial assistance with regard to the spectrum occupancy measurement campaign.
- My fellow engineering colleagues, Kahesh Dhuness, Simon Barnes and Thinus Prinsloo, for their thoughtful help with regard to various aspects of my Masters work.

LIST OF ABBREVIATIONS

2D	Two-dimensional
3D	Three-dimensional
AN	Anchor Node
AOA	Angle of Arrival
AWGN	Additive White Gaussian Noise
BS	Base Station
BD	Bandwidth Determination
CPS	Cognitive Positioning System
CR	Cognitive Radio
CRLB	Cramer-Rao Lower Bound
CWN	Cognitive Wireless Network
EDSM	Enhanced Dynamic Spectrum Management
FIM	Fisher Information Matrix
GNSS	Global Navigation Satellite System
GPS	Global Positioning System
LOS	Line-of-sight
LTE	Long Term Evolution
LLS	Linear Least Squares
MAC	Medium Access Control
MIMO	Multiple-input-multiple-output
ML	Maximum-likelihood
MT	Mobile Terminal
NLOS	Non-line-of-sight
NLS	Non-linear Least Squares
PDF	Probability Density Function
PHY	Physical
PU	Primary User
QoS	Quality of Service
RF	Radio Frequency
RKRL	Radio Knowledge Representation Language

RMSE	Root Mean Square Error
RSS	Received Signal Strength
SDR	Software Defined Radio
SISO	Single-input-single-output
SIMO	Single-input-multiple-output
SNR	Signal-to-noise Ratio
SU	Secondary User
TDOA	Time-difference-of-arrival
TN	Target Node
TOA	Time-of-arrival
TSML	Two-step Maximum-likelihood
UHF	Ultra-high Frequency
WLAN	Wireless Local Area Network
WRAN	Wireless Regional Area Network

LIST OF TABLES

LIST OF FIGURES

NOTATION

$\mathbf{A}$	Matrix A
$\mathbf{a}$	Column vector A
$\mathbf{H}$	Hessian matrix
∇	Gradient vector
$[.]^T$	Transpose of matrix
$E[.]$	Expectation operator
$var(.)$	Variance operator
$diag(x)$	Diagonal matrix with x on the main diagonal
$\lvert\mathbf{A}\rvert$	Determinant or magnitude of $\mathbf{A}$
$\mathbf{0}$	Zero vector

COMMON SYMBOLS

$\mathbf{e}_{nl}$	Non-linear error function
$\mathbf{e}_{lin}$	Linear error function
α	Complex channel coefficient
β	Bandwidth
μ	Stability and convergence
τ	Delay of transmitted signal
$\mathbf{\Psi}$	Noise covariance vector
$\hat{\theta}$	Location estimate
γ_s	Signal-to-noise ratio
$r(t)$	Received signal
$s(t)$	Transmitted signal
$P(\hat{d})$	Positional accuracy

TABLE OF CONTENTS

CHAPTER 1

INTRODUCTION

The demand for voice and high data rate applications has drastically increased over the past few years, partly in response to the introduction of smartphone and tablet devices, which are capable of performing various functions, such as multitasking, document editing and high-definition video streaming, all of which were traditionally performed by personal computers. The addition of social networking and cloud storage have provided people with different ways of exchanging and storing various multimedia, including videos, photos and music with the aid of these mobile devices. Next generation wireless communication systems therefore have to cater for this increasing demand by optimising radio and network resources, as well as different transmission parameters such as throughput and QoS.

The management of the radio frequency (RF) spectrum, which is an integral part of wireless communications, has garnered interest among the research community. Studies [1–6] have shown that there is a definite lack of efficient spectrum utilisation based on the current fixed spectrum allocation policy, which is determined by telecommunication regulators. In addition, the usable RF spectrum for wireless communications is a limited resource. The results of these investigations have revealed that large percentages of the RF band are underutilised and in certain cases, extremely congested. As a result, this brought about the need for increased spectrum efficiency and awareness for mobile communication devices. Cognitive radio (CR) and cognitive wireless networks (CWNs) have been regarded as proposed solutions to enhance spectrum utilisation using concepts derived from a Software Defined Radio (SDR) and machine learning perspective. Cognitive radio's primary

capabilities involve the dynamic utilisation of specific spectrum gaps (also termed white spaces) in an opportunistic manner that is non-interfering with existing licensed users, such as mobile telecommunication operators. Research in the CR field has expanded into different areas ranging from adaptive wireless systems, spectrum sensing and resource allocation to cross-layer optimisation, as well as various other issues.

1.1 BACKGROUND

1.1.1 Software Defined Radio

The basic structure of a digital communication system has remained unchanged since its original development. The first component of such a system may include an analogue or digital source containing the information to be transmitted. This particular signal can be efficiently represented as a series of binary symbols through a source encoder. The output of the source encoder is passed through a channel encoder, which then compensates for the degrading channel effects such as interference and noise through the introduction of redundancy into the transmitted message. The digital modulator then translates the binary symbol output of the channel encoder into signal waveforms for transmission over the channel. At the receiver end, the demodulator converts the noise-corrupted signal into a series of symbols, which is then passed through the channel decoder and source decoder in order to construct the original transmitted information [7]. The introduction of microelectronics has allowed the aforementioned communication subsystems, such as the antenna, the modem and codecs, to be encased in a single integrated chip (IC). The concept of SDR aims to replace currently implemented radio hardware with configurable software for all communication layers, including the physical (PHY) layer right up to the application layer. For example, PHY layer modules that can be reconfigured include the antenna system, RF conversion and amplifiers. Conventional wireless radios consisted of ICs optimised for small or fixed RF ranges and bandwidths such as frequency modulation (FM) broadcast (88-108 MHz), GSM communications (850-950 MHz) and wireless fidelity (WiFi) at 2.4 GHz. One of the key capabilities of SDR is to reconfigure the analogue RF components in a digital manner to operate across a single frequency range while catering for different technologies that operate over different

frequency bands. The SPEAKeasy Phase-2 system was one of the earlier implementations of SDR, which was designed specifically for the military program to operate between the 2 MHz and 2 GHz frequency range [8]. Hence, the idea of reconfigurability aims to provide a generalised framework for multiple air interfaces, different protocols and various applications which enhance the network and terminal efficiency and capabilities. There are a specific set of goals for reconfigurability with regard to mobile communication systems, such as [9]:

- Reconfiguration control and adaptation of the radio interface based on various environments and standards.
- Service design and provision to reconfigurable terminals across all network types and various radio access modes.
- Environment user management with regard to location, user profiles, access networks and terminals.

SDR therefore serves as an underlying technology for future implementations of CR.

1.1.2 Cognitive Radio

SDR became the foundation of 'cognitive radio' which was a concept initially devised by Mitola [10, 11]. This article described the radio knowledge representation language (RKRL) as a viable method to increase the efficiency and flexibility of wireless services. Through the RKRL, it was possible to distinguish several key characteristics of CR which, included awareness, intelligence, learning, adaptation, reliability and efficiency. The multifaceted concept of CR makes this next generation communication technology a real possibility owing to the advances and progress made over the years in digital signal processing hardware, software, networking and machine learning [12].

Spectrum awareness is a prominent feature of CR and has become vital in order to fulfil the requirements of efficient spectrum usage. Interference avoidance is a classical

challenge affecting existing mobile networks. Communication regulators are tasked with assigning a fixed frequency spectrum to telecommunication operators and various organisations in such a manner that these bodies can co-exist without interfering with one other. In a congested spectrum environment, the task of conducting effective and efficient mobile communications, coupled with the process of interference avoidance, becomes a challenging issue. In a typical CR scenario, interference can be broadly categorised into two types, viz. interference in the presence of a primary user (PU) (user licensed to utilise a specific portion of the spectrum) causing disruption to real-time communications and interference in the absence of the PU. Both of these cases can have a negative impact on the channel capacity and QoS. It is envisioned that a secondary user (SU) (CR user who has unlicensed access to the spectrum) has the inherent ability to compensate for PU interference by implementing a coordinated strategy to locate and utilise unused portions of the spectrum in seamless and non-interfering fashion [13]. Various spectrum sharing models have been developed in relation to the fundamentals of game theory. A basic dynamic spectrum sharing model can be considered as multiple games between numerous PUs and SUs, where the optimal behaviour and actions of these players can be studied from a game theoretic perspective [14]. Figure 1.1 illustrates the exploitation of white spaces using dynamic spectrum access. The challenge for the SU, is to maintain reliable communications without interfering with any of the PUs, as shown in Figure 1.1. Therefore it is imperative to sense channel occupancy in order to take advantage of the available white spaces. Adaptation and awareness are therefore key enabling factors, which will aid CR in correct decision-making. In addition to spectrum awareness, CR should be able to characterise signal propagation conditions and dynamically adapt accordingly [15].

Figure 1.2 is an example of a typical CR scenario. Primary network access refers to the existing radio network infrastructure, which has the required access to utilise the spectrum band, such as TV broadcasters and telecommunication operators. Similarly, the PUs have the required licenses to operate in the spectrum band. The CR (secondary) network, together with CR unlicensed users, can only opportunistically access the spectrum. There are a number of enabling technologies that can drive CR. One such technology is the ability of CR to gather and maintain immediate location data using a variety of existing techniques such as the Glo-

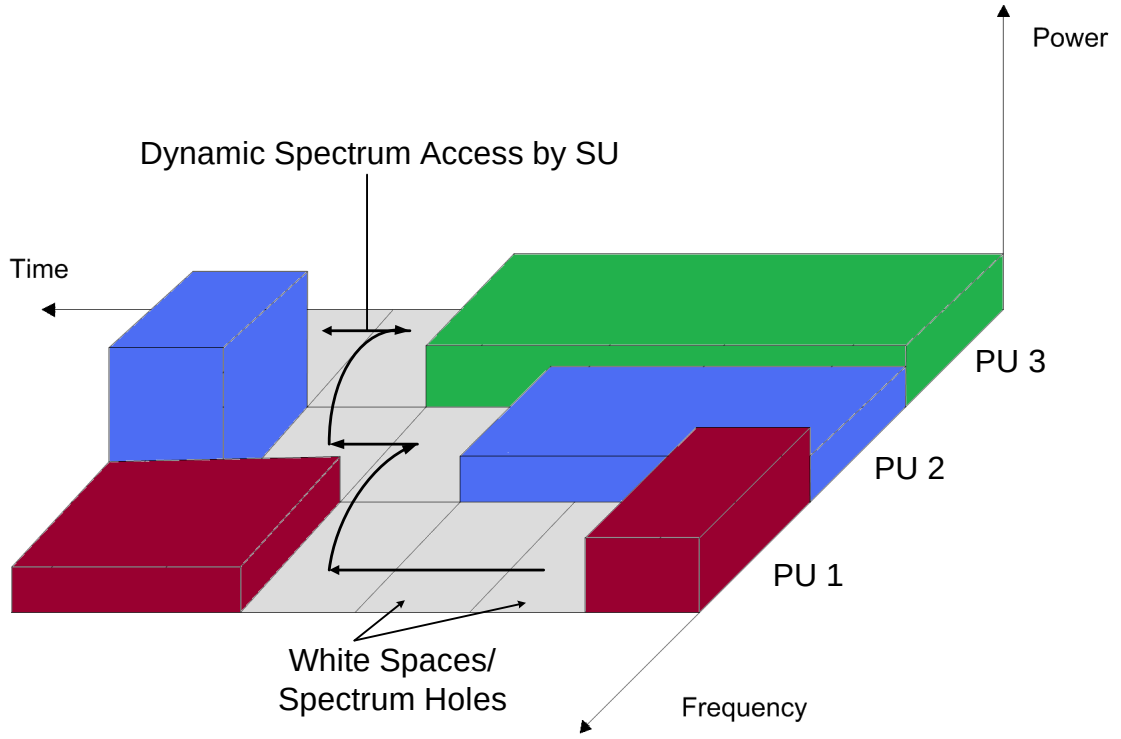

Figure 1.1: Basic illustration of dynamic spectrum access [13]

bal Positioning System (GPS), cellular-aided positioning or even cooperative localisation. The knowledge and understanding of a radio's node location forms an important part of the overall CR architecture. CWN applications that are capable of utilising location-assisted data to the maximum benefit include dynamic spectrum management, dynamic channel allocation algorithms, automatic network expansion procedures, handover algorithms and adaptive coverage systems. Location awareness for CR also enables optimised scheduling of tasks and routing both in space and time, which enable more efficient communications [16]. Therefore the motivation and focus of this dissertation pertains to certain aspects of location awareness for CR and more specifically the optimisation of dynamic spectrum access assisted positioning techniques.

1.2 RESEARCH OBJECTIVES

The objectives of this research study aims to optimise the existing time-based localisation techniques in order to enable CR location awareness and therefore this research work can be

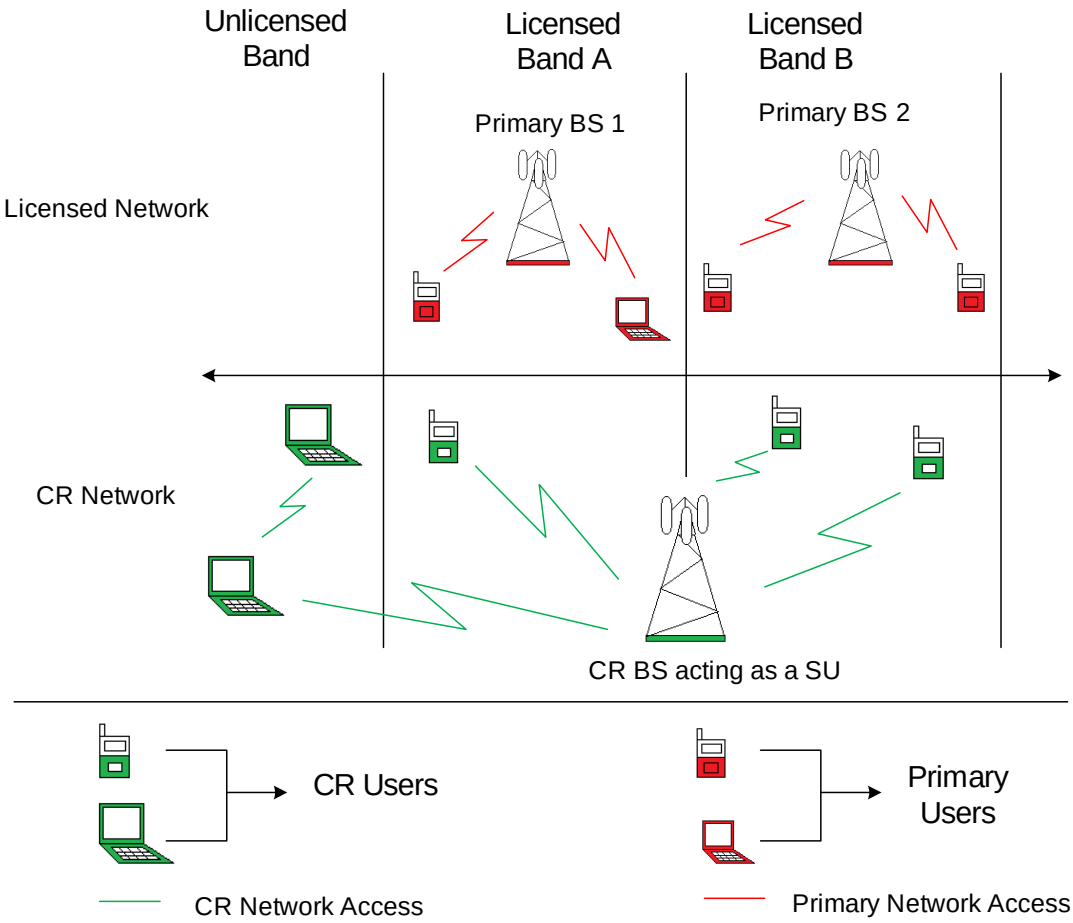

Figure 1.2: Overview of a typical CR environment [13]

broadly divided into two aspects:

- The first objective is the development of an efficient bandwidth determination (BD) model for the cognitive positioning system (CPS) using a multiple receive antenna system, which is based on the Cramer-Rao lower bound (CRLB) principle. The performance advantages of the single-input-multiple-output (SIMO) BD positioning scheme are compared with the conventional single-input-single-output (SISO) scheme, using the linear least squares (LLS) technique and two-step maximum-likelihood (TSML) location estimation algorithms. The proposed efficient BD model is also compared under different environmental models with various propagation characteristics. These include a generalised rural scenario where line-of-sight (LOS) is the dominant signal component, as well as urban and suburban environments where non-line-of-sight

(NLOS) components can affect the positional accuracy of a CR user.

- The second objective involves the proposed formulation of a single-path multiband time-of-arrival (TOA) positioning technique for CR, which follows indirectly from the first research objective. The positional accuracy of a conventional single band TOA system is compared with the proposed multiband TOA estimation technique. An overall time delay estimate is developed, which is based on the CRLB derivation of a combining estimation technique. The performance of the localisation technique is analysed using a set of linear and non-linear location estimation algorithms. In the context of a CR scenario, the multiband positioning technique is validated using a fixed bandwidth availability model and a practical ultra-high frequency (UHF) bandwidth availability model, which is based on spectrum occupancy measurement data.

1.3 CONTRIBUTIONS

The analysis and evaluation of a bandwidth efficient CPS and the development of a multiband TOA estimation technique would be a significant next step in the optimised development of location awareness engines for CR transceivers. The following research contributions are pertinent to this study:

- One of the main contributions of this research study would be the development of a more spectrally efficient CPS for CR, i.e. the CPS would require less bandwidth to achieve the desired positional accuracy when compared to the current system. This technique highlights the advantages of multi-antenna schemes for positioning in addition to its benefits in wireless communications.

- An evaluation of the proposed bandwidth efficient model is presented under two main types of scenarios, LOS and NLOS environments. The extent to which either system outperforms the other will be quantified, using two linear estimation algorithms, viz. two-step maximum likelihood (TSML) and linear least squares (LLS) estimation.

- Knowledge regarding the state (LOS/NLOS) of the transmitted signals and required

compensation thereof to improve positional accuracy, can also be utilised to significantly increase the performance of the autonomous and adaptive capabilities of CR. The resulting outcome of this research may significantly aid in decision-directed selection of optimal modulation schemes, as well as appropriate frequency band selection. This is provided that a CR receiver can accurately determine its position, irrespective of the state of the signals, while at the same time achieving the desired requirements of dynamic spectrum access.

- TOA ranging has traditionally been implemented in many positioning applications and determines the position of a mobile user by estimating the signal time delay between the transmitter and the receiver. The multiband TOA method also aims to exploit a typical CR scenario where varying discrete bandwidths are utilised in an opportunistic fashion to enable improved TOA location awareness. The novelty of this work is the estimation combining technique, which involves the selection of an overall optimum delay estimate to enhance the two-dimensional location estimation accuracy of a mobile user.

The development of these environment and location awareness applications could pave the way for advanced autonomous location-based services, which will inevitably form part of the overall CR architecture [15]. The concept of CR has been considered the recommended solution for problems associated with spectrum scarcity and autonomous functionality and awareness of local surroundings has become an integral part of wireless adaptive communication systems.

1.4 RESEARCH OUTPUTS

The following conference proceeding and journal letter was published during the course of this research study:

1. R.R. Thomas, B. Zayen, R. Knopp and B.T. Maharaj, "A multiband TOA positioning technique for CR systems", in *22nd Personal Indoor Mobile Radio Communications (PIMRC) Workshop on Cognitive Radio and Networking: Solutions and Challenges*

Ahead, Toronto, Canada, September 2011, pp. 2315-2319.

2. R.R. Thomas and B.T. Maharaj, "Towards a bandwidth efficient cognitive positioning system", *IET Electronic Letters*,vol. 48, no. 12, pp. 736-737, June 2012.

The following journal paper was submitted and is in review:

- An article titled "Multiband TOA positioning technique using an UHF Bandwidth Availability model for Cognitive Radio" authored by R.R. Thomas, B.T. Maharaj, B. Zayen and R. Knopp was submitted for review to the IET Journal of Radar, Sonar and Navigation.

1.5 DISSERTATION OUTLINE

Chapter 2 provides a conceptual overview of existing ranging techniques utilised for mobile positioning systems. Thereafter a scholarly review of the different positioning applications which may be suitable for CR is given, with emphasis on Global Navigation Satellite Systems (GNSSs), multiple-input-multiple-output (MIMO) and wireless local area network (WLAN) positioning systems. Thereafter a discussion on the role of location awareness in CR and its relation to various other CR functions is provided.

Chapter 3 takes a closer look into the existing location estimation algorithms from a mathematical standpoint. Two general types of location estimation algorithms are covered, viz. linear and non-linear techniques. Issues relating to the performance of these algorithms such as the convergence of the final solution, are discussed. The chapter concludes with an overview of the effect of NLOS signal components on positioning accuracy.

Chapter 4 provides a brief discussion of the cognitive positioning system (CPS) and thereafter the CRLB derivation of the proposed efficient BD model using multiple receive antennas is analysed. Thereafter the enhanced dynamic spectrum management (EDSM) component of the CPS is discussed.

The concept of the multiband TOA technique in the context of CR systems is then introduced in Chapter 5. An analytical derivation of the combining estimation technique for the estimated parameters of the received baseband signal is given. The UHF spectrum occupancy measurement campaign which led to the development of the bandwidth availability model is then discussed. This dynamic model is then used to validate the performance of the multiband TOA positioning technique.

Chapter 6 provides a detailed analysis of the results related to the proposed optimised positioning technique presented in Chapters 4 and 5.

In Chapter 7, conclusions are drawn about the overall study and any possibilities for future research related to this study are suggested.

CHAPTER 2

REVIEW OF LOCALISATION TECHNIQUES AND APPLICATIONS

This chapter presents a detailed and conceptual review of the key signal processing techniques currently employed to aid in the determination of the two-dimensional (2D) location estimate of a mobile user. Section 2.2 examines the different positioning systems applicable to CR. Thereafter in Section 2.3, the importance of location awareness in the overall CR architecture is elaborated upon.

2.1 EXISTING RANGING TECHNIQUES

According to current literature, there are several distance estimation methods that rely on signal processing of the received signal, viz. received signal strength (RSS), time-of-arrival (TOA), time-difference-of-arrival (TDOA) and angle-of-arrival (AOA). Table 2.1 outlines each of these ranging techniques and its associated applications.

2.1.1 Received Signal Strength

The key metric for estimating the distance between a transmitting (anchor) and receiving (target) node is the RSS. Multiple nodes are required to triangulate a user's position according to this particular ranging technique. The path-loss model plays an important role in location estimation, as it describes the attenuation of a signal as a function of distance.

Table 2.1: Application of the different ranging techniques

Ranging Technique	Usage Application
RSS	Utilised where approximate positional accuracy is required with emphasis on robustness.
TOA	Usually utilised in cellular networks.
TDOA	Mainly applied in wireless sensor networks.
AOA	Hardware complexity is high to accommodate antenna arrays and hence suitable for implementation at base station (BS).
Fingerprinting	Commonly applied in WLAN or cellular networks in conjunction with RSS or TOA as a metric for the database.

Different path loss models have been developed according to the type of environment (e.g. urban, suburban or rural environment), due to the variation in signal attenuation in various terrains. As a result the position estimate becomes dependent on a parameter known as the path loss coefficient, which varies according to the type of environment setting. These path-loss models are usually based on assuming an ideal free-space channel or by conducting extensive channel measurements and modelling. Received signal strength positioning schemes are known to provide low positional accuracy, since variations in channel behaviour induce large estimation errors. However, the key advantages of this technique include the low cost of implementation as well as low complexity of the algorithm [17]. Figure 2.1 illustrates the basic concept of RSS positioning with the aid of the log-distance path loss model, which has been validated through various empirical measurements. The following equation describes the log-distance path loss (PL) equation and underscores the relationship between the received signal energy and distance [18]:

$$PL = P_{Tx|dB} - P_{Rx|dB} = PL(d_o)|_{dB} + 10n\log\frac{d}{d_o}, \tag{2.1}$$

where $P_{Tx|dB}$ and $P_{Rx|dB}$ represent the transmit and receive power in dB units respectively, d_o is the reference path loss at a fixed distance of 1 km, d is the true distance between the transmitter and receiver. The path-loss coefficient is given by n and has a direct influence on the received strength of a signal. As a result this technique is heavily dependent on the channel and can therefore lead to inaccuracies due to the variable nature of the propagation channel.

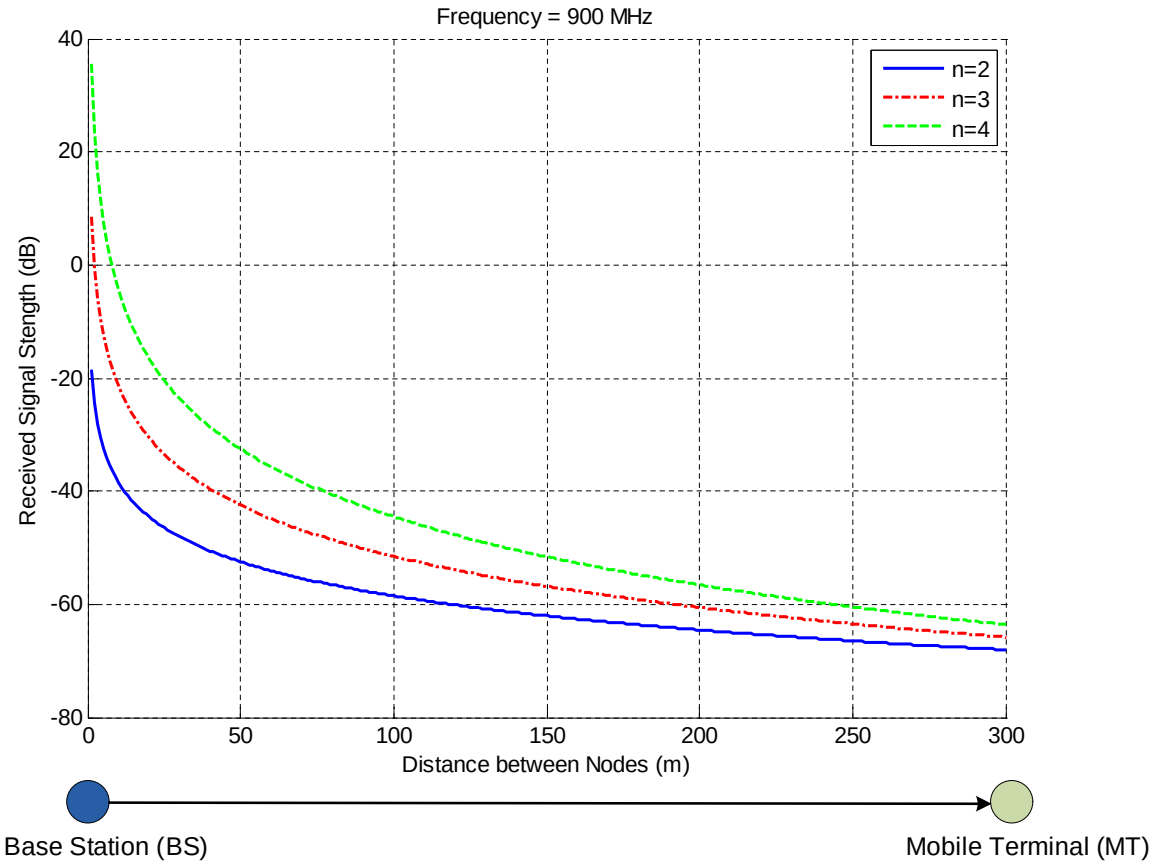

Figure 2.1: RSS positioning technique

The 2D coordinates of i base stations (BS) are given by the vector $\mathbf{x}_i = [\ x_i \quad y_i\ ]^T$, and for the mobile terminal (MT), given by the vector $\mathbf{x} = [\ x \quad y\ ]^T$. Let it be defined that the Euclidean distance between the base station and MT be represented by d_i, which can be represented as:

$$d_i = ||\mathbf{x} - \mathbf{x}_i|| = \sqrt{(x-x_i)^2 + (y-y_i)^2}. \qquad i = 1,2,...,N \tag{2.2}$$

The RSS measurement model, which is a manipulation of eq. (2.1), can be alternatively shown as [19]:

$$P_{Rx,i} = K_i P_{Tx} d_i^{-n} = K_i P_{Tx} ||\mathbf{x} - \mathbf{x}_i||^{-n}, \tag{2.3}$$

where K_i represents a factor encompassing the antenna gains, antenna heights, etc. Accordingly eq. (2.3) follows a lognormal distribution and can be expressed as:

$$\ln(P_{Rx,i}) = \ln(K_i) + \ln(P_{Tx}) - n\ln(d_i) + j_{RSS,i}, \tag{2.4}$$

where $j_{RSS,i}$ follows a zero mean uncorrelated Gaussian distribution with variance $\sigma^2_{RSS,i}$. In order to simplify eq. (2.4), let [19]:

$$r_{RSS,i} = -n\ln(d_i) + j_{RSS,i}. \tag{2.5}$$

All the BSs represented in eq. (2.5) can be condensed into vector form:

$$\mathbf{r}_{RSS} = \mathbf{f}_{RSS}(\mathbf{x}) + \mathbf{j}_{RSS}, \tag{2.6}$$

where the vectors $\mathbf{r}_{RSS}$, $\mathbf{j}_{RSS}$ and $\mathbf{f}_{RSS}(\mathbf{x})$ are represented as follows:

$$\mathbf{r}_{RSS} = \left[r_{RSS,1}, r_{RSS,2}, \ldots, r_{RSS,N}\right]^T, \tag{2.7}$$

$$\mathbf{j}_{RSS} = \left[j_{RSS,1}, j_{RSS,2}, \ldots, j_{RSS,N}\right]^T, \tag{2.8}$$

$$\mathbf{f}_{RSS}(\mathbf{x}) = -n \begin{bmatrix} \ln\left(\sqrt{(x-x_1)^2 + (y-y_1)^2}\right) \\ \ln\left(\sqrt{(x-x_2)^2 + (y-y_2)^2}\right) \\ \vdots \\ \ln\left(\sqrt{(x-x_N)^2 + (y-y_N)^2}\right) \end{bmatrix}. \tag{2.9}$$

2.1.2 Time-of-arrival

The TOA positioning technique is one of two time-based schemes to estimate the location of a node. In a similar manner to RSS, multiple anchor nodes (e.g. BSs) are also required to triangulate the position estimate of the target node (MT). The distance estimate can be obtained from the propagation signal delay between an anchor and target node. For a coplanar case, a minimum of three anchors are required to determine the position of a target node. However, in a non-coplanar case a minimum of four anchors are required to triangulate a user's position [19]. This particular technique has always been applied to cellular networks where MTs are inherently synchronised to base stations. The signal-to-noise ratio (SNR) of a signal, as well as the signal bandwidth, has a direct impact on the accuracy of TOA positioning systems. The TOA ranging technique is well suited for CR systems, since the bandwidth of the signal can be adaptively adjusted according to dynamic spectrum availability. The position of a target's node can be localised with a sphere of radius r_i, where i represents the identifier of each BS. Figure 2.2 is a conceptual diagram of the TOA technique.

The time delay (τ) of the signal from each BS is characterised by a circle with a radius (r). In an ideal scenario the intersection of all the circles represents the 2D location of the MT. A few issues relating to the TOA ranging method need to be considered [20]:

- Lack of synchronisation between the BS (anchor node) and the MT (target node) may lead to large location estimation errors.

- Additional complexity is introduced to the transmitted signal by adding a time stamp. This time stamp enables the anchor node to determine the time at which the signal was transmitted by the target node.

- The BS's location coordinates are a prerequisite in order to perform TOA ranging.

Let the propagation delay between each of the N base stations and the MT be represented by t_i. The TOAs of each signal can then be expressed as:

$$t_i = \frac{d_i}{c}, \tag{2.10}$$

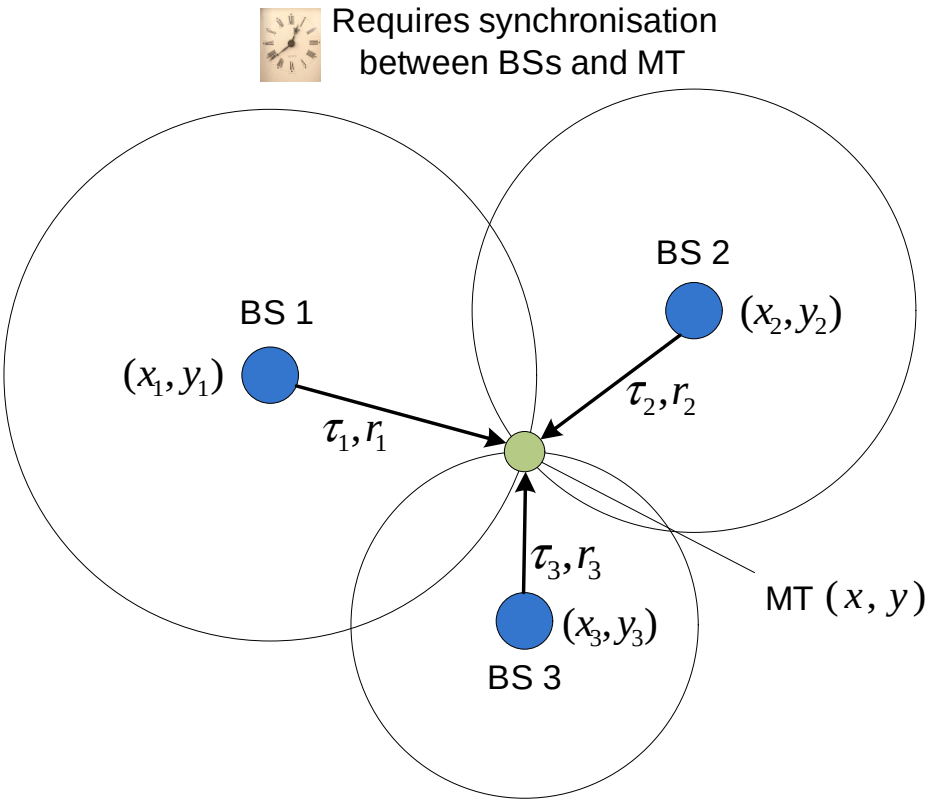

Figure 2.2: TOA positioning technique

where d_i has been defined in eq. (2.2) and c is the speed of an electromagnetic wave. However, in reality the time delay estimation is susceptible to measurement errors, which could arise from certain factors such as the effects of the propagation channel and random noise. Taking these impairments into account, the following expression can be derived, based on eq. (2.10):

$$r_{TOA,i} = d_i + j_{TOA,i}, \tag{2.11}$$

where $r_{TOA,i} = ct_i$ and $j_{TOA,i}$ is the aforementioned TOA measurement error. Eq. (2.11) can be further expanded into signal vector form as follows:

$$\mathbf{r}_{TOA} = \mathbf{f}_{TOA}(\mathbf{x}) + \mathbf{j}_{TOA,} \tag{2.12}$$

where in a similar case to the RSS model the vector variables are defined as:

$$\mathbf{r}_{TOA} = \left[r_{TOA,1}, r_{TOA,2}, ..., r_{TOA,N}\right]^T, \tag{2.13}$$

$$\mathbf{j}_{TOA} = \left[j_{TOA,1}, j_{TOA,2}, ..., j_{TOA,N}\right]^T, \tag{2.14}$$

$$\mathbf{f}_{TOA}(\mathbf{x}) = \begin{bmatrix} \sqrt{(x-x_1)^2 + (y-y_1)^2} \\ \sqrt{(x-x_2)^2 + (y-y_2)^2} \\ \vdots \\ \sqrt{(x-x_N)^2 + (y-y_N)^2} \end{bmatrix}. \tag{2.15}$$

In the case of TOA ranging, the expression given in (2.15) is assumed to be known and is free from any noise corruption. Therefore, let each scalar value ($j_{TOA,i}$) be characterised by a zero-mean Gaussian process with variance $\sigma^2_{TOA,i}$. It is then possible to develop an expression for the scalar probability density function (pdf) [19]:

$$p(r_{TOA,i}) = \frac{1}{\sqrt{2\pi\sigma^2_{TOA,i}}} \exp\left(-\frac{1}{2\sigma^2_{TOA,i}}\left(r_{TOA,i} - d_i\right)^2\right), \tag{2.16}$$

where the mean is given by d_i. The vector form of the pdf is given by:

$$p(\mathbf{r}_{TOA}) = \frac{1}{(2\pi)^{N/2}\left|\mathbf{C}_{TOA}\right|^{1/2}} \exp\left(-\frac{1}{2}\left(\mathbf{r}_{TOA} - \mathbf{d}\right)^T \mathbf{C}^{-1}_{TOA}\left(\mathbf{r}_{TOA} - \mathbf{d}\right)\right), \tag{2.17}$$

where $\mathbf{C}_{TOA}$ is the covariance matrix, which can be alternatively written as:

$$\begin{aligned} \mathbf{C}_{TOA} &= E\left\{\mathbf{j}_{TOA}\mathbf{j}^T_{TOA}\right\} \\ &= diag\left\{\sigma^2_{TOA,1}, \sigma^2_{TOA,2}, ..., \sigma^2_{TOA,N}\right\}. \end{aligned} \tag{2.18}$$

Considering eq. (2.17) and (2.18), the final expression for the vectorised pdf can be given as [19]:

$$p(\mathbf{r}_{TOA}) = \frac{1}{(2\pi)^{N/2}\prod_{i=1}^{N}\sigma_{TOA,i}} \exp\left(-\frac{1}{2}\sum_{i=1}^{N}\frac{\left(r_{TOA,i} - d_i\right)^2}{\sigma^2_{TOA,i}}\right). \tag{2.19}$$

Eq. (2.19) is an important relationship with regard to the TOA location estimation algorithm.

2.1.3 Time-difference-of-arrival

TDOA is a variation of the TOA technique where two or more anchor nodes utilise each individual TOA signal data to estimate a target node's location. A hyperbola characterises the TOA difference between anchor nodes where the differences between two distances from any two points on the hyperbola curve are constant (also known as foci points). For a coplanar case, three anchor nodes and two TDOA measurements are required. In a non-coplanar case, similar to TOA estimation, four anchor nodes with three TDOA measurements are required. A key advantage of the TDOA method, is that synchronisation between the anchor nodes and the target node is not required, but among the different anchor nodes, the clocks have to be perfectly synchronised. Some of the enabling applications include military and emergency aid systems [19]. Two or more nodes are required to perform localisation and therefore it is more suitable for wireless sensor networks, as indicated in Table 2.1 [21]. Figure 2.3 illustrates the basic concept of the TDOA positioning technique. According to Figure 2.3, the point of intersection of the two TDOA hyperbola curves characterises the MT's (target node's) location. The corresponding two TDOA measurements are obtained by choosing BS 1 as the reference node.

As a result the corresponding mathematical model can be defined by assuming that the MT transmits a signal at time t_0 and base station i receives the signal at time t_i where $i = 1,2,...,N$. For TDOA, the minimum number of base stations required is given by $N \geq 3$. Since the time difference between the base stations are taken into account, there are $\frac{N(N-1)}{2}$ unique combinations of TDOAs between all possible base station pairs, which is best described by the following equation:

$$t_{m,i} = (t_m - t_0) - (t_1 - t_0) = t_m - t_i, \quad i = 1,2,...,N \quad and \quad k > 1 \tag{2.20}$$

where m represents the selected reference node. In order to avoid redundant TDOA pairs, a

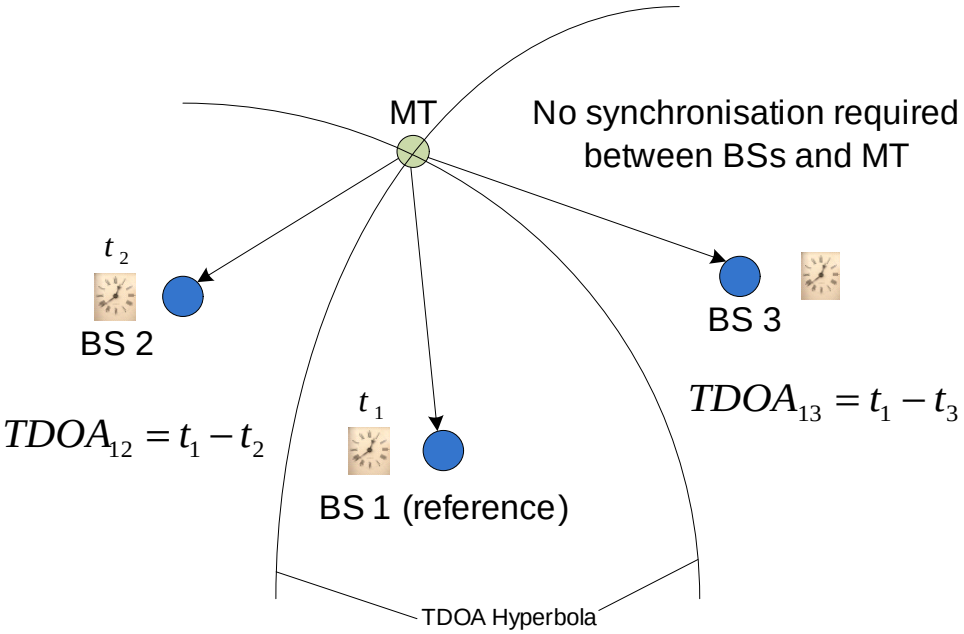

Figure 2.3: TDOA positioning technique

reference base station has to be chosen. In this case, the first base station will be considered as the reference. Similar to eq. (2.11), the TDOA measurement can be given as [19]:

$$r_{TDOA,i} = d_{i,1} + j_{TDOA,i}, \quad i = 1,2,...,N \tag{2.21}$$

where $d_{i,1}$ is the distance to the reference base station given as:

$$d_{i,1} = d_i - d_1. \tag{2.22}$$

Eq. (2.21) can also be expressed in vector form as:

$$\mathbf{r}_{TDOA} = \mathbf{f}_{TDOA}(\mathbf{x}) + \mathbf{j}_{TDOA}, \tag{2.23}$$

where these can be shown as:

$$\mathbf{r}_{TDOA} = \left[r_{TDOA,1}, r_{TDOA,2}, ..., r_{TDOA,N}\right]^T, \tag{2.24}$$

$$\mathbf{j}_{TDOA} = \left[j_{TDOA,1}, j_{TDOA,2}, \ldots, j_{TDOA,N} \right]^T, \tag{2.25}$$

$$\mathbf{f}_{TDOA}(\mathbf{x}) = d_1 = \begin{bmatrix} \sqrt{(x-x_2)^2+(y-y_2)^2} - \sqrt{(x-x_1)^2+(y-y_1)^2} \\ \sqrt{(x-x_3)^2+(y-y_3)^2} - \sqrt{(x-x_1)^2+(y-y_1)^2} \\ \vdots \\ \sqrt{(x-x_N)^2+(y-y_N)^2} - \sqrt{(x-x_1)^2+(y-y_1)^2} \end{bmatrix}. \tag{2.26}$$

If $\mathbf{j}_{TDOA}$ follows a zero mean Gaussian distribution, then in a similar fashion to eq. (2.17), the pdf of $\mathbf{r}_{TDOA}$ can be written as:

$$p(\mathbf{r}_{TDOA}) = \frac{1}{(2\pi)^{(N-1)/2} |\mathbf{C}_{TDOA}|^{1/2}} \exp\left(-\frac{1}{2} (\mathbf{r}_{TDOA} - \mathbf{d}_1)^T \mathbf{C}_{TDOA}^{-1} (\mathbf{r}_{TDOA} - \mathbf{d}_1) \right). \tag{2.27}$$

In this particular case the covariance matrix ($\mathbf{C}_{TDOA}$) is not a diagonal matrix, since all TDOA calculations are with respect to the first base station and hence $j_{TDOA,i} = 1,2,..,N$ is correlated.

2.1.4 Angle-of-arrival

The distance estimate is obtained by computing the angles of arrival (AOA) of the MT (target node) as seen from each of the BSs (anchor nodes). An important advantage of AOA systems is that a lower number of anchor nodes are required to localise a target when compared to TOA or TDOA systems. However, there are a few drawbacks with respect to this technique [21]:

- Cost becomes an issue, since additional hardware has to be implemented in the form of antenna arrays, which increases the overall complexity of the system.
- This technique is very susceptible to multipath and scattering, which results in complex computation of angles, inducing large distance estimation errors. This method also performs poorly in NLOS environments.

The AOA technique best outperforms TOA and RSS in inhomogeneous mediums, e.g. water, and as such is suitable for localisation sensors in body area networks (BANs) [19]. Figure 2.4 illustrates the concept of AOA.

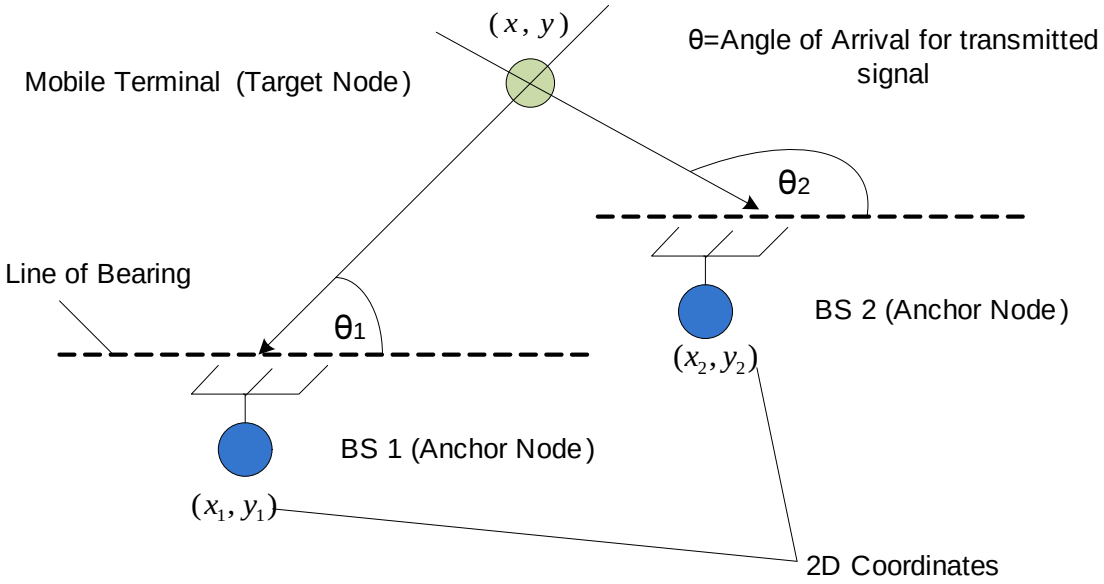

Figure 2.4: AOA positioning technique

The position of the MT is determined through the juncture point of two lines of which the direction is obtained through energy peaks of two different signals received at BS 1 and BS 2. Both anchor nodes as seen in Figure 2.4 are equipped with antenna arrays, which are used to compute the AOA. It is further possible to derive a generalised mathematical model by letting the AOA between the MT and BS i be given as θ_i. Using the 2D coordinates, it can be shown that:

$$\tan\theta_i = \frac{y-y_i}{x-x_i}. \quad i = 1,2,...,N \tag{2.28}$$

Since AOA requires fewer BSs to localise a target, it follows that $N \geq 2$. The AOA measurement can therefore be given as [19]:

$$r_{TDOA,i} = \theta_i + j_{AOA,i} = \arctan\left(\frac{y-y_i}{x-x_i}\right) + j_{AOA,i}. \quad i = 1,2,...,N \tag{2.29}$$

The above expression can then be translated into the following vector form:

$$\mathbf{r}_{AOA} = \mathbf{f}_{AOA}(\mathbf{x}) + \mathbf{j}_{AOA}, \tag{2.30}$$

where

$$\mathbf{r}_{AOA} = \left[r_{AOA,1}, r_{AOA,2}, ..., r_{AOA,N}\right]^T, \tag{2.31}$$

$$\mathbf{j}_{AOA} = \left[j_{AOA,1}, j_{AOA,2}, ..., j_{AOA,N}\right]^T, \tag{2.32}$$

$$\mathbf{f}_{TDOA}(\mathbf{x}) = \theta_i = \begin{bmatrix} \arctan\left(\frac{y-y_1}{x-x_1}\right) \\ \arctan\left(\frac{y-y_2}{x-x_2}\right) \\ \vdots \\ \arctan\left(\frac{y-y_N}{x-x_N}\right) \end{bmatrix}. \tag{2.33}$$

Similarly, if $\mathbf{j}_{AOA}$ assumes a zero mean Gaussian process with variance $\sigma^2_{AOA,i}$, then the corresponding pdf of $\mathbf{r}_{AOA}$ is given by:

$$p(\mathbf{r}_{AOA}) = \frac{1}{(2\pi)^{N/2}|\mathbf{C}_{AOA}|^{1/2}} \exp\left(-\frac{1}{2}(\mathbf{r}_{AOA} - \theta)^T \mathbf{C}^{-1}_{AOA}(\mathbf{r}_{AOA} - \theta)\right), \tag{2.34}$$

where $\mathbf{C}_{AOA}$ is a covariance matrix expressed as a diagonal matrix of elements $\sigma^2_{AOA,i}$, ranging from $i = 1, 2, ..., N$.

2.1.5 Fingerprinting

The positional accuracy of the aforementioned techniques, including RSS, TOA and AOA, degrade significantly in heavy or dense multipath environments [22]. The fingerprinting positioning technique serves as a solution to this problem. This involves mapping the characteristics of the multipath environment in dense urban areas using pattern recognition where key signal parameters of a specific area are stored in a database on a server. These signal parameters may include received signal characteristics and time delay parameters [23].

2.2 POSITIONING SYSTEMS

The following positioning applications have an important role to play in future location awareness of CR and will therefore be discussed in detail.

2.2.1 Satellite-based Positioning

Satellite-based positioning systems that utilise a constellation of satellites to determine a user's terrestrial coordinates are referred to as Global navigation satellite systems (GNSSs) [24]. The Global Positioning System (GPS) and the future Galileo [25] are well-known examples of positioning satellites. There are currently 24 operational GPS satellites in orbit, of which four are always available at any given location on earth. These four satellites can determine the 3D position of a user in terms of three key parameters: latitude, longitude and altitude [26]. Although GPS is a popular positioning method, it has a few drawbacks. GPS is unable to perform positioning in certain environments, such as underground mines and within indoor structures (buildings), mainly owing to the degradation of the signal quality. GPS also performs very poorly in dense urban environments, where multipath signals are frequent. Prerequisite information about the distance between the GPS receiver and satellite has to be known in order for GPS positioning to take place. Furthermore, the 3D co-ordinates of the four satellites involved in determining the position of the user also have to be known [19]. The core function of a standard GNSS is to utilise pseudorange measured data to estimate the location of a GNSS receiver, which can be mathematically modelled as follows [24]:

$$p^k(t) = r^k(t, t-\tau) + c[\delta t_u(t) - \delta t^k(t-\tau)] + I^k(t) + T^k(t) + \varepsilon^k(t). \tag{2.35}$$

Table 2.2 describes each of the parameters from eq. (2.35).

GNSS distance measurement is carried out using TOA and hence the delay (τ) parameter in eq. (2.35) is one of the main variables in the estimation process. The pseudorange measurement can be determined for each satellite corresponding to k. The receiver clock offset

Table 2.2: Parameter description of the pseudorange measurement model for GNSS

Symbol	Description
$p^k(t)$	pseudorange measurement
k	individual identifier for transmitting satellite
t	signal receive time in seconds
τ	signal delay of the transmitted signal between the transmitter and receiver
$r^k(t,t-\tau)$	geometric range between the received signal at time t and the transmitting satellite k at time $t-\tau$
c	speed of light
$\delta t_u(t)$	receiver clock offset relative to GPS time at time of reception
$\delta t^k(t-\tau)$	transmitting satellite clock offset relative to GPS time at time of transmission
$I^k(t)$	Ionosphere-induced propagation delay for satellite k
$T^k(t)$	Troposphere-induced propagation delay for satellite k
$\varepsilon^k(t)$	miscellaneous unmodelled range error for satellite k which may include multipath effects and receiver noise

($\delta t_u(t)$) is a parameter generalised to all satellites and as a result eq. (2.35) can be further simplified by concatenating all errors into one term ($\widetilde{\varepsilon}^k_{Total}$). The error from each satellite can therefore be expressed as [24]:

$$\rho^k_c = r^k + c\delta t_u + \widetilde{\varepsilon}^k_{Total}. \tag{2.36}$$

The actual range (r^k) and the receiver clock offset (δt_u) represent the unknowns in eq. (2.36). The accuracy of the position, velocity and time solution is affected by the statistics and magnitude of $\widetilde{\varepsilon}^k_{Total}$. The actual range ($r^k$) between the GNSS receiver and satellite k can be expressed as Cartesian co-ordinates [24]:

$$r^k = \sqrt{\left(x^k - x\right) + \left(y^k - y\right) + \left(z^k - z\right)} = ||\mathbf{x}^k - \mathbf{x}_u||, \tag{2.37}$$

where the receiver's and satellite's 3D co-ordinates are respectively given as $\mathbf{x}_u = (x, y, z)$ and $\mathbf{x}^k = \left(x^k, y^k, z^k\right)$. Figure 2.5 is a simplified diagram showing the utilisation of four pseudorange measurements to localise a GNSS user.

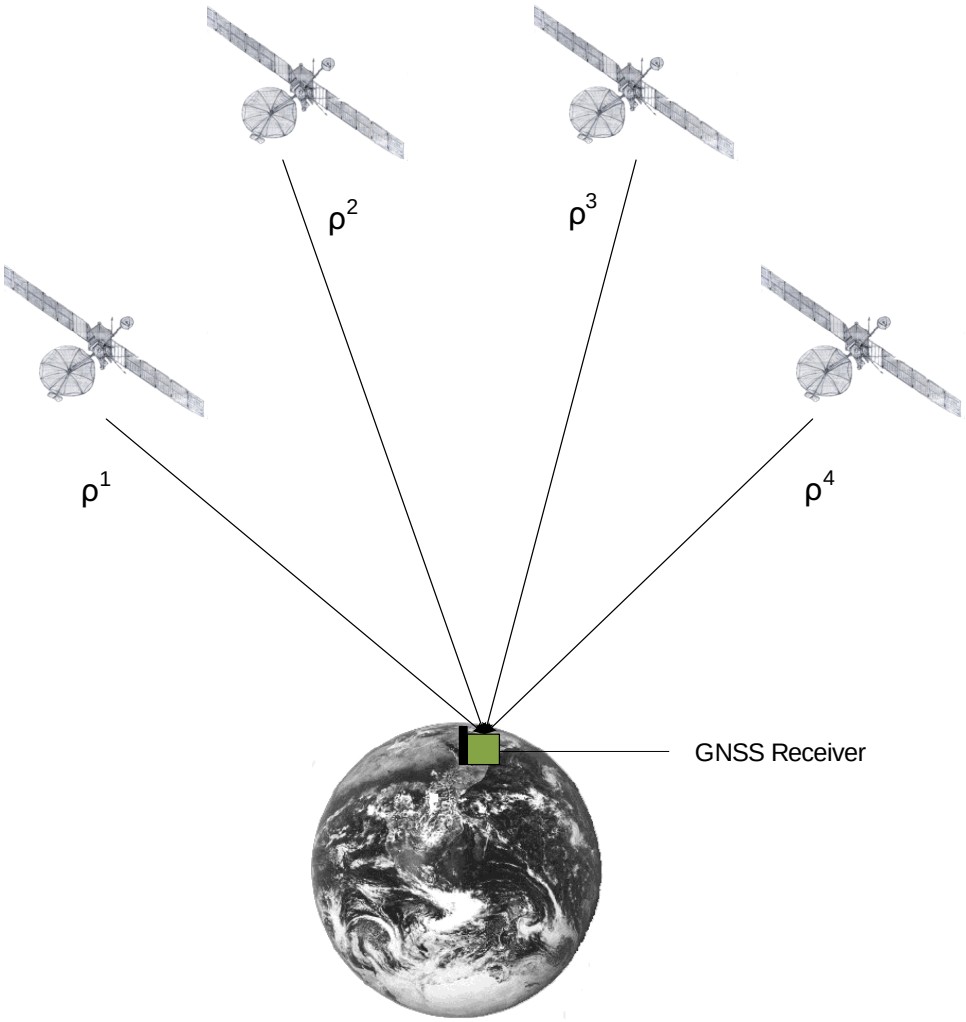

Figure 2.5: User position tracking using pseudorange measurements from 4 GNSSs

2.2.2 MIMO Positioning Systems

The use of multi-input-multiple-output (MIMO) antenna systems have been extensively employed in wireless communication systems to improve channel capacity performance

and achieve both diversity and array gains. MIMO systems have also been implemented to achieve higher positioning accuracy in radar and positioning applications. The main advantage of this approach is the exploitation of the information contained within each of the different received signal components. MIMO positioning systems may also take into account the effects of multipath and NLOS conditions to improve system accuracy. A direct location estimation method has been proposed which utilises MIMO techniques and ML estimation and as a result the overall distance estimation error is reduced. This method also considers the localisation of dynamic MTs as opposed to static MTSs and can ascertain the mobile user's position with the aid of only one base station [27]. Another technique utilises a combination of RSS ranging and spatial diversity to provide an improved distance estimation error between a single transmitter and receiver pair. The advantage of exploiting the overall received power of signal is the low complexity and low cost. The implementation of MIMO can eliminate deep fades that tend to hamper the estimation of the ranging error and hence the location of the MT (user) [28].

The TOA of a signal has also been implemented in conjunction with multiple antennas at the transmitter and receiver to improve positioning system performance by using the minimal selection algorithm [29]. Particle filtering algorithms also exploit the characteristics of MIMO to achieve higher positioning accuracy for mobile users. The choice of propagation channel model is an important aspect that has to be taken into account when considering the localisation of a user using MIMO techniques [30]. Hybrid signal processing techniques usually outperform the individual algorithms. One such MIMO method employs a combination of AOA, angle of departure and TDOA to estimate a user's location by using a single base station. The results reveal that by utilising multipath channel parameters, such as path delay and angle of arrival or departure, the location estimation error can be reduced and the measurement noise arising from this can be mitigated [31].

Three key points are evident from the implementation of MIMO positioning systems:

- Instead of mitigating the effects of multipath signals on location estimation, the MIMO systems exploit these signals by taking advantage of spatial diversity. It can also be

noted that MIMO systems can better exploit the a priori information contained in a NLOS signal when compared to SISO systems.

- MIMO systems can also take advantage of multiple estimation parameters to improve accuracy, such as the time delay of the signal, as well as the angle of arrival or departure of the signal, since closely spaced antennas act as phase array structures. Therefore the implementation of hybrid algorithms are particularly apt for these particular positioning systems.

- The selection of an appropriate channel model is another important factor that has to be taken into account. As a result, MIMO positioning systems are able to perform well under realistic propagation channel conditions.

The benefits of using multiple antennas at the transmitter and receiver can provide increased location awareness capabilities and increased spectral efficiency with respect to CR networks. Not much work has been done, to the best of the author's knowledge, in the area of applying MIMO techniques to improve environment location awareness in CR wireless networks.

2.2.3 WLAN Positioning

Wireless local area network (WLAN) positioning systems are limited in proximity and therefore suitable for indoor localisation. A variety of techniques are employed for WLAN positioning, such as RSS identification, which makes use of multiple distance measurements from predefined locations (also known as trilateration). A WLAN-based positioning scenario (refer to Figure 2.6) typically involves implementation of multiple access points to localise a MT as demonstrated in [32], where the estimation error performance of different RSS positioning algorithms such as distance variance, probabilistic estimation and nearest neighbour are investigated. One can consider dividing an indoor environment into a number of subspaces and thereafter develop a database of RSS signal characteristics for each subspace. A pattern-matching algorithm can then be utilised to localise a mobile host's location. In order to complement the system, a set of reference points are also included to compensate for any

changes in RSS in order to improve positional accuracy [33]. Another notion involves the use of WLAN in infrastructure mode where indoor localisation is performed using a set of access points and RSS data collectors. This technique comprises of two stages: offline training, where RSS measurements are collected and regarded as observed data, and then online location processing, where real-time RSS data of a MT is collected and thereafter location prediction is performed [34].

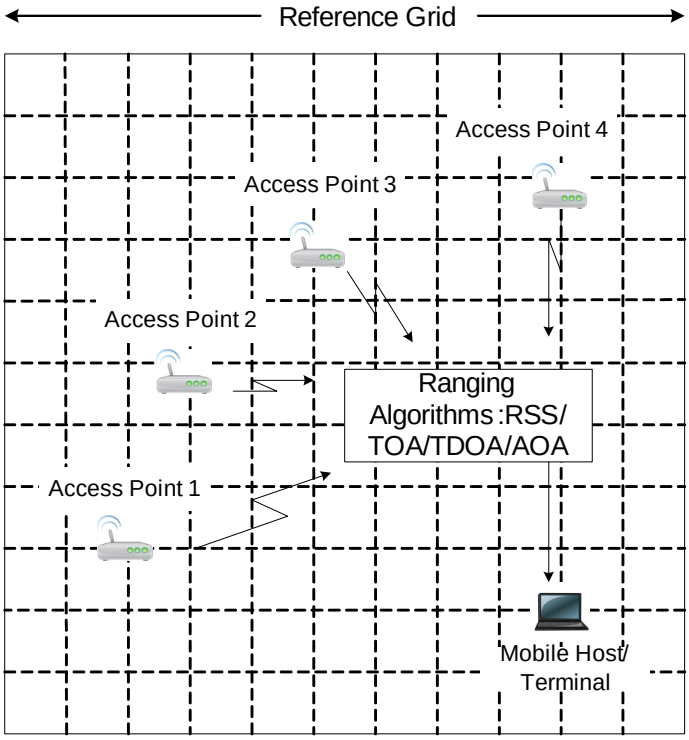

Figure 2.6: A typical WLAN-based positioning scenario

A number of TOA-based and AOA-based WLAN positioning schemes have also been considered. A key aspect of these particular ranging techniques in WLAN systems is the avoidance of any intricate databases which depend on RSS signal measurements. Certain TOA WLAN positioning schemes have been known to perform with better accuracy than traditional correlation methods [35]. TOA ranging can also be implemented using the existing WLAN infrastructure mode (as previously mentioned with RSS) using round-trip measurements (also commonly known as two-way ranging). The results show that three access points are sufficient in order to achieve 90 % accuracy in the order of 2 m [36]. Certain comparative studies have also shown that TOA ranging can offer superior performance in terms of posi-

tional accuracy when compared to RSS ranging in WLAN systems [37, 38]. TOA ranging can also be manipulated in software as proposed in [39], where timing measurements are observed at operating system level using a CPU clock at the receiver side (MT). Existing strategies involved minor hardware modifications to the WLAN network interface card to achieve cost-effective and accurate TOA estimates, but the TOA software technique aims to further reduce the reduce the complexity and implementation cost.

2.3 COGNITIVE RADIO: LOCATION AND ENVIRONMENT AWARENESS

An environment and location awareness conceptual model has been proposed to serve as a subsystem within the overall CR architecture and is shown in Figure 2.7. This model has been chosen to serve as a preliminary guideline in order to gain an overall picture of the problem and garner an understanding of how the proposed techniques in this research study can be integrated into this model. Figure 2.7 illustrates the relation of location and environmental awareness as a subsystem of the overall core architecture of CR. The real-time spectrum sensing component gathers information on the channel availability using signal processing techniques such as energy detection, match filtering, waveform-based sensing, etc. The location awareness component is responsible for intelligently (using machine learning techniques) managing the positioning data gathered from the various adaptive positioning schemes. A positioning system can be adaptive in the following ways [40]:

- Different types of usage applications may require different levels of accuracy such as accident and emergency services, where the required resolution accuracy is between 50 m and 300 m, as opposed to asset and vehicle tracking management services, where the resolution accuracy requirement is between 0.05 m and 30 m.

- Environment type can greatly influence the accuracy of positioning systems, e.g. there is a significant difference in accuracy between outdoor and indoor environments.

- Signalling technologies, such as wide-band code division multiple access (WCDMA) or ultra-wideband (UWB), can also have an impact on the performance of a positioning system.

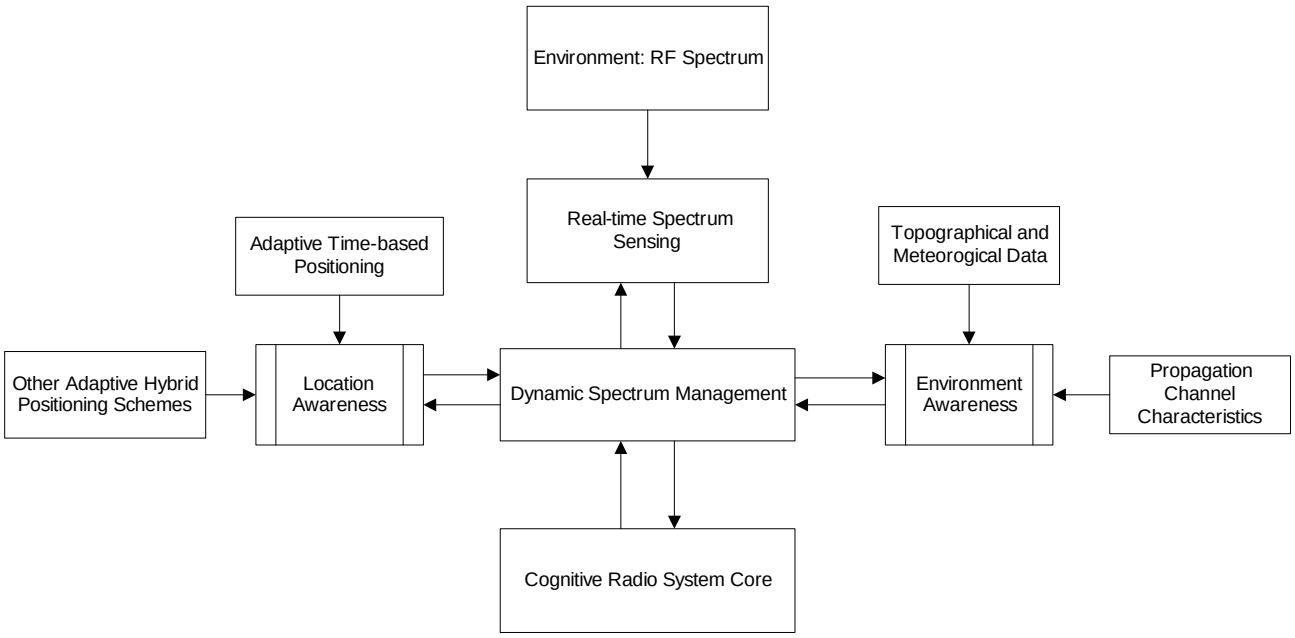

Figure 2.7: CR Subsystem consisting of the environment and location awareness model

The environmental awareness component takes advantage of surrounding environmental information such as the topographical data of a CR user to enhance various cognition capabilities. The dynamic spectrum management modules coordinate spectral, location and environment awareness information to optimise key tasks such as dynamic channel allocation and other transmission-related parameters.

The aforementioned ranging techniques, such as RSS and AOA, lack the required adaptive capabilities for CR. According to existing literature, conceptual architectures and models have been proposed with regard to location and environmental awareness [40–43]. The implications for location and environmental awareness for CR system design have been analysed. In order to optimise transmissions, CR must be able to display awareness of the wireless channel and adapt to parameter changes. Path-loss, delay spread, Doppler spread, angular spread, LOS/NLOS components and noise characteristics are examples of such wireless transmission parameters [43].

The IEEE 802.22 Wireless Regional Area Network (WRAN) standard employs concepts from CR that enable the sharing of unused spectrum with existing television broadcasters. The objective is to provide wireless broadband services to areas lacking in network infra-

structure, such as rural and sparsely populated environments. Figure 2.8 shows a segment of the overall IEEE 802.22 architecture that involves the use of location data [44].

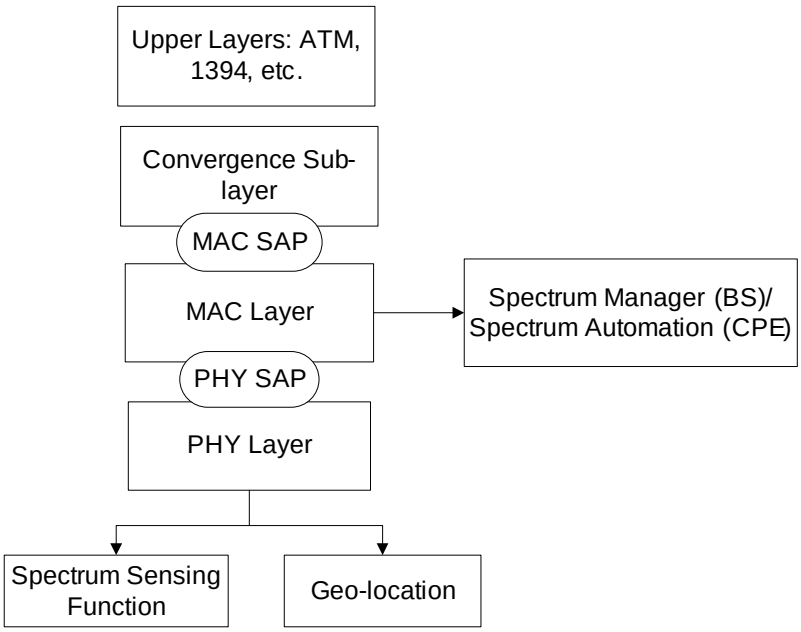

Figure 2.8: IEEE 802.22 architecture [44]

According to Figure 2.8 the Medium Access Control (MAC) layer is interfaced to the Physical (PHY) layer via the service access point (SAP). Utilisation of a geo-location database is an important component of the PHY layer and together with the spectrum sensing function, dynamic channel allocation can be performed [44].

Various candidate technologies exist for the CPS. For example, the following characteristics make UWB highly suited to indoor CR positioning as well as certain radar applications [21,45]:

- The large transmission bandwidth can inherently increase the positional accuracy of a system.
- The reliability of the link is improved, since the transmitted signal performs well in LOS and especially in NLOS environments.
- Large transmission bandwidths also mitigate the effects of small-scale fading.

- Interference is also reduced by spreading the signal over a large bandwidth and as a result reducing the power spectral density.

However, the primary drawback in the context of CR is the inability to adapt positional accuracy. Range accuracy adaptation is one of the key performance criteria of environmental and location awareness systems. This particular idea stems from the bat echolocation system, which is a well-known adaptive mechanism for bats. Bats adjust certain physical parameters with regard to their echo, such as bandwidth, repetition rate and transmitted signal duration, to track their prey. The same principle is being applied to CR in order to develop the range accuracy adaptation capability so that these devices can effectively and more efficiently recognise the immediate environment and location in a multi-user scenario. Range accuracy adaptation is susceptible to errors arising from dynamic spectrum effects, transceiver impairments, environmental and interference effects. Location and environmental awareness aims to draw its inspiration from biological organisms which possess the same capability and knowledge of this has been widely applied in the electronics field, e.g. robotics. Until recently, cognisance of the surrounding location and type of environment has been mainly limited to existing location-based services and mobile positioning systems [40].

The CPS has been proposed to tackle awareness of the location (position) in CRs by accomplishing accuracy adaptation for indoor and outdoor environments. This particular technique operates in two modes designed specifically for CR, viz. the bandwidth determination (BD) mode and enhanced dynamic spectrum management (EDSM) mode. The first mode ascertains the bandwidth required for a specific positional accuracy. The second mode uses a set of decision criteria to determine if the required bandwidth is physically available in the spectrum at any given time. The study reveals that there is an inherent trade-off between the complexity and accuracy of the CPS algorithms. Maximum-likelihood time-of-arrival performance evaluations pertaining to range accuracy adaptation of CPS systems have also been carried out and the results prove that it is possible to adapt the range accuracy of the positioning system based on the environment (indoor and outdoor) [45, 46].

CHAPTER 3

LOCATION ESTIMATION ALGORITHMS

The TOA ranging technique is suitable for implementation in CR owing to its adaptive capabilities. These algorithms can be broadly divided into two categories, viz. non-linear and linear techniques. The estimation of a mobile user's position in a wireless environment is susceptible to measurement errors including NLOS errors, and therefore the following distance estimation model for a single user can be derived [47]:

$$\tilde{d}_i = d_i + b_i + j_i, \tag{3.1}$$

where i represents the base station identifier, d_i is given in eq. (2.2), j_i represents additive white Gaussian noise (AWGN) with zero mean and variance σ_i^2 ($j_i \sim \aleph(0, \sigma_i^2)$). The positive bias error given by b_i, is also introduced into the model depending on whether the signal has a LOS or NLOS component. Alternatively, it can be shown that:

$$b_i = \begin{cases} 0 & if \quad BS_i \quad LOS \\ \psi_i & if \quad BS_i \quad NLOS. \end{cases} \tag{3.2}$$

The NLOS error can be modelled using a variety of techniques including the use of an empirical model derived from measurements, a constant time window scheme or according to a specific type of distribution, e.g. Gaussian, uniform, etc [47]. A more detailed discussion on NLOS error modelling is provided later on in Section 3.5. Eq. (3.1) can be extended into vector form as in eq. (2.12) and can be written as:

$$\tilde{\mathbf{r}} = \mathbf{f}(\mathbf{x}) + \mathbf{b} + \mathbf{j}, \tag{3.3}$$

where $\mathbf{f}(\mathbf{x})$ is a distance vector between each of the base stations and the single MT while $\mathbf{b}$ is a vector representing the positive bias errors from each base station.

3.1 TOA NON-LINEAR METHODS

The position estimation process in a non-linear case involves solving for $\mathbf{x}$ in eq. (3.3) by minimising the cost function based on the following error function:

$$\mathbf{e}_{nl} = \tilde{\mathbf{r}} - \mathbf{f}(\tilde{\mathbf{x}}) - \mathbf{b}, \tag{3.4}$$

where the optimisation variable for $\mathbf{x}$ is given by $\tilde{\mathbf{x}} = [\ \tilde{x} \quad \tilde{y}\ ]^T$ which relates to the ML or non-linear least squares (NLS) estimator [19].

3.1.1 Maximum-likelihood Estimation

Maximum-likelihood estimation involves the computation of the pdf of a data set, which characterises the most probable observed data. This requires the determination of the scalar parameter (θ), which maximises the likelihood function ($p(\mathbf{x};\theta)$) for a constant $\mathbf{x}$ over an allowable range Λ. The corresponding scalar parameter is referred to as the ML estimate (MLE), which is obtained by searching through multi-dimensional parameter space [48–50]. This can be expressed as:

$$\hat{\theta}(\mathbf{x};\theta)_{ML} = \arg\left\{\max_{\theta \varepsilon \Lambda} p(\mathbf{x};\theta)\right\}. \tag{3.5}$$

The maximum of the log-likelihood function ($\log p(\mathbf{x};\theta)$) corresponds to the maximum of $p(\mathbf{x};\theta)$, provided this function has sufficient smoothness. A key prerequisite of an MLE involves satisfaction of the following relationship:

$$\frac{\partial}{\partial \theta} \log p(\mathbf{x};\theta) \mid_{\theta=\hat{\theta}(\mathbf{x};\theta)_{ML}} = 0. \tag{3.6}$$

The ML technique relies on the fact that information about the error distribution is known a priori in order to maximise the pdf of the TOA measurement model. The initial step involves the maximisation of eq. (2.17) which, as shown in eq. (3.6), is equivalent to taking the natural logarithm of both sides of the equation as shown below:

$$\ln p(\mathbf{r}_{TOA,i}) = \ln \left((2\pi)^{N/2} |\mathbf{C}_{TOA}|^{1/2} \right)^{-1} - \frac{1}{2} (\mathbf{r}_{TOA} - \mathbf{d})^T \mathbf{C}_{TOA}^{-1} (\mathbf{r}_{TOA} - \mathbf{d}). \tag{3.7}$$

Maximising eq. (3.7) is equivalent to minimising the second term, since the first term is independent of $\mathbf{x}$, which is contained in $\mathbf{d}$ (refer to eq. (2.2)). The resulting expression becomes [19]:

$$\hat{\mathbf{x}} = \arg\min_{\hat{\mathbf{x}}} (\mathbf{r}_{TOA} - \mathbf{f}_{TOA}(\tilde{\mathbf{x}}))^T \mathbf{C}_{TOA}^{-1} (\mathbf{r}_{TOA} - \mathbf{f}_{TOA}(\tilde{\mathbf{x}})), \tag{3.8}$$

where the minimisation term is regarded as the ML cost function:

$$J_{ML-TOA}(\hat{\mathbf{x}}) = (\mathbf{r}_{TOA} - \mathbf{f}_{TOA}(\tilde{\mathbf{x}}))^T \mathbf{C}_{TOA}^{-1} (\mathbf{r}_{TOA} - \mathbf{f}_{TOA}(\tilde{\mathbf{x}})). \tag{3.9}$$

The cost function can be expanded further by substituting eqs. (2.13), (2.15) and (2.18):

$$J_{ML-TOA}(\hat{\mathbf{x}}) = \sum_{i=1}^{N} \frac{\left(r_{TOA,i} - \sqrt{(\tilde{x}-x_i)^2 + (\tilde{y}-y_i)^2} \right)}{\sigma_{TOA,i}^2}. \tag{3.10}$$

Therefore eq. (3.8) can be simply expressed as:

$$\hat{\mathbf{x}} = \arg\min_{\hat{\mathbf{x}}} \sum_{i=1}^{N} \frac{\left(r_{TOA,i} - \sqrt{(\tilde{x}-x_i)^2 + (\tilde{y}-y_i)^2} \right)}{\sigma_{TOA,i}^2}. \tag{3.11}$$

The final step involves the computation of $\hat{\mathbf{x}}$ in eq. (3.11). Iterative numerical methods are used to solve for the MLE. The first numerical method is the Newton-Raphson technique, which can be expressed as follows:

$$\hat{\mathbf{x}}^{k+1} = \hat{\mathbf{x}}^{k} - \mathbf{H}^{-1}(J_{ML-TOA}(\hat{\mathbf{x}}^{k}))\nabla(J_{ML-TOA}(\hat{\mathbf{x}}^{k})), \tag{3.12}$$

where $\mathbf{H}(J_{ML-TOA}(\mathbf{x}))$ represents a 2×2 Hessian matrix and $\nabla(J_{ML-TOA}(\mathbf{x}))$ is the gradient vector, all of which are computed for k iterations. The Hessian matrix is expressed in the following form [19]:

$$\mathbf{H}(J_{ML-TOA}(\mathbf{x})) = \begin{bmatrix} \frac{\partial^2(J_{ML-TOA}(\mathbf{x}))}{\partial x^2} & \frac{\partial^2(J_{ML-TOA}(\mathbf{x}))}{\partial x \partial y} \\ \frac{\partial^2(J_{ML-TOA}(\mathbf{x}))}{\partial y \partial x} & \frac{\partial^2(J_{ML-TOA}(\mathbf{x}))}{\partial y^2} \end{bmatrix}. \tag{3.13}$$

The computed Hessian matrix elements are shown as:

$$\frac{\partial^2\left(J_{ML-TOA}(\mathbf{x})\right)}{\partial x^2} = \sum_{i=1}^{N} \frac{2}{\sigma_{TOA,i}^2}\left(\frac{(x-x_i)^2}{(x-x_i)^2+(y-y_i)^2} - \frac{\left(r_{TOA,i}-d_i\right)(y-y_i)^2}{\left[(x-x_i)^2+(y-y_i)^2\right]^{3/2}}\right), \tag{3.14}$$

$$\frac{\partial^2\left(J_{ML-TOA}(\mathbf{x})\right)}{\partial x \partial y} = \frac{\partial^2\left(J_{ML-TOA}(\mathbf{x})\right)}{\partial y \partial x} = \sum_{i=1}^{N} \frac{2r_{TOA,i}(x-x_i)(y-y_i)}{\sigma_{TOA,i}^2\left[(x-x_i)^2+(y-y_i)^2\right]^{3/2}}, \tag{3.15}$$

$$\frac{\partial^2\left(J_{ML-TOA}(\mathbf{x})\right)}{\partial y^2} = \sum_{i=1}^{N} \frac{2}{\sigma_{TOA,i}^2}\left(\frac{(y-y_i)^2}{(x-x_i)^2+(y-y_i)^2} - \frac{\left(r_{TOA,i}-d_i\right)(x-x_i)^2}{\left[(x-x_i)^2+(y-y_i)^2\right]^{3/2}}\right), \tag{3.16}$$

where d_i has been defined in eq. (2.2). The gradient vector is a 2×1 matrix and is represented as:

$$\begin{aligned}\nabla(J_{ML-TOA}(\mathbf{x})) &= \begin{bmatrix} \frac{\partial J_{ML-TOA}(\mathbf{x})}{\partial x} \\ \frac{\partial J_{ML-TOA}(\mathbf{x})}{\partial y} \end{bmatrix} \\ &= -2\begin{bmatrix} \sum_{i=1}^{N} \frac{\left(r_{TOA,i}-d_i\right)(x-x_i)}{\sigma^2_{TOA,i}d_i} \\ \sum_{i=1}^{N} \frac{\left(r_{TOA,i}-d_i\right)(y-y_i)}{\sigma^2_{TOA,i}d_i} \end{bmatrix}. \end{aligned} \tag{3.17}$$

The second numerical technique employed to solve for $\hat{\mathbf{x}}$, is referred to as the Gauss-Newton method:

$$\hat{\mathbf{x}}^{k+1} = \hat{\mathbf{x}}^k + \left(\mathbf{G}^T\left(\mathbf{f}_{TOA}(\hat{\mathbf{x}}^k)\right)\mathbf{C}^{-1}_{TOA}\mathbf{G}\left(\mathbf{f}_{TOA}(\hat{\mathbf{x}}^k)\right)\right)^{-1}\mathbf{G}^T\left(\mathbf{f}_{TOA}(\hat{\mathbf{x}}^k)\right)\mathbf{C}^{-1}_{TOA}\left(\mathbf{r}_{TOA}-\mathbf{f}_{TOA}(\hat{\mathbf{x}}^k)\right), \tag{3.18}$$

where $\mathbf{G}\left(\mathbf{f}_{TOA}(\hat{\mathbf{x}}^k)\right)$ is a Jacobian matrix of $\mathbf{f}_{TOA}(\hat{\mathbf{x}})$ which is updated at every k^{th} iteration and can be expressed as:

$$\begin{aligned}\mathbf{G}\left(\mathbf{f}_{TOA}(\hat{\mathbf{x}}^k)\right) &= \begin{bmatrix} \frac{\partial d_1}{\partial x} & \frac{\partial d_1}{\partial y} \\ \frac{\partial d_2}{\partial x} & \frac{\partial d_2}{\partial y} \\ \vdots & \vdots \\ \frac{\partial d_N}{\partial x} & \frac{\partial d_N}{\partial y} \end{bmatrix} \\ &= \begin{bmatrix} \frac{x-x_1}{d_1} & \frac{y-y_1}{d_1} \\ \frac{x-x_2}{d_2} & \frac{y-y_2}{d_2} \\ \vdots & \vdots \\ \frac{x-x_N}{d_N} & \frac{y-y_N}{d_N} \end{bmatrix}. \end{aligned} \tag{3.19}$$

The third iterative numerical method is the steepest descent method:

$$\hat{\mathbf{x}}^{k+1} = \hat{\mathbf{x}}^k - \mu\nabla\left(J_{ML-TOA}(\hat{\mathbf{x}}^k)\right), \tag{3.20}$$

where μ is a factor controlling the stability and convergence rate of the algorithm.

In order to indicate sufficient convergence after k iterations, the required stopping criterion must satisfy the following condition:

$$||\hat{\mathbf{x}}^{k+1} - \hat{\mathbf{x}}^{k}|| < \kappa, \tag{3.21}$$

where κ is a positive small constant.

3.1.2 Least Squares Estimation

According to parametric estimation theory, a suitable estimator satisfies two key conditions, viz. it has to be unbiased and have a minimum variance. An unbiased estimator refers to a type of estimator where the mean value approaches the true value of the parameter to be estimated. The motivation behind parameter estimation is to inherently minimise the error between the estimator and actual/true parameter value. The least squares (LS) principle involves minimising the squared difference between the estimated or given data and the true data set.

This concept can be further elaborated through a basic example relating to signal theory, which is illustrated in Figure 3.1. Let θ characterise an unidentified parameter to be estimated, which forms part of a generated signal model $y[n]$. Consider that $y[n]$ is a deterministic signal and the corrupted version of $y[n]$, denoted by $w[n]$, is observed as a result of factors such as model discrepancies and system noise. Unlike MLE, there is no a priori information on the probability distribution characteristics of $w[n]$. A parameter value is computed using LS estimation, which ascertains the degree of similarity between the signal $y[n]$ and the observed data $w[n]$.

This degree of similarity (closeness) of the data sets is defined by the following least square error criterion:

$$L(\theta) = \sum_{n=0}^{N-1} (w[n] - y[n])^2, \tag{3.22}$$

where the observation interval ranges from $n = 0, 1, 2, ..., N-1$. The value of θ that minimises $L(\theta)$ is defined as the least squares estimate [50].

The NLS cost function to be minimised is represented as:

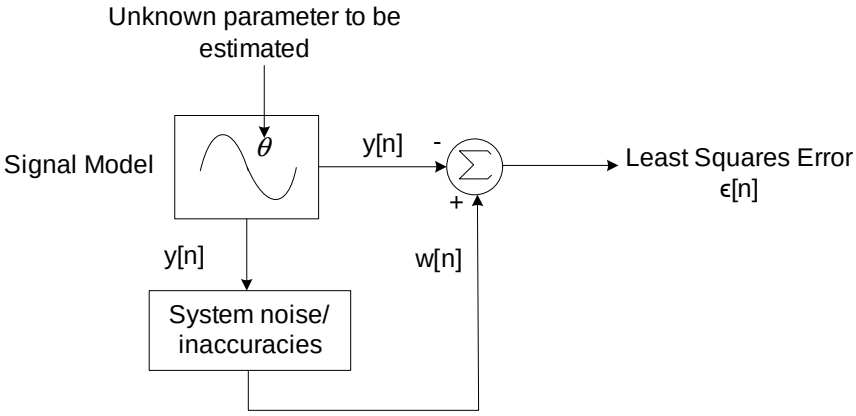

Figure 3.1: Least squares estimation

$$J_{NLS-TOA}(\tilde{\mathbf{x}}) = \sum_{i=1}^{N} \left(r_{TOA,i} - \sqrt{(\tilde{x}-x_i)^2 + (\tilde{y}-y_i)^2} \right)^2, \tag{3.23}$$

which alternatively can be represented in vector form as:

$$J_{NLS-TOA}(\tilde{\mathbf{x}}) = \left(\mathbf{r}_{TOA} - \mathbf{f}_{TOA}(\tilde{\mathbf{x}})\right)^T \left(\mathbf{r}_{TOA} - \mathbf{f}_{TOA}(\tilde{\mathbf{x}})\right). \tag{3.24}$$

The NLS estimate is equivalent to the smallest value of $J_{NLS-TOA}(\tilde{\mathbf{x}})$:

$$\hat{\mathbf{x}} = \arg\min_{\tilde{\mathbf{x}}} J_{NLS-TOA}(\tilde{\mathbf{x}}). \tag{3.25}$$

As with the MLE, numerical methods are also used to compute $\hat{\mathbf{x}}$. The Newton-Raphson expression for solving eq. (3.25) is given as:

$$\hat{\mathbf{x}}^{k+1} = \hat{\mathbf{x}}^k - \mathbf{H}^{-1}(J_{NLS-TOA}(\hat{\mathbf{x}}^k))\nabla(J_{NLS-TOA}(\hat{\mathbf{x}}^k)), \tag{3.26}$$

where similar to eq. (3.12), $\mathbf{H}(J_{NLS-TOA}(\mathbf{x}))$ and $\nabla(J_{NLS-TOA}(\mathbf{x}))$ represent the Hessian matrix and gradient vector respectively. The matrix is of the same form as shown in eq. (3.13). Hence the Hessian matrix elements are shown as:

$$\frac{\partial^2\left(J_{NLS-TOA}(\mathbf{x})\right)}{\partial x^2} = \sum_{i=1}^{N} 2\left(\frac{(x-x_i)^2}{(x-x_i)^2+(y-y_i)^2} - \frac{\left(r_{TOA,i}-d_i\right)(y-y_i)^2}{\left[(x-x_i)^2+(y-y_i)^2\right]^{3/2}}\right) \tag{3.27}$$

$$\frac{\partial^2\left(J_{NLS-TOA}(\mathbf{x})\right)}{\partial x\partial y} = \frac{\partial^2\left(J_{NLS-TOA}(\mathbf{x})\right)}{\partial y\partial x} = \sum_{i=1}^{N} \frac{2r_{TOA,i}(x-x_i)(y-y_i)}{\left[(x-x_i)^2+(y-y_i)^2\right]^{3/2}} \tag{3.28}$$

$$\frac{\partial^2\left(J_{NLS-TOA}(\mathbf{x})\right)}{\partial y^2} = \sum_{i=1}^{N} 2\left(\frac{(y-y_i)^2}{(x-x_i)^2+(y-y_i)^2} - \frac{\left(r_{TOA,i}-d_i\right)(x-x_i)^2}{\left[(x-x_i)^2+(y-y_i)^2\right]^{3/2}}\right) \tag{3.29}$$

where d_i is the distance between the MT (target node) and BS (anchor node) as expressed in eq. (2.2). The gradient vector is shown as:

$$\nabla\left(J_{NLS-TOA}(\mathbf{x})\right) = -2\begin{bmatrix} \sum_{i=1}^{N} \frac{\left(r_{TOA,i}-d_i\right)(x-x_i)}{d_i} \\ \sum_{i=1}^{N} \frac{\left(r_{TOA,i}-d_i\right)(y-y_i)}{d_i} \end{bmatrix}. \tag{3.30}$$

The Gauss-Newton technique for the NLS estimation technique is similar to the MLE technique as shown in eq. (3.18). The expression for the steepest descent method is given as:

$$\hat{\mathbf{x}}^{k+1} = \hat{\mathbf{x}}^{k} - \mu\nabla\left(J_{NLS-TOA}(\hat{\mathbf{x}}^{k})\right), \tag{3.31}$$

where μ indicates the convergence rate.

3.2 LINEAR TECHNIQUES

These particular techniques aim to linearise eq. (3.3) into a defined set of linear equations that can be represented as:

$$\mathbf{k} = \mathbf{A}\mathbf{x} + \mathbf{B} + \mathbf{q}, \tag{3.32}$$

where information about **k** and **A** are known a priori and **B** and **q** are the transformation of the NLOS and noise vector respectively. The following linear error function can be derived [19]:

$$\mathbf{e}_{lin} = \mathbf{k} - \mathbf{A}\tilde{\mathbf{x}}. \tag{3.33}$$

3.2.1 Linear Least Squares

The linear least squares (LLS) technique aims to initially transform the TOA model based on eq. (2.11) into a linear equation in order to solve for **x** and thereafter the MT's position is estimated using the conventional LS approach as described in Section 3.1.2. The linear algorithm involves the addition of an intermediate variable, which is a function of the target node's position. Expanding on eq. (2.11), the following expression is obtained [19, 47, 51, 52]:

$$r_{TOA,i} = \sqrt{(x-x_i)^2 + (y-y_i)^2} + j_{TOA,i}. \tag{3.34}$$

The first step involves the squaring of eq. (3.34) on both sides as follows:

$$r_{TOA,i}^2 = (x-x_i)^2 + (y-y_i)^2 + 2j_{TOA,i}\sqrt{(x-x_i)^2 + (y-y_i)^2} + j_{TOA,i}^2. \tag{3.35}$$

Let the range (intermediate) variable be given as: $R = \sqrt{x^2+y^2}$. After some algebraic manipulation of eq. (3.35):

$$xx_i + yy_i - \frac{1}{2}R^2 - z_{noise} = \frac{1}{2}\left(x_i^2 + y_i^2 - r_{TOA,i}^2\right), \quad i = 1,2,...,N \tag{3.36}$$

where $z_{noise} = 2j_{TOA,i}\sqrt{(x-x_i)^2 + (y-y_i)^2} + j_{TOA,i}^2$ which represents the noise component of eq. (3.35). Eq. (3.36) can now be expressed in the following linear standard form:

$$\mathbf{A}\boldsymbol{\theta} + \mathbf{q} = \mathbf{b}, \tag{3.37}$$

where:

$$\mathbf{A} = \begin{bmatrix} x_1 & y_1 & -\frac{1}{2} \\ x_2 & x_2 & -\frac{1}{2} \\ \vdots & \vdots & \vdots \\ x_N & y_N & -\frac{1}{2} \end{bmatrix}, \tag{3.38}$$

and:

$$\mathbf{b} = \frac{1}{2} \begin{bmatrix} x_1^2 + y_1^2 - r_{TOA,1}^2 \\ x_2^2 + y_2^2 - r_{TOA,2}^2 \\ \vdots \\ x_N^2 + y_N^2 - r_{TOA,N}^2 \end{bmatrix}, \tag{3.39}$$

while:

$$\mathbf{q} = \begin{bmatrix} -2j_{TOA,1}\sqrt{(x-x_1)^2 + (y-y_1)^2} - j_{TOA,1}^2 \\ -2j_{TOA,2}\sqrt{(x-x_2)^2 + (y-y_2)^2} - j_{TOA,2}^2 \\ \vdots \\ -2j_{TOA,N}\sqrt{(x-x_N)^2 + (y-y_N)^2} - j_{TOA,N}^2 \end{bmatrix}, \tag{3.40}$$

and:

$$\boldsymbol{\theta} = \begin{bmatrix} x \\ y \\ R^2 \end{bmatrix}. \tag{3.41}$$

Assuming that $\mathbf{q}$ is a noise process with an approximated zero mean, eq. (3.37) can be simply written as:

$$\mathbf{A}\boldsymbol{\theta} \approx \mathbf{b}. \tag{3.42}$$

Similar to eq. (3.25), the estimated position vector ($\hat{\boldsymbol{\theta}}$) can be computed using the conventional LS method, which utilises the cost function defined by $J_{LLS-TOA}(\tilde{\boldsymbol{\theta}})$:

$$\hat{\boldsymbol{\theta}} = \arg\min_{\tilde{\theta}} J_{LLS-TOA}(\tilde{\boldsymbol{\theta}}), \tag{3.43}$$

where $\tilde{\boldsymbol{\theta}}$ represents an optimisation vector and the corresponding cost function is derived using eq. (3.42):

$$J_{LLS-TOA}(\tilde{\boldsymbol{\theta}}) = \left(\mathbf{A}\tilde{\boldsymbol{\theta}} - \mathbf{b}\right)^T \left(\mathbf{A}\tilde{\boldsymbol{\theta}} - \mathbf{b}\right). \tag{3.44}$$

As a result eq. (3.43) can be determined by differentiating eq. (3.44) with respect to $\tilde{\boldsymbol{\theta}}$ while setting the expression to zero, as follows:

$$\frac{\partial J_{LLS-TOA}(\tilde{\boldsymbol{\theta}})}{\partial \tilde{\boldsymbol{\theta}}}|_{\tilde{\boldsymbol{\theta}}=\boldsymbol{\theta}} = \mathbf{0}, \tag{3.45}$$

and leads to:

$$\hat{\boldsymbol{\theta}} = \left(\mathbf{A}^T\mathbf{A}\right)^{-1}\mathbf{A}^T\mathbf{b}, \tag{3.46}$$

which represents the LLS estimate.

3.2.2 Two-step Maximum-likelihood

The estimation performance of the LLS approach hinges on whether the noise in eq. (3.37) is an independent identically distributed (iid) random process. A technique in literature [53] shows that the addition of a symmetric weighted matrix can provide increased positioning

accuracy. The TSML technique and the weighted LLS (WLLS) algorithm share a similar approach with the inclusion of the weighted matrix. As a result the cost function found in eq. (3.44) can be slightly modified as follows [47, 50]:

$$J_{TSML-TOA}(\tilde{\boldsymbol{\theta}}) = \left(\mathbf{A}\tilde{\boldsymbol{\theta}} - \mathbf{b}\right)^T \boldsymbol{\Psi}^{-1} \left(\mathbf{A}\tilde{\boldsymbol{\theta}} - \mathbf{b}\right), \tag{3.47}$$

where $\boldsymbol{\Psi}$ represents the weighted matrix. It can be shown that the weighted matrix is equivalent to the covariance of the noise vector denoted by:

$$\begin{aligned} \boldsymbol{\Psi} &= E[\mathbf{j}_{TOA}\mathbf{j}_{TOA}] \\ &= diag\left\{4\sigma_{TOA,1}^2 d_1^2, 4\sigma_{TOA,2}^2 d_2^2, ..., 4\sigma_{TOA,N}^2 d_N^2\right\}. \end{aligned} \tag{3.48}$$

The distances (d_i) in eq. (3.48) are unknown and therefore a more viable approach to the solution would be to use $r_{TOA,i}$ (eq. (2.11)), which is sufficient for an initial solution with a small error requirement.

In a similar fashion to the LLS estimate, the TSML estimate is determined using the following expression:

$$\hat{\boldsymbol{\theta}} = \arg\min_{\tilde{\theta}} J_{TSML-TOA}(\tilde{\boldsymbol{\theta}}), \tag{3.49}$$

where differentiating with respect to $\tilde{\boldsymbol{\theta}}$ will yield the global minima. As a result the TSML estimate can be determined using:

$$\frac{\partial J_{TSML-TOA}(\tilde{\boldsymbol{\theta}})}{\partial \tilde{\boldsymbol{\theta}}}|_{\tilde{\boldsymbol{\theta}}=\boldsymbol{\theta}} = \mathbf{0}, \tag{3.50}$$

which leads to the resulting TSML estimate:

$$\hat{\boldsymbol{\theta}} = \left(\mathbf{A}^T\mathbf{A}\boldsymbol{\Psi}^{-1}\right)^{-1}\mathbf{A}^T\mathbf{b}\boldsymbol{\Psi}^{-1}. \tag{3.51}$$

3.3 ALGORITHM EVALUATION

The performances of the non-linear and linear algorithmic techniques are investigated in terms of complexity and accuracy.

3.3.1 Maximum-likelihood

Four base stations within a 100×100 grid were chosen to estimate the position of the MT. The MT's 2D position co-ordinates were chosen to be fixed at $\mathbf{x} = \begin{bmatrix} 20 & 20 \end{bmatrix}^T$ while the SNR was set constant at 15 dB. In the case of the steepest-descent technique, the stability factor (μ) was set to 0.5. Figures 3.2 and 3.3 represent the convergence rate of the x and y coordinates respectively, using the three iterative numerical techniques discussed in Section 3.1.1. According to both the aforementioned plots, the Gauss-Newton and Newton-Raphson techniques display similar convergence at around two iterations, while the steepest descent method takes 20 iterations to converge to the final position estimate.

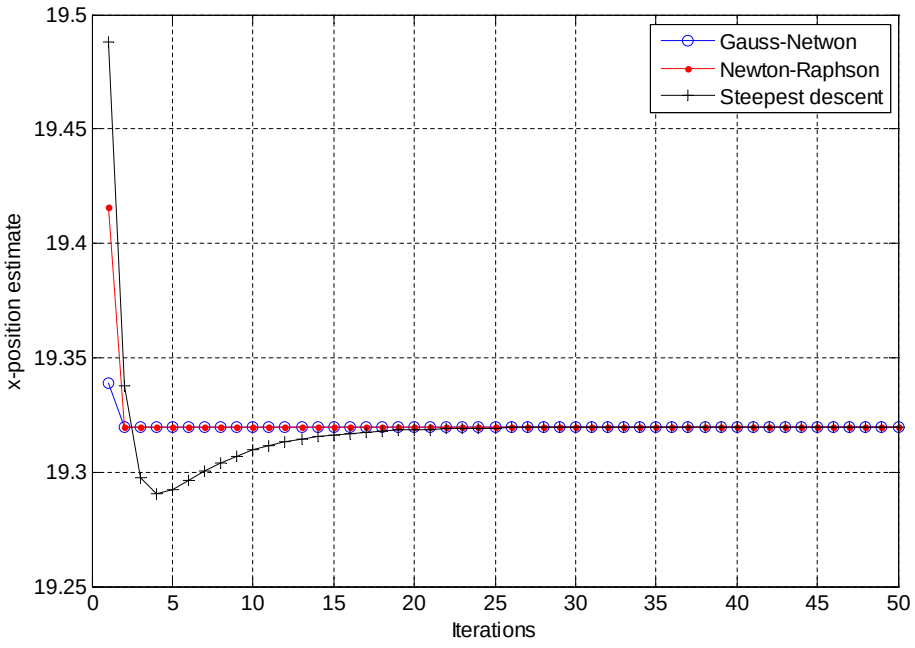

Figure 3.2: ML convergence rate of position estimate x

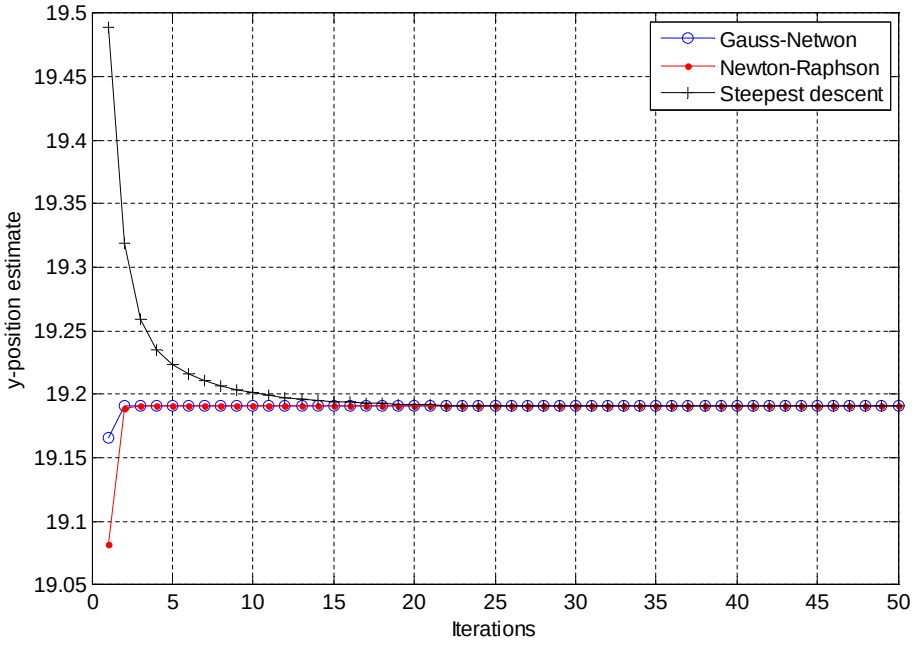

Figure 3.3: ML convergence rate of position estimate y

3.3.2 Non-linear Least Squares

The same scenario in Section 3.3.1 was simulated for the Non-linear least squares (NLS) technique. Figure 3.4 shows the number of iterations required for the estimated x-coordinate of the MT to converge for the three investigated numerical methods using the NLS estimation algorithm. Similarly, Figure 3.5 also illustrates the same principle for the y-coordinate of the MT using NLS estimation. As in the case of the ML technique, the Gauss-Newton and Newton-Raphson numerical methods converge comparatively faster than the steepest-descent technique. However, the ML estimation technique tends to converge faster than the NLS algorithm due to the inclusion of the noise covariance vector ($\mathbf{C}_{TOA}$).

3.3.3 Positioning Accuracy

The accuracy of the non-linear and linear estimation algorithms was analysed in terms of the root mean square error (RMSE) of the position estimates over a defined signal-to-noise (SNR) range. This particular RMSE is characterised by the following equation:

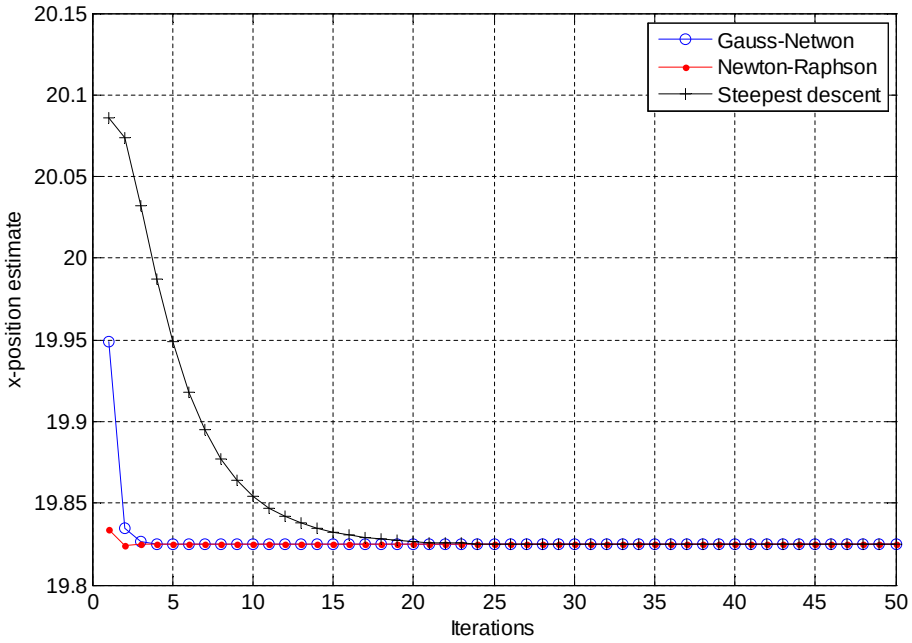

Figure 3.4: NLS convergence rate of position estimate x

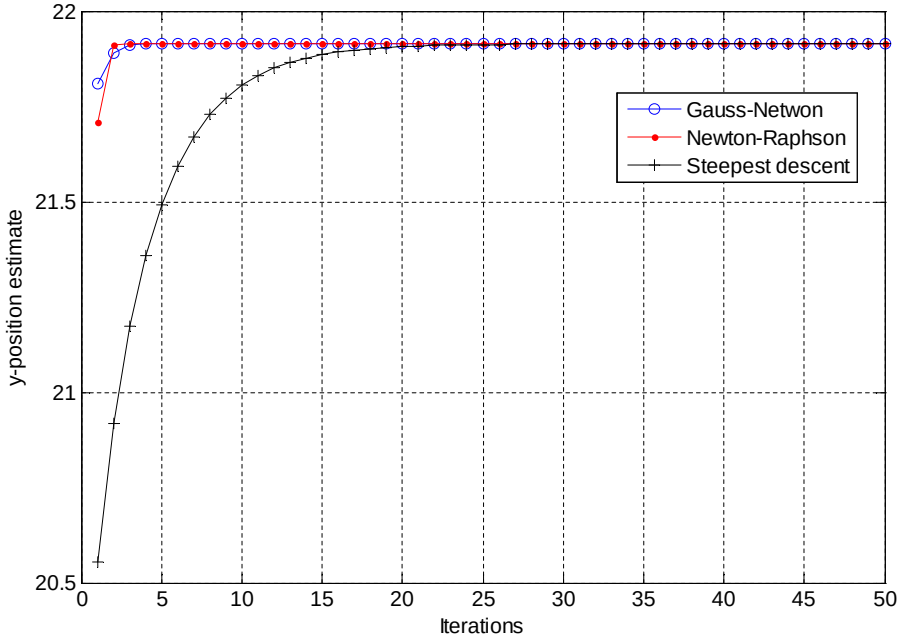

Figure 3.5: NLS convergence rate of position estimate y

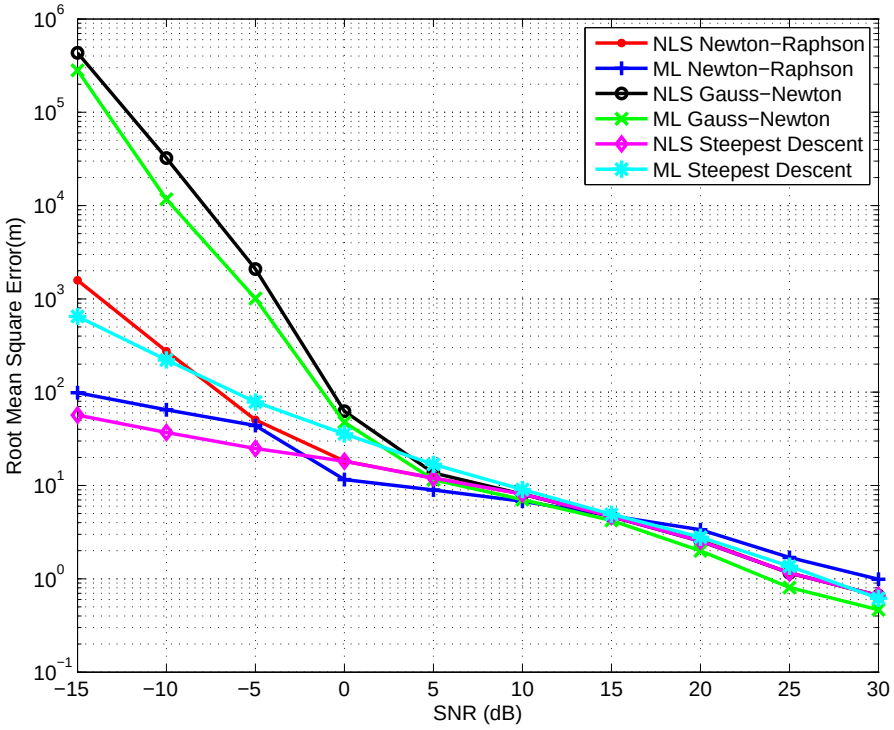

Figure 3.6: SNR performance of the non-linear algorithms

$$RMSE = \sqrt{\frac{\sum_{n=1}^{N}\left[(\hat{x}_n - x)^2 + (\hat{y}_n - y)^2\right]}{N}}, \tag{3.52}$$

where N represents the number of samples and $\begin{bmatrix} \hat{x}_n & \hat{y}_n \end{bmatrix}^T$ is the iterative position estimate according to n samples. Figure 3.6 illustrates the performance of the Newton-Raphson (NR), Gauss-Newton (GN) and steepest-descent (SD) numerical methods for the two non-linear algorithms, NLS and ML. In this particular scenario 3 iterations were sufficient for the NR and GN methods to achieve convergence, while 20 iterations were required to achieve convergence with the SD method. The GN method, however, performs poorly at lower SNRs which may be due to the rough initial estimates of the Jacobian matrix. The GN estimates gradually improve with an increase in SNR. The NR and SD perform comparably at lower SNRs, while at higher SNRs the accuracy improves. Figure 3.7 illustrates the positional accuracy between the LLS and TSML. According to Figure 3.7, the TSML

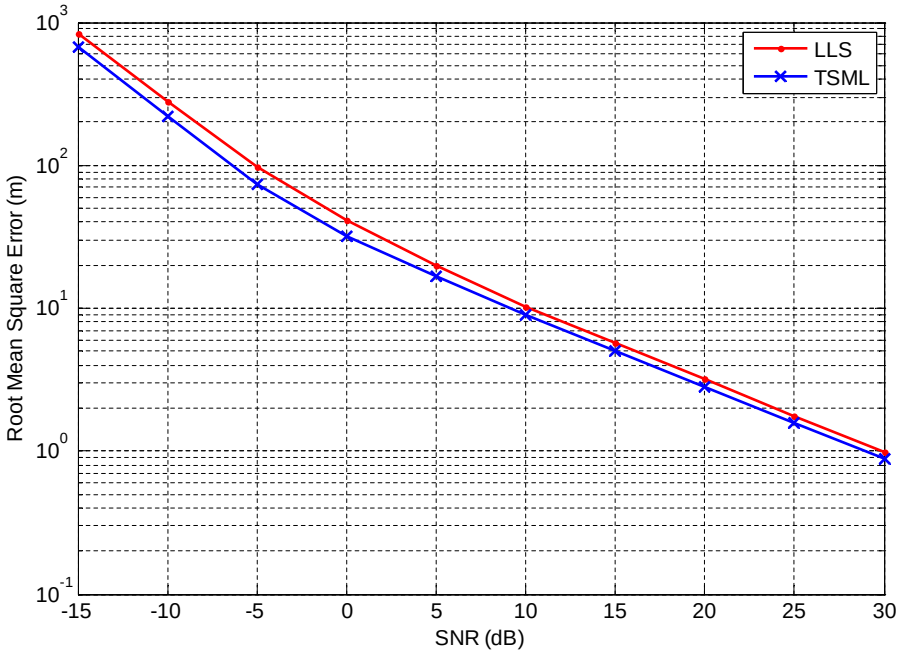

Figure 3.7: SNR performance of the linear estimation algorithms

location estimation technique slightly outperforms the LLS technique, by displaying a lower RMSE.

It can be noted that the SD convergence rate for the ML and NLS techniques are quite slow when compared to the NR and GN methods. The is due to the selection of a small μ which ensures algorithm stability. A large μ increases the convergence rate but causes the SD algorithm to be highly unstable. The linear estimation techniques exhibit less variation in RMSE at lower SNRs when compared to the non-linear estimation algorithms.

3.4 CRAMER-RAO LOWER BOUND

Positioning algorithms such as TOA are based on fundamental principles in signal and parameter estimation theory. The basic problem involves estimating certain values (which in this case, is the signal time delay) given a set of parameters. In most systems this involves the extraction of parameter values from continuous-time waveforms such as in the case of TOA, where the parameter values have to be extracted from the received waveform. Assessing an

estimator's performance is critical in achieving the best accuracy with respect to the actual value that is being estimated, which in this particular application is the target's location as well as range accuracy. Using an unbiased estimator is the primary way of performing optimal parameter estimation, since the mean value of the estimator will yield the actual value of the unknown parameter. It can be represented mathematically as follows [50]:

$$E\left[\hat{\theta}\right] = \theta, \qquad for \quad a < \theta < b \tag{3.53}$$

where $\hat{\theta}$ represents the estimator, θ represents the true value and (a,b) is the range of possible values of θ. An optimal unbiased estimator that exhibits the least variability is referred to as the minimum variance unbiased (MVU) estimator. The following methods are used to compute the MVU estimator under certain conditions [50]:

- Application of the CRLB principle and ascertaining whether the estimator satisfies these bounds.
- Application of the Rao-Blackewell-Lehmann-Scheffe theorem and using sufficient statistics to determine the MVU estimator.
- Restricting the class of estimators to being unbiased as well linear and thereafter determining the MVU estimator within this predefined set.

The basic principle behind the CRLB is that the variance of any unbiased estimator must be greater or equal to a given quantity. This given quantity is usually referred to as the Fisher information (I_θ) for estimating θ from Y. The information inequality can be represented as follows:

$$Var_\theta[\hat{\theta}(Y)] \geq \frac{\left[\frac{\partial}{\partial\theta}E_\theta\left\{\hat{\theta}(Y)\right\}\right]^2}{I_\theta}. \tag{3.54}$$

The information equality is directly dependent on the information measure of a specific model and as a result a higher information measure provides a lower bound on the estimation

accuracy. Since the estimator is unbiased and following from eq. (3.53), the information equality reduces to:

$$Var_{\theta}[\hat{\theta}(Y)] \geq \frac{1}{I_{\theta}}, \tag{3.55}$$

which represents the CRLB [49].

3.5 NLOS EFFECT ON USER POSITIONING

Time-based and AOA localisation techniques are susceptible to errors, which include the negative effects of NLOS signal components. LOS and NLOS identification has usually been applied to mitigate the errors resulting from the ranging acquisition process between the transmitter and receiver, as well as in various location-based tracking algorithms [40]. Figure 3.8 is a basic illustration of a NLOS scenario. It can be observed that the reflected and obstructed signals can cause inaccuracies relating to the position estimate of a mobile user.

During a typical ranging process, it is usually possible to identify and disregard the NLOS measurements, thus only exploiting LOS measurements. A less complex and computationally inexpensive LOS and NLOS identification technique has been proposed which specifically caters to the requirements of CR systems with the objective of increasing performance as quickly and as accurately as possible. This method is based on the premise that the LOS component of the initial signal path has a much higher correlation in comparison to other NLOS paths [54]. One of the first techniques that has been extensively employed to characterise LOS and NLOS components, is the binary hypothesis test. This method utilises a decision theoretic framework, as well as certain input parameters, such as ranging measurements and TOA data, to construct suitable pdfs of the amplitudes of various multipath components [55, 56]. Let H_0 and H_1 represent a LOS output and NLOS output respectively. The following conditional pdfs are then defined on observations that are completely arbitrary: $f(.|H_0)$ and $f(.|H_1)$. A threshold (δ) is defined and compared with the likelihood ratio given by:

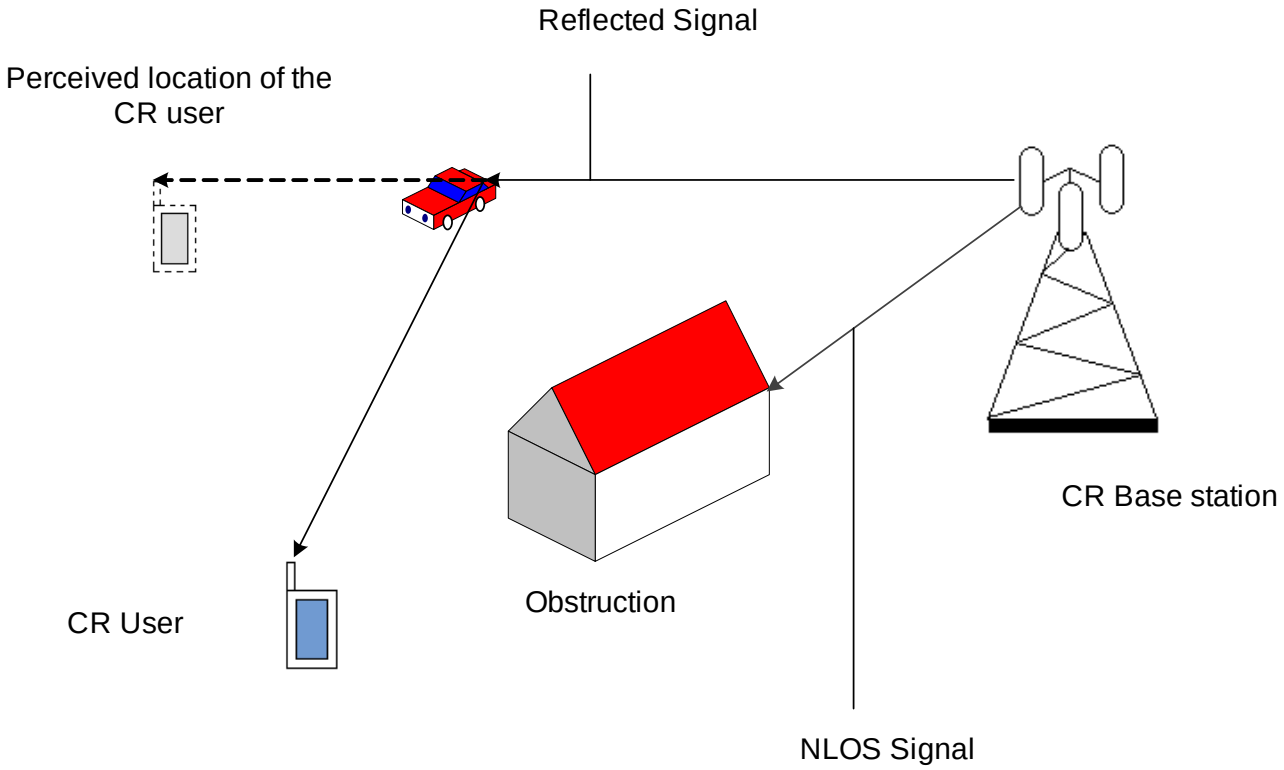

Figure 3.8: Simplified NLOS scenario

$$L_{ratio} = \frac{f(.|H_0)}{f(.|H_1)} = \begin{cases} H_0 & when \quad L_{ratio} < \delta \\ H_1 & when \quad L_{ratio} > \delta \end{cases}. \tag{3.56}$$

However, the drawback of this method is its computational complexity. A NLOS identification technique using statistical decision theory has also been proposed for mobile positioning using the Neyman-Pearson theorem, which implements a combination of the AOA principle, a TOA-based method and RSS data [57].

It is also possible to exploit various NLOS measurements to improve localisation accuracy. For example, one NLOS classification algorithm seeks to take advantage of the NLOS propagation path characteristics rather than mitigate the errors resulting from them. The technique is a geometrically-based solution ascertaining the location of the mobile user and the performance is evaluated using the CRLB [58]. Received signal statistics and scattering-based models have also been used to identify the NLOS condition of transmitted

signals in UWB systems and wireless environments respectively [59, 60].

Three main NLOS identification techniques can be identified with respect to single anchor node position estimation [19]:

- Use of TOA statistical information to identify a NLOS signal component. The general TOA error is characterised by a Gaussian distribution, which is also the LOS component. The NLOS signal component can be added to the model as a positive bias and displays a pdf that is non-Gaussian.

- Parameter extraction of the power delay profile, e.g. delay spread, Rician K-factor.

- Hybrid ranging approaches that involve the utilisation of TOA statistics, path-loss information derived from the RSS as well as direction information from the AOA technique [57].

In the case of narrowband and wideband systems, NLOS identification is applied using the first aforementioned technique. The received power envelope distribution is utilised to identify the status of the signal component. The NLOS component is therefore Rayleigh-distributed while the LOS component follows a Rician distribution, since the initial arriving path has the strongest signal component [57, 61].

It can be noted that various LOS or NLOS identification techniques have been developed in literature with the objective of computing the location of a mobile user. In order to realise environmental and location awareness for CR, current positioning algorithms require an additional cognitive capability and this includes the ability to accurately distinguish between LOS and NLOS signals and thereafter adapt accordingly without degrading positioning accuracy, depending on the type of environment. The effects of LOS and NLOS have yet to be investigated with regard to bandwidth efficiency in CPSs. Therefore a bandwidth efficient CPS is investigated and its performance studied under LOS and NLOS conditions.

CHAPTER 4

A BANDWIDTH EFFICIENT COGNITIVE POSITIONING SYSTEM

The CPS concept draws its inspiration from nature, where location and environmental awareness are embedded biological features in certain animal species. Dolphins and bats are well known examples of species that rely on echo location to traverse their natural environment and to hunt prey. Echolocation has evolved as the primary sensory mechanism for these animals. Dolphins possess the capability to track long-range targets through a series of emitted clicks, as well as perform object recognition and tracking. Adaptation of echolocating signal parameters such as interclick intervals, frequency content and source level modulation are key biological characteristics in dolphins. The required adaptation feature is based on the type of echolocation scenario, distance to the target and any interference that may occur, such as clutter in the environment and any background noise [62, 63]. Studies have also shown that echolocation and adaptation play a vital role in bats, especially with regard to navigation and foraging [64, 65]. Bats share many of the aforementioned adaptation features with dolphins. Bats also possess the ability to perform adaptive acoustic interference management in the presence of other bats by offsetting the timing between pulse transmissions [66].

It is envisioned that many of the adaptive capabilities of dolphins and bats can be applied to CR to enable location and environmental awareness. These may include aspects such as adaptive waveform generation, software adaptable networks, location and environ-

ment adaptation, adaptable transmit power, multiple access and cross-layer adaptation [15]. In the context of location awareness, there are numerous types of antenna-based ranging techniques (RSS, AOA, hybrid schemes, etc.) which have been developed to improve localisation accuracy for a variety of positioning systems. These techniques have tradeoffs in terms of accuracy, complexity and environmental application. A key feature, which is absent in existing positioning systems, is the ability to adapt according to the positional accuracy or usage environment. A notable example is GPS, where the accuracy significantly degrades in indoor environments. The CPS proposed in [45, 67] serves to deal with the issue of adaptivity in positioning systems.

This chapter provides an overview of the CPS and then focuses on the derivation of the CRLB for a spectrally efficient bandwidth determination (BD) model for the CPS using multiple receive antennas. The end goal is to improve the bandwidth utilisation in a LOS and NLOS scenario by comparing the performance with the existing single-input-single-output (SISO) model. A look into the role of the EDSM component of the CPS is also presented.

4.1 COGNITIVE POSITIONING SYSTEM

In order to achieve adaptivity with regard to positioning in CR, at least one of the ranging signal parameters should be independent of channel effects. For example, the accuracy of the RSS ranging technique is dependent on the log-distance model, which in turn is dependent on the path-loss factor and as a result the CR device cannot adaptively control these parameters to improve positional accuracy. In the case of time-based localisation schemes such as TOA and TDOA, adjusting the bandwidth of the ranging signal can have a significant influence on the positional accuracy. The CPS exploits this characteristic to achieve adaptive positioning.

According to Figure 4.1, the CPS consists of two key interdependent phases, viz. the bandwidth determination (BD) mode and enhanced dynamic spectrum management (EDSM) mode [45]. The BD mode, as the name suggests, ascertains the amount of bandwidth required to perform TOA estimation using CRLB derivations. This bandwidth is calculated

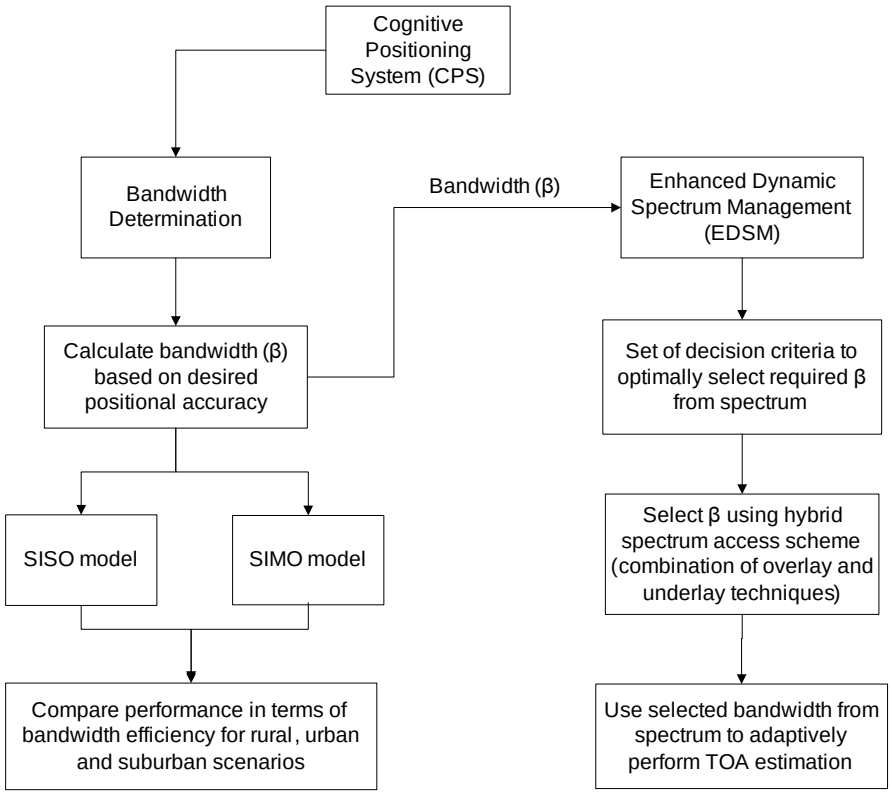

Figure 4.1: Overall CPS model

according to the required positional accuracy. The existing BD mode makes use of a SISO model, which is currently bandwidth-inefficient, and therefore the proposed SIMO model aims to improve this bandwidth efficiency. Furthermore, the performance of this SIMO model is analysed under different LOS and NLOS scenarios. Once the required bandwidth has been computed, the EDSM mode checks whether the actual bandwidth is physically available from the spectrum. This is achieved using a combination of overlay and underlay spectrum access techniques to select the best approximate bandwidth to perform TOA estimation of a CR user.

4.2 BANDWIDTH DETERMINATION MODEL

Adaptive time-of-arrival (A-TOA) is a relatively new concept, which has been developed specifically to address the needs of CR and therefore has been implemented in the CPS model [45]. The BD mode essentially involves the derivation of a CRLB for a received

single-path AWGN signal and thereafter the development of a mathematical relationship between the estimated amount of required bandwidth and the positional accuracy.

4.2.1 Bandwidth Determination: SISO Model

The existing CPS utilises UWB as the main signal for positioning in order to exploit its high bandwidth resolution. However, the main drawback would be the range, as UWB is only effective over short distances. The following UWB pulse signal was transmitted over a single path AWGN channel in the model described in [45]:

$$s(t) = \sqrt{\varepsilon}\sum_{k} p(t - kT_s), \tag{4.1}$$

where $p(t)$ describes a single pulse, T_s is the symbol duration and ε is symbol energy. The received baseband signal ($r(t)$), which is processed at the receiver end, is given by:

$$r(t) = \alpha s(t - \tau) + n(t), \tag{4.2}$$

where the channel coefficient (α) is assumed to be unity, $s(t)$ is a generalised transmitted signal which can be given by eq. (4.1) and τ represents the signal path delay. After performing some mathematical manipulations, the bandwidth determination equation was found to be [45]:

$$\beta = \sqrt{\frac{c^2 P(\hat{d})}{G\gamma_s|\alpha|}} \tag{4.3}$$

where $c = 3 \times 10^8\, m/s$ and represents the speed of the electromagnetic wave (speed of light), G represents the number of transmitted symbols, while the positional accuracy ($P(\hat{d})$) can be described in terms of the variance of the distance estimate ($var(\hat{d})$):

$$P(\hat{d}) = \frac{1}{var(\hat{d})}. \tag{4.4}$$

The SNR is given by:

$$\gamma_s = \frac{\varepsilon}{N_o}. \tag{4.5}$$

4.2.2 Bandwidth Determination: SIMO Model

The advantages of multiple antenna techniques have been realised in wireless communications and it will be shown that similar techniques can improve the spectrum efficiency of A-TOA algorithms and consequently less bandwidth would be required for a specific positional accuracy. The novelty of the proposed technique involves the utilisation of a SIMO model, which is then verified with two different location estimation algorithms to improve the spectrum efficiency of the CPS. In a similar fashion to eq. (4.2), let the SIMO baseband received signal be mathematically modelled as:

$$r_l(t) = \alpha_l s(t-\tau_o) + n_l(t), \qquad 0 \leq t \leq T \tag{4.6}$$

where every l^{th} antenna can range from $l = 1,...,N$, α_l is the complex channel coefficient, $s(t)$ represents the original transmitted signal, which for the purposes of this study is a general narrowband signal, τ_o is the path delay and $n(t)$ represents an AWGN process with a zero mean and power spectral density (PSD) of σ_l^2. It has been assumed that the signal delays (τ_o) for the different antennas are identical, since the first arriving signal has the strongest component for a single-path scenario. A 1×2 vector of signal parameters has to be estimated, which can be represented as $\theta = [\ \tau_o \quad (\alpha_1,...,\alpha_l)\ ]$. The channel coefficient forms part and parcel of the estimation problem, since it directly affects each received signal at each antenna. The assumption is also made that over the interval between 0 and T_s (symbol time), the $s(t)$ pulse is non-zero (and band-limited to f_B Hz). It is also assumed that a fixed number of symbols (G) are transmitted. As as result, the observation interval encompasses

the symbol time, number of symbols and maximum time delay. Therefore, it can be shown that:

$$T = GT_s + \tau_{o_{max}}. \tag{4.7}$$

The pdf of the AWGN noise variance of eq. (4.6) is given as follows:

$$\begin{aligned} p(r;\theta) &= \prod_{n=0}^{N-1} \frac{1}{\left(2\pi\sigma_l^2\right)^{\frac{1}{2}}} \exp\left(\sum_{l=1}^{N}\left[-\frac{1}{2\sigma^2}\left\{r_l(t)-\alpha_l s(t-\tau_o)\right\}^2\right]\right) \\ &= \frac{1}{\left(2\pi\sigma_l^2\right)^{\frac{N}{2}}} \exp\left(\sum_{l=1}^{N}\left[-\frac{1}{2\sigma^2}\sum_{n=0}^{t=T}\left\{r_l(t)-\alpha_l s(t-\tau_o)\right\}^2\right]\right) \end{aligned} \tag{4.8}$$

If the pdf given by eq. (4.8) is a function of one or more unknown parameters, it is referred to as the likelihood function. The curvature of the likelihood function ascertains the degree of estimation accuracy of the unknown parameter and is determined by the log-likelihood function, which is the negative of the second derivative of the natural logarithm of the likelihood function [48, 50]. Therefore, the log-likelihood function is given as:

$$\begin{aligned} \ln p(r;\theta) &= -\ln\left(2\pi\sigma_l^2\right)^{\frac{N}{2}} - \sum_{l=1}^{N}\frac{1}{2\sigma_l^2}\int_0^T \left(r_l(t)-\alpha_l s(t-\tau_o)\right)^2 dt \\ &= -\frac{N}{2}\ln\left(2\pi\sigma_l^2\right) - \sum_{l=1}^{N}\frac{1}{2\sigma_l^2}\int_0^T \left(r_l(t)-\alpha_l s(t-\tau_o)\right)^2 dt \\ &= -\frac{N}{2}\ln\left(2\pi\right) - \frac{N}{2}\ln\left(\sigma_l^2\right) - \sum_{l=1}^{N}\frac{1}{2\sigma_l^2}\int_0^T \left(r_l(t)-\alpha_l s(t-\tau_o)\right)^2 dt \\ &= A - \sum_{l=1}^{N}\frac{1}{2\sigma_l^2}\int_0^T \left(r_l(t)-\alpha_l s(t-\tau_o)\right)^2 dt, \end{aligned} \tag{4.9}$$

where A is given by:

$$A = -\frac{N}{2}\ln(2\pi) - \frac{N}{2}\ln(\sigma_l^2). \tag{4.10}$$

The CRLB of a vector of unknown parameters is given by the first row and first column of an inverse matrix and is represented as follows:

$$var(\hat{\theta}_i) \geq \left[\mathbf{I}^{-1}(\theta)\right]_{ii}, \tag{4.11}$$

where $\mathbf{I}(\theta)$ is a $p \times p$ Fisher Information Matrix (FIM) and p is defined by the number of unknown parameters to estimate. In this particular case, the elements of the 2×2 FIM are determined by taking the negative expectation of the second derivative of the log-likelihood function [50]:

$$[\mathbf{I}(\theta)]_{ij} = -E\left[\frac{\partial^2 \ln p(r;\theta)}{\partial\theta_i \partial\theta_j}\right]. \tag{4.12}$$

From observing eq. (4.9) and eq. (4.12), determining the Fisher information elements can be quite involved. However, a less complicated mathematical model for the general Gaussian case can be utilised to derive each of the Fisher information elements for the 2×2 case with a complex channel coefficient:

$$[\mathbf{I}(\theta)]_{ij} = \sum_{l=1}^{N} \frac{1}{\sigma_l^2} \sum_{k=0}^{K-1} \frac{\partial s[k;\theta]}{\partial\theta_i} \frac{\partial s[k;\theta]}{\partial\theta_j}, \tag{4.13}$$

where k represents a set of discrete points of a signal. The general form 2×2 FIM for this particular estimation problem is given as:

$$\mathbf{I}(\theta) = \begin{bmatrix} I_{\tau\tau} & \mathbf{I}_{\tau\boldsymbol{\alpha}} \\ \mathbf{I}_{\boldsymbol{\alpha}\tau} & \mathbf{I}_{\boldsymbol{\alpha}\boldsymbol{\alpha}} \end{bmatrix}. \tag{4.14}$$

The FIM elements are determined using eq. (4.13) (refer to Appendix A for full discrete signal derivation):

$$I_{\tau\tau} = \hat{\varepsilon} \sum_{l=1}^{N} \frac{|\alpha_l|^2}{\sigma_l^2 T_{samp}}, \tag{4.15}$$

$$\mathbf{I}_{\tau\boldsymbol{\alpha}} = \mathbf{I}_{\boldsymbol{\alpha}\tau} = -\tilde{\varepsilon}\left[\frac{|\alpha_1|}{T_{samp}\sigma_1^2},\ldots,\frac{|\alpha_l|}{T_{samp}\sigma_l^2}\right], \tag{4.16}$$

$$\mathbf{I}_{\boldsymbol{\alpha}\boldsymbol{\alpha}} = \frac{\varepsilon}{T_{samp}} \times diag\left[\frac{1}{\sigma_1^2},\ldots,\frac{1}{\sigma_N^2}\right], \tag{4.17}$$

where T_{samp} is the sampling period of the continuous waveform given in eq. (4.6) and the corresponding energy transformations are given by:

$$\hat{\varepsilon} = G\int_0^{T_s}\left|\frac{ds(t)}{dt}\right|^2 dt = \int_0^{T_s}\left|s'(t)\right|^2 dt, \tag{4.18}$$

$$\tilde{\varepsilon} = G\int_0^{T_s}\left|\frac{ds(t)}{dt}\right||s(t)|^2 dt, \tag{4.19}$$

$$\varepsilon = G\int_0^{T_s}|s(t)|^2 dt. \tag{4.20}$$

It can be noted that the Fisher elements $\mathbf{I}_{\tau\boldsymbol{\alpha}}$ and $\mathbf{I}_{\boldsymbol{\alpha}\tau}$ are $1\times N$ Hessian matrices, while $\mathbf{I}_{\boldsymbol{\alpha}\boldsymbol{\alpha}}$ is an $N\times N$ Hessian matrix where N is the number of receive antennas. The inverse elements of the FIM are equivalent to the variance on the time delay estimate and channel coefficients, which are respectively given as:

$$[I_{\tau\tau}]^{-1} = \left(\mathbf{I}_{\tau\tau} - \mathbf{I}_{\tau\boldsymbol{\alpha}}\mathbf{I}_{\boldsymbol{\alpha}\boldsymbol{\alpha}}^{-\mathbf{1}}\mathbf{I}_{\boldsymbol{\alpha}\tau}^{T}\right)^{-1}, \tag{4.21}$$

$$[\mathbf{I}_{\boldsymbol{\alpha}\boldsymbol{\alpha}}]^{-1} = \left(\mathbf{I}_{\boldsymbol{\alpha}\boldsymbol{\alpha}} - \mathbf{I}_{\boldsymbol{\alpha}\tau}\mathbf{I}_{\tau\tau}^{-\mathbf{1}}\mathbf{I}_{\tau\boldsymbol{\alpha}}^{T}\right)^{-1}, \tag{4.22}$$

Since a single time delay is estimated, $[I_{\tau\tau}]^{-1}$ is a scalar value. As a result, according to eq. (4.21):

$$[I_{\tau\tau}]^{-1} = \left(\hat{\varepsilon} - \frac{\tilde{\varepsilon}^2}{\varepsilon}\right) \sum_{l=1}^{N} \frac{|\alpha_l|^2}{T_{samp}\sigma_l^2}, \tag{4.23}$$

$$[\mathbf{I}_{\boldsymbol{\alpha\alpha}}]^{-1} = D_{i,j}\Big|_{\substack{i=1..N \\ j=1..N}}, \tag{4.24}$$

where $i = 1,...,N$ and $j = 1,...,N$ and $[\mathbf{I}^{-1}]_{\boldsymbol{\alpha\alpha}}$ is a $N \times N$ matrix containing elements $D_{i,j}$. It follows that eq. (4.24) can be expanded into:

$$D_{i,j} = \begin{cases} \dfrac{\varepsilon}{T_{samp}\sigma_i^2} - \dfrac{\tilde{\varepsilon}^2 \sum_{l=1}^{N} \frac{|\alpha_l|^2}{(\sigma_l^2)^2}}{\hat{\varepsilon} T_{samp} \sum_{l=1}^{N} \frac{|\alpha_l|^2}{\sigma_l^2}} & i = j \\ -\dfrac{\tilde{\varepsilon}^2 \sum_{l=1}^{N} \left(\frac{|\alpha_l|^2}{T_{samp}\sigma_l^2}\right)^2}{\hat{\varepsilon} T_{samp} \sum_{l=1}^{N} \frac{|\alpha_l|^2}{T_{samp}\sigma_l^2}} & i \neq j. \end{cases} \tag{4.25}$$

Therefore, from eq. (3.55) and assuming that the a priori information about the channel coefficients are known (i.e. $\tilde{\varepsilon} = 0$), the time delay and channel coefficient estimate can be respectively given as:

$$var(\hat{\tau}_o) = \frac{1}{\hat{\varepsilon} \sum_{l=1}^{N} \frac{|\alpha_l|^2}{T_{samp}\sigma_l^2}}, \tag{4.26}$$

$$var(\hat{\alpha}) = diag\{\frac{\varepsilon}{T_{samp}\sigma_1^2}, ..., \frac{\varepsilon}{T_{samp}\sigma_N^2}\}. \tag{4.27}$$

According to eq. (4.27), the variance on the channel coefficient estimate is essentially a diagonal matrix of received SNR values at each antenna branch. The variance on the time delay estimate ($var(\hat{\tau}_o)$) can be expressed in terms of the variance on the distance estimate ($var(\hat{d})$) and the electromagnetic wave speed (c):

$$var(\hat{\tau}_o) = \frac{var(\hat{d})}{c^2}, \tag{4.28}$$

where $\hat{d}$ is the distance estimate while $c = 3 \times 10^8 m/s$. Using eq. (4.26) and eq. (4.28), the variance on the distance can be expressed as:

$$var(\hat{d}) = \frac{c^2}{\hat{\varepsilon} \sum_{l=1}^{N} \frac{|\alpha_l|^2}{T_{samp}\sigma_l^2}}, \tag{4.29}$$

then assuming a constant noise spectral density across all N receive branches,

$$\sigma_l^2 = \sigma^2, \tag{4.30}$$

and according to the PSD of white Gaussian noise band-limited to f_B Hz:

$$\sigma^2 = N_o f_B, \tag{4.31}$$

and utilising the sampling period (T_{samp}):

$$T_{samp} = \frac{1}{2f_B}, \tag{4.32}$$

Eq. (4.29) can be re-written as:

$$var(\hat{d}) = \frac{c^2}{\hat{\varepsilon} \sum_{l=1}^{N} \frac{|\alpha_l|^2}{\frac{N_0}{2}}}. \tag{4.33}$$

The energy of a signal is given by eq. (4.20). The bandwidth of a signal in the time domain can be represented as:

$$\beta^2 = \frac{\hat{\varepsilon}}{\varepsilon}. \tag{4.34}$$

Transforming the time domain signal bandwidth representation in eq. (4.34) into the frequency domain yields (using Fourier transforms) [7]:

$$\beta^2 = \frac{\int_{-\infty}^{\infty} f^2 |S(f)|^2 df}{\int_{-\infty}^{\infty} |S(f)|^2 df}, \tag{4.35}$$

where $S(f)$ is the Fourier transform of $s(t)$. Using eqs. (4.33), (4.34) and (4.35), the variance of the distance estimate is now given as:

$$var(\hat{d}) = \frac{c^2}{\varepsilon \beta^2 \sum_{l=1}^{N} \frac{|\alpha_l|^2}{\frac{N_0}{2}}}. \tag{4.36}$$

Since $\gamma_s = \frac{\varepsilon}{N_o/2}$ represents the SNR, eq. (4.36) can be simplified to yield:

$$var(\hat{d}) = \frac{c^2}{\gamma_s \beta^2 \sum_{l=1}^{N} |\alpha_l|^2}. \tag{4.37}$$

Following eq. (4.37), the resulting proposed SIMO bandwidth determination model is shown to be:

$$\beta = \sqrt{\frac{c^2 P(\hat{d})}{G \gamma_s \sum_{l=1}^{N} |\alpha_l|^2}}, \tag{4.38}$$

where G represents the number of symbols according to the defined pulse-shape as shown in eq. (4.1). For a generalised signal the G parameter is a constant factor. Theoretical comparisons of the SISO BD model and SIMO BD model are shown in Figure 4.2. These are based on eqs. (4.3) and (4.38) for Rician fading coefficients with a K-factor of 4 dB (dominant LOS component). The 1×8 case was shown to level off at a utilised bandwidth of approximately 5 MHz for the Rician case.

Figure 4.3 illustrates the results for a Rayleigh fading scenario (strong NLOS component). Similarly, it was observed that for the 1×8 case (Rayleigh), the curve tended to level off

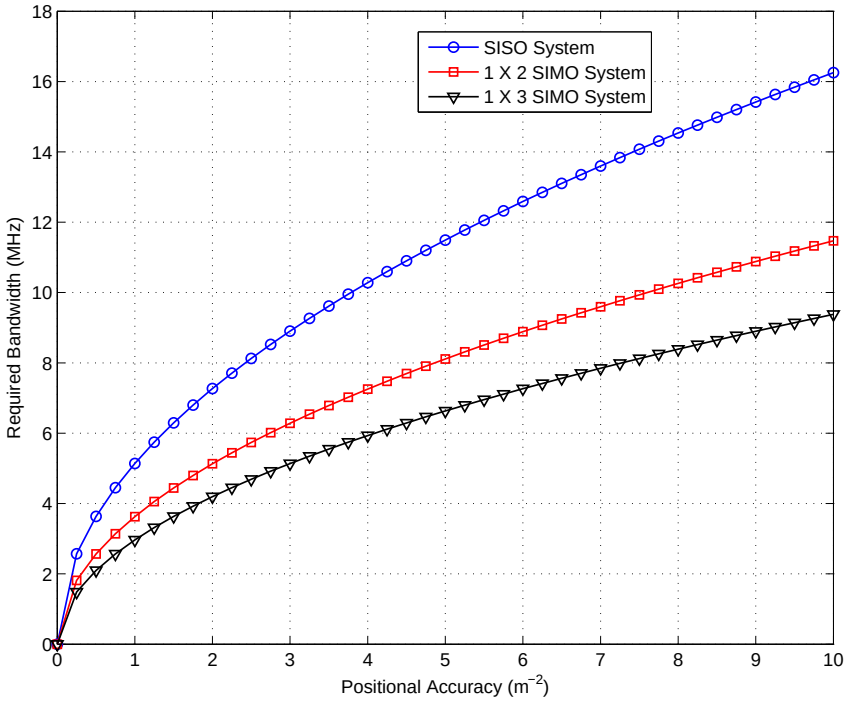

Figure 4.2: Comparison of a SISO and SIMO BD model for a Rician case (K = 4 dB)

at a required bandwidth of approximately 17 MHz. According to Figure 4.3, the different SIMO cases can exploit NLOS components to achieve better theoretical performance over the SISO case. In addition, for $N \geq 8$, a minimal change in theoretically utilised bandwidth was observed for both the Rician and Rayleigh cases.

4.2.3 Enhanced Dynamic Spectrum Management

Dynamic spectrum management is a vital component of CR and it involves the efficient and optimal management of spectrum utilisation between primary and secondary users. Centralised (with a primary controller) and decentralised (distributed approach) schemes have been investigated as possible spectrum sharing techniques. A variety of spectrum sharing models have been proposed, such as the competition-based model [68, 69] and auction-based model [70, 71], which rely on game theoretic approaches. A biologically inspired spectrum sharing model uses an insect colony to perform adaptive task allocation and the corresponding results reveal efficient dynamic spectrum sharing [72].

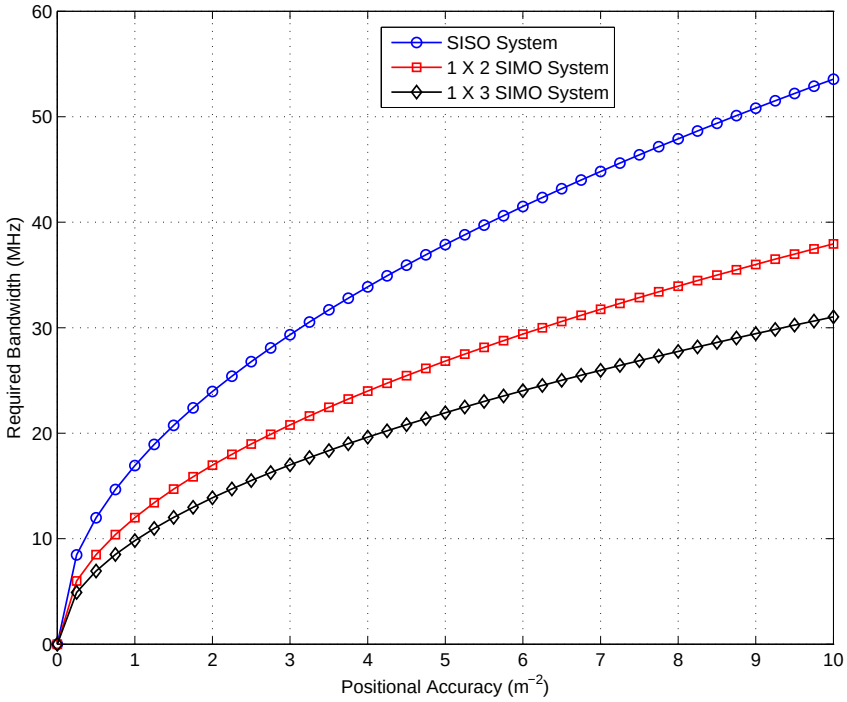

Figure 4.3: Comparison of a SISO and SIMO BD model for a Rayleigh case

As mentioned earlier in the chapter, the EDSM component of the CPS follows from the BD model and extracts the required bandwidth using a set of decision criteria as determined by the available bandwidth from the available spectrum. Important parameters, such as carrier frequency, PSD or transmit power, number of available bands and associated bandwidth, have to be taken into account when modelling dynamic spectrum utilisation. Therefore in the context of CR there are two proposed approaches, viz. overlay (opportunistic) spectrum access and hybrid (combination of overlay and underlay) spectrum access. Overlay spectrum usage may entail the use of adaptive frequency transmitters that focus on 'holes' within the spectrum and transmit within these gaps without causing interference to existing wireless technologies. There have been numerous studies on overlay access techniques for CR, such as the optimisation of transmission times for the SU in an overlay setting [73]. A cooperative decode-and-forward spectrum sharing scheme has also been proposed where the PU and SU can transmit simultaneously [74]. The concept of underlay

spectrum access involves the utilisation of the frequency band at well below the noise floor of the PU. Hence optimal power control by the SU is an inherent requirement [75]. Therefore unlicensed users are able to transmit overlay waveforms required for A-TOA estimation within the licensed bands in an opportunistic and non-interfering manner. The proposed technology for underlay spectrum usage is UWB, since the signal is characterised by a large bandwidth with a relatively low PSD. The premise behind implementing UWB for underlay spectrum usage is the fact that primary users can tolerate an acceptable level of interference. As a result, unlicensed users will be able to operate at the noise floor of licensed users [76]. Hybrid schemes exploit the advantages of both types of spectrum access techniques, as demonstrated in [77] where the throughput of the SU is maximised.

CHAPTER 5

MULTIBAND TOA POSITIONING TECHNIQUE FOR COGNITIVE RADIO

The CPS proposed in [45] utilises a combination of adaptive bandwidth selection as well as dynamic spectrum allocation techniques to address the location awareness requirements of CR. Time-based ranging schemes such as TOA are particularly suited for such localization systems employing UWB or orthogonal frequency division multiplexing (OFDM) in CR, since the bandwidth and SNR of the signal, play an important role in the positional accuracy of the receiver [21]. Previous works [78, 79] have shown that conventional TOA ranging is a suitable technique for single band positioning systems. It has also been shown that optimal two-step time-delay estimation can be conducted simultaneously on dispersed bands for CR systems using a variety of combining schemes, each with different degrees of performance under various modulation schemes [80, 81]. There has not been any work to date, to the best of the author's knowledge, which investigates the 2D positioning accuracy of multiband TOA systems and the benefits over legacy single band TOA band systems.

In this chapter, an analytic approach for performing two dimensional (2D) location estimation over multiple (unoccupied) bands in the context of opportunistic spectrum access for CR networks is proposed. The best achievable positioning accuracy is achieved through the generalised derivation of the CRLB time delay and channel coefficient estimates for multiple bands. A combining technique using the computed estimates for each band is then derived to obtain an optimal time delay estimate (and channel coefficient estimate), which

results in improved user location estimation when compared to a single band system. In order to validate the outcome in a practical scenario, the multiband positioning technique is applied to a spectrum occupancy pdf model, which is based on measurements conducted at the University of Pretoria, Hatfield campus, in the ultra-high frequency (UHF) band. The performance was analysed using the NLS, LLS and TSML location estimation algorithms. This proposed positioning technique has been developed in the context of future application for various multicarrier communication standards, most of which are fundamentally based on OFDM such as Long term evolution (LTE), DVB-T2, WiMax, etc [82].

In Section 5.1 of this chapter, an overview of the multiband signal model is proposed. Section 5.2 provides the derived CRLB estimate of the time delay and channel coefficients for multiple bands. The combining technique for the estimates is presented in Section 5.3. In Section 5.4, the UHF spectrum occupancy measurement results are discussed where the pdf for this particular band is determined.

5.1 SIGNAL MODEL

The mathematical signal model for deriving the CRLB and required estimates forms the initial basis of this particular study. It has been assumed that the MT to be localised, is synchronised with the different base stations, each of which is transmitting single-path signals over multiple bands. The signal delay (τ) has also been assumed to be constant for all transmitted signals, as the delay is based on the power of the first arriving path. In a typical CR scenario, it is envisioned that discrete multiple bands can be opportunistically accessed and utilised for TOA positioning. The baseband representation of each received signal ($r(t)$) can be represented as:

$$r_i(t) = \alpha_i s_i(t-\tau) + n_i(t), \quad 0 \leq t \leq T,\ i \in [1..N], \tag{5.1}$$

where α_i is the channel-fading coefficient of each band identified by i, $s_i(t-\tau)$ is the delayed transmitted signal occupying a specific bandwidth (β_i), N is the total number of discrete bands and $n_i(t)$ represents a zero mean AWGN process with variance, σ_i^2.

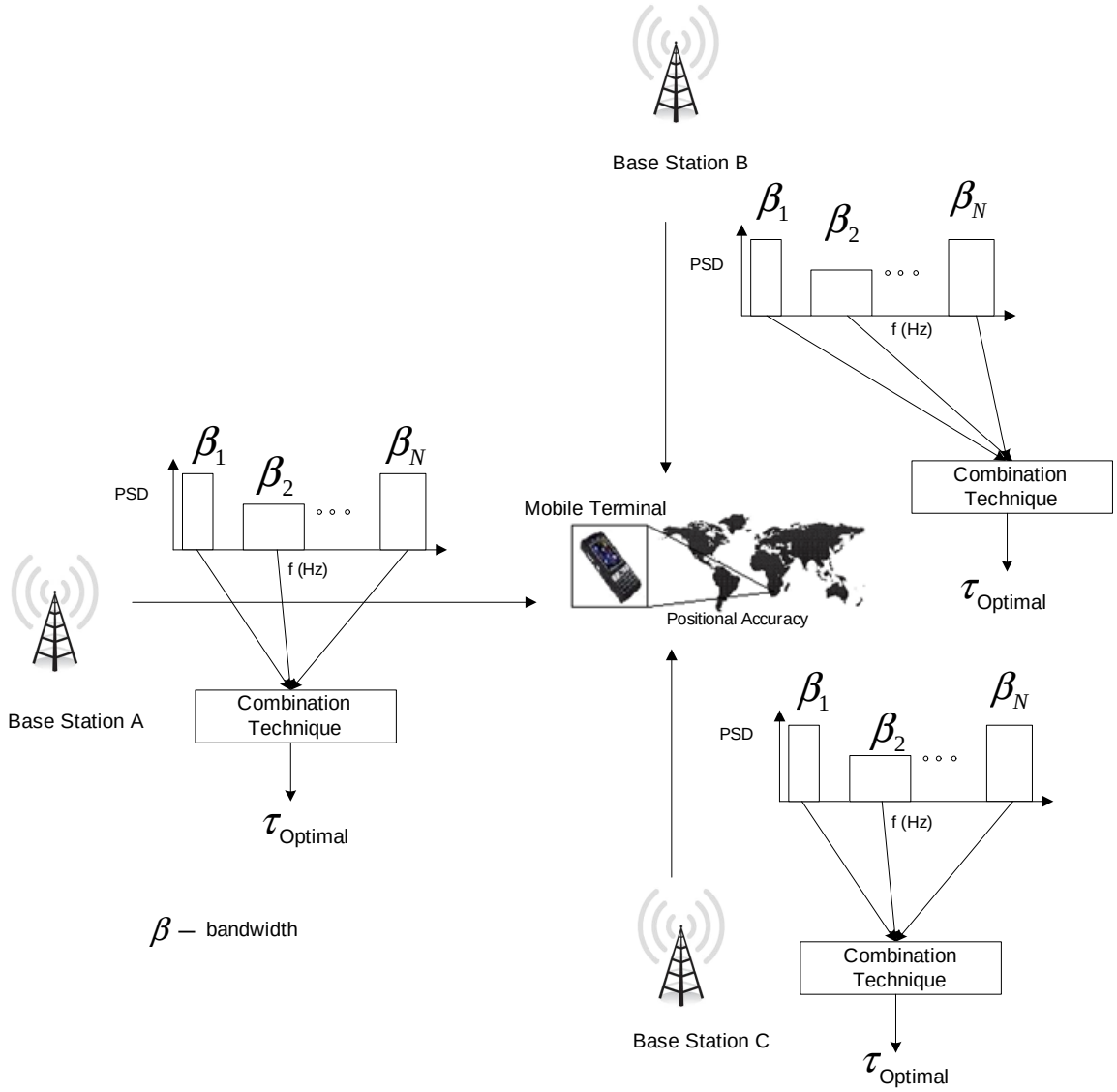

Figure 5.1: Overall multiband TOA model

Figure 5.1 displays the conceptual system model for the multiband TOA positioning system. In the case of any TOA ranging system, there are a minimum of three base stations (which can play the role of an SU) required to localise a mobile user. These SU base stations can dynamically access the spectrum and transmit TOA ranging signals using different bandwidths of varying magnitude. The estimated amount of discrete bandwidths available from each base station can range from $\hat{\beta}_1, ..., \hat{\beta}_N$, depending on the availability at any given point in time.

The main advantage of the model shown in Figure 5.1 is that varying bandwidths of different

magnitudes are exploited (depending on the availability) to obtain an improved location estimate by considering multiple time delays to obtain a final optimal time delay estimate. The combining technique considers the CRLB estimate of each band and thereafter computes the mean estimate for all N bands to obtain an overall optimal time delay estimate for TOA ranging.

5.2 CRLB OF TIME DELAY AND CHANNEL COEFFICIENT ESTIMATES

Figure 5.2 displays the proposed receiver model for the multiband TOA positioning system where $\hat{\beta}_1, ..., \hat{\beta}_N$ represents the bandwidth magnitude of each band. The time delay and channel coefficient are estimated for the overall multiband system. The measured signal characteristics are obtained and thereafter the positional accuracy for the MT can be obtained using a suitable location estimation algorithm.

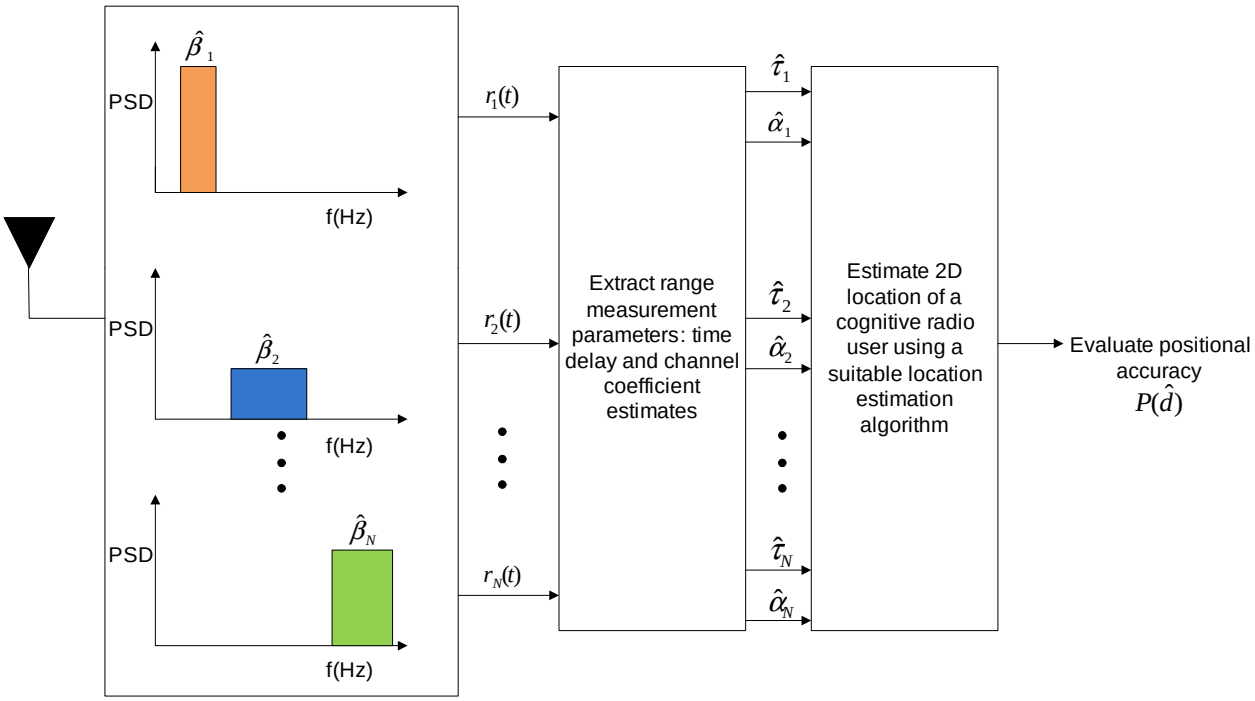

Figure 5.2: Multiband receiver model

The CRLB for the time delay and channel coefficients can be derived according to the multiband signal model represented in eq. (5.1). Accordingly (similar to Section 4.2.2), the following vector of unbiased signal parameters are estimated:

$$\Theta = [\tau \;\; \boldsymbol{\alpha}], \tag{5.2}$$

where τ is the signal time delay and $\boldsymbol{\alpha} = [\alpha_1 ... \alpha_N]$ represents the vector of complex channel coefficients corresponding to N bands, which describe the fading of each received signal. The assumption is made that over the interval between 0 and T_s (symbol time), the transmitted pulse given by $s(t)$ is non-zero and band-limited to B Hz. As a result the observation interval encompasses the symbol time and maximum time delay, which can be also shown as follows: $T = T_s + \tau_{max}$. The CRLB of eq. (5.2) is given by the first row and first column of an inverse matrix and represented as follows [50]:

$$var(\hat{\Theta}_i) \geq \left[\mathbf{I}^{-1}(\Theta)\right]_{ii}, \tag{5.3}$$

where $\mathbf{I}(\Theta)$ is a $q \times q$ FIM and q is defined by the number of unknown parameters to estimate. In this case, $\Theta_1 = \tau$ and $\Theta_2 = \boldsymbol{\alpha}$. The elements of the 2×2 FIM have been determined for a general Gaussian case for a discrete received signal using (refer to Appendix A):

$$\mathbf{I}(\Theta) = \sum_{i=1}^{N} \frac{1}{\sigma_i^2} \sum_{k=0}^{K-1} \frac{\partial s_i[k;\Theta]}{\partial \Theta_i} \frac{\partial s_i[k;\Theta]}{\partial \Theta_j}, \tag{5.4}$$

where $i = 1, 2, .., q$ and $j = 1, 2, ..., q$ and N is the total number of bands. The FIM is therefore represented as:

$$\mathbf{I}(\Theta) = \begin{bmatrix} I_{\tau\tau} & \mathbf{I}_{\tau\boldsymbol{\alpha}} \\ \mathbf{I}_{\boldsymbol{\alpha}\tau} & \mathbf{I}_{\boldsymbol{\alpha}\boldsymbol{\alpha}} \end{bmatrix}. \tag{5.5}$$

The following FIM elements can be derived using eq. (5.4) [83]:

$$I_{\tau\tau} = \sum_{i=1}^{N} \frac{|\alpha_i|^2 \hat{\varepsilon}_i}{\sigma_i^2}, \tag{5.6}$$

$$\mathbf{I}_{\tau\boldsymbol{\alpha}} = \mathbf{I}_{\boldsymbol{\alpha}\tau}^{T} = -\left[\frac{|\alpha_1|\tilde{\varepsilon}_1}{\sigma_1^2}, \ldots, \frac{|\alpha_N|\tilde{\varepsilon}_N}{\sigma_N^2}\right], \tag{5.7}$$

$$\mathbf{I}_{\boldsymbol{\alpha}\boldsymbol{\alpha}} = diag\left[\frac{\varepsilon_1}{\sigma_1^2}, \ldots, \frac{\varepsilon_N}{\sigma_N^2}\right], \tag{5.8}$$

where $\hat{\varepsilon}_i$ and $\tilde{\varepsilon}_i$ are respectively given as:

$$\hat{\varepsilon}_i = \int_0^T \left|\tilde{\lambda}\right|^2 dt, \tag{5.9}$$

$$\tilde{\varepsilon}_i = \int_0^T |\tilde{\lambda}||\lambda| dt. \tag{5.10}$$

The first derivative of the signal energy λ is given by $\tilde{\lambda} = s_i'(t-\tau)$, while the energy ($\varepsilon_i$) of the signal $\lambda = s_i(t-\tau)$ is shown as:

$$\varepsilon_i = \int_0^T |s_i(t-\tau)|^2 dt. \tag{5.11}$$

The CRLB of the time delay estimate can be obtained using the matrix algebraic manipulations given in eq. (4.21) and eq. (4.22).

The time delay estimate of the signal is therefore shown as:

$$
\begin{aligned}
[I_{\tau\tau}]^{-1} =& \sum_{i=1}^{N} \frac{|\alpha_i|^2 \hat{\varepsilon}_i}{\sigma_i^2} - \left[\frac{|\alpha_1|\tilde{\varepsilon}_1}{\sigma_1^2}, \ldots, \frac{|\alpha_N|\tilde{\varepsilon}_N}{\sigma_N^2} \right] \\
& \times diag \left[\frac{\varepsilon_1}{\sigma_1^2}, \ldots, \frac{\varepsilon_N}{\sigma_N^2} \right]^{-1} \times \begin{bmatrix} \frac{|\alpha_1|\tilde{\varepsilon}_1}{\sigma_1^2} \\ \vdots \\ \frac{|\alpha_N|\tilde{\varepsilon}_N}{\sigma_N^2} \end{bmatrix} \\
=& \sum_{i=1}^{N} \frac{|\alpha_i|^2 \hat{\varepsilon}_i}{\sigma_i^2} - \left[\frac{\tilde{\varepsilon}_1|\alpha_1|}{\varepsilon_1}, \ldots, \frac{\tilde{\varepsilon}_N|\alpha_N|}{\varepsilon_N} \right] \times \begin{bmatrix} \frac{\tilde{\varepsilon}_1|\alpha_1|}{\sigma_1^2} \\ \vdots \\ \frac{\tilde{\varepsilon}_N|\alpha_N|}{\sigma_N^2} \end{bmatrix} \\
=& \sum_{i=1}^{N} \frac{|\alpha_i|^2}{\sigma_i^2} \left(\hat{\varepsilon}_i - \frac{\tilde{\varepsilon}_i^2}{\varepsilon_i} \right) \qquad (5.12) \\
=& var(\hat{\tau})^{-1}. \qquad (5.13)
\end{aligned}
$$

It can be noted that the overall estimated time delay is dependent on the channel coefficient for each band. Using eq. (5.12), it is possible to derive a relationship between the CRLB time delay estimate and the positional accuracy of the MT:

$$
var(\hat{\tau}) = \frac{1}{c^2 P(\hat{d})}, \qquad (5.14)
$$

where c is the speed of light and $P(\hat{d})$ is the positional accuracy of the MT. Using eq. (5.12), eq. (5.14) and the bandwidth representation in the Fourier domain, which can be expressed as:

$$
\hat{\varepsilon}_i = \varepsilon_i \hat{\beta}_i^2, \qquad (5.15)
$$

the overall positional accuracy is shown to be:

$$
P(\hat{d}) = \frac{1}{c^2} \sum_{i=1}^{N} \frac{|\alpha_i|^2}{\sigma_i^2} \left(\varepsilon_i \hat{\beta}_i^2 - \frac{\tilde{\varepsilon}_i^2}{\varepsilon_i} \right). \qquad (5.16)
$$

It can be also shown that the CRLB estimate of the channel coefficient for all dispersed bands can be computed using eq. (4.22), resulting in:

$$\begin{aligned}[\mathbf{I}_{\boldsymbol{\alpha\alpha}}]^{-1} &= diag\left[\frac{\varepsilon_1}{\sigma_1^2},\ldots,\frac{\varepsilon_N}{\sigma_N^2}\right] - \left[\frac{|\alpha_1|\tilde{\varepsilon}_1}{\sigma_1^2},\ldots,\frac{|\alpha_N|\tilde{\varepsilon}_N}{\sigma_N^2}\right] \\ &\times \left(\frac{1}{\sum_{i=1}^{N}\hat{\varepsilon}_i\frac{|\alpha_i|^2}{\sigma_i^2}}\right) \times \begin{bmatrix} \frac{|\alpha_1|\tilde{\varepsilon}_1}{\sigma_1^2} \\ \vdots \\ \frac{|\alpha_N|\tilde{\varepsilon_N}}{\sigma_N^2} \end{bmatrix} \\ &= diag\left[\frac{\varepsilon_1}{\sigma_1^2},\ldots,\frac{\varepsilon_N}{\sigma_N^2}\right] - \frac{\sum_{i=1}^{N}\frac{|\alpha_i|^2\tilde{\varepsilon}_i^2}{(\sigma_i^2)^2\varepsilon_i}}{\sum_{i=1}^{N}\hat{\varepsilon}_i\frac{|\alpha_i|^2}{\sigma_i^2}}. \end{aligned} \tag{5.17}$$

The channel coefficient vector ($[\mathbf{I}_{\boldsymbol{\alpha\alpha}}]^{-1}$) can be represented in condensed form (in a similar manner to eq. (4.24)):

$$[\mathbf{I}_{\boldsymbol{\alpha\alpha}}]^{-1} = var(\hat{\alpha}) = D_{i,j}\Big|_{\substack{i=1..N \\ j=1..N}}, \tag{5.18}$$

where N represents the total number of bands and each element $D_{i,j}$ is given by:

$$D_{i,j} = \begin{cases} \dfrac{\varepsilon_i}{\sigma_i^2} - \dfrac{\sum_{i=1}^{N}\frac{|\alpha_i|^2\tilde{\varepsilon}_i^2}{(\sigma_i^2)^2\varepsilon_i}}{\sum_{i=1}^{N}\hat{\varepsilon}_i\frac{|\alpha_i|^2}{\sigma_i^2}} & \text{if } i=j \\ -\dfrac{\sum_{i=1}^{N}\frac{|\alpha_i|^2\tilde{\varepsilon}_i^2}{(\sigma_i^2)^2\varepsilon_i}}{\sum_{i=1}^{N}\hat{\varepsilon}_i\frac{|\alpha_i|^2}{\sigma_i^2}} & \text{if } i\neq j. \end{cases} \tag{5.19}$$

Location accuracy adaptation is dependent on the available bandwidth in the spectrum. According to eq. (5.16), it is inherently impossible to extract the required bandwidth for a specific positional accuracy. Therefore an alternative combining estimation technique has to be proposed, which allows the extraction of the estimated required bandwidth, which in turn provides the location accuracy adaptation functionality for CR.

5.3 TIME DELAY AND CHANNEL COEFFICIENT COMBINATION ESTIMATION TECHNIQUE

Section 5.2 provided the CRLB time delay estimates and channel coefficient estimates for the overall multiband system. Using similar methods, it is possible to derive the estimates for each band, and utilise each estimate individually to obtain an overall optimal solution that enables bandwidth-accuracy adaptation. The vector representation of the estimation parameters based on a single transmitted signal is given as [83]:

$$\Theta_i = [\tau_i \;\; \alpha_i], \tag{5.20}$$

where α is a scalar value. This results in a 2×2 FIM given by:

$$\mathbf{I}(\Theta) = \begin{bmatrix} I_{\tau_i\tau_i} & I_{\tau_i\alpha_i} \\ I_{\alpha_i\tau_i} & I_{\alpha_i\alpha_i} \end{bmatrix}. \tag{5.21}$$

Using eq. (5.4), each FIM element is given by:

$$I_{\tau_i\tau_i} = \frac{|\alpha_i|^2\hat{\varepsilon}_i}{\sigma_i^2}, \tag{5.22}$$

$$I_{\tau_i\alpha_i} = I_{\alpha_i\tau_i} = -\frac{|\alpha_i|\tilde{\varepsilon}_i}{\sigma_i^2}, \tag{5.23}$$

$$I_{\alpha_i\alpha_i} = \frac{\varepsilon_i}{\sigma_i^2}. \tag{5.24}$$

The CRLB of the time delay estimate can be computed in a similar way to eq. (4.21), bearing in mind that the elements in this case are all scalar:

$$[I_{\tau_i\tau_i}]^{-1} = \left(I_{\tau_i\tau_i} - I_{\tau_i\alpha_i} I_{\alpha_i\alpha_i}^{-1} I_{\alpha_i\tau_i}\right)^{-1}. \tag{5.25}$$

Therefore, the CRLB of the time delay estimate for an individual band is given as:

$$\begin{aligned}
[I_{\tau_i\tau_i}]^{-1} &= \frac{|\alpha_i|^2\hat{\varepsilon}_i}{\sigma_i^2} - \frac{|\alpha_i|\tilde{\varepsilon}_i}{\sigma_i^2} \times \frac{\sigma_i^2}{\varepsilon_i} \times \frac{|\alpha_i|\tilde{\varepsilon}_i}{\sigma_i^2} \\
&= \frac{|\alpha_i|^2}{\sigma_i^2}\left(\hat{\varepsilon}_i - \frac{\tilde{\varepsilon}_i^2}{\varepsilon_i}\right) \\
&= var(\hat{\tau}_i)^{-1} = c^2 P(\hat{d}).
\end{aligned} \tag{5.26}$$

According to eq. (5.15), one can obtain a bandwidth determination equation based on the required positional accuracy of the MT, which can be adapted based on the availability of the required number of bands:

$$\begin{aligned}
\frac{|\alpha_i|^2}{\sigma_i^2}\left(\hat{\varepsilon}_i - \frac{\tilde{\varepsilon}_i^2}{\varepsilon_i}\right) &= c^2 P(\hat{d}) \\
\frac{|\alpha_i|^2}{\sigma_i^2}\left(\varepsilon_i\hat{\beta}_i^2 - \frac{\tilde{\varepsilon}_i^2}{\varepsilon_i}\right)^2 &= c^2 P(\hat{d}) \\
\varepsilon_i\hat{\beta}_i^2 &= \frac{c^2 P(\hat{d})\sigma_i^2}{|\alpha_i|^2} + \frac{\tilde{\varepsilon}_i^2}{\varepsilon_i} \\
\hat{\beta}_i &= \sqrt{\frac{c^2 P(\hat{d})\sigma_i^2}{|\alpha_i|^2\varepsilon_i} + \frac{\tilde{\varepsilon}_i^2}{\varepsilon_i^2}}.
\end{aligned} \tag{5.27}$$

It can be noted that the derivative of the signal energy (constant) is zero, which results in

$\tilde{\varepsilon} = 0$. The estimated required bandwidth for a specified positioning accuracy is therefore shown as:

$$\hat{\beta}_i = \sqrt{\frac{c^2 P(\hat{d})}{|\alpha_i|^2 \gamma_i}}, \tag{5.28}$$

where γ_i is the SNR of the received signal. The CRLB of the channel coefficient estimate for an individual band is calculated using:

$$[I_{\alpha_i\alpha_i}]^{-1} = \left(I_{\alpha_i\alpha_i} - I_{\alpha_i\tau_i} I_{\tau_i\tau_i}^{-1} I_{\tau_i\alpha_i}\right)^{-1}. \tag{5.29}$$

This leads to the following CRLB for the channel coefficient estimate:

$$\begin{aligned} [I_{\alpha_i\alpha_i}]^{-1} &= \frac{\varepsilon_i}{\sigma_i^2} - \frac{\tilde{\varepsilon}_i^2}{\sigma_i^2 \hat{\varepsilon}_i} \\ &= \frac{1}{\sigma_i^2}\left(\varepsilon_i - \frac{\tilde{\varepsilon}_i^2}{\hat{\varepsilon}_i}\right) \\ &= var(\hat{\alpha}_i)^{-1}. \end{aligned} \tag{5.30}$$

Two combining estimation techniques were investigated. The first method involved the averaging of the delay estimates over the total number of bands and the second method involved determining the minimum estimate over all the discrete bandwidths. For a fixed bandwidth availability model, the average delay combining estimate scheme was shown to display optimal performance. However, for a dynamic bandwidth availability model the minimum estimate combining scheme was shown to provide an improved performance in positioning accuracy. According to eq. (5.16), the channel coefficient and SNR of the received signal, together with the total number of bands, are therefore important parameters which affect the TOA location estimate.

5.4 UHF SPECTRUM OCCUPANCY MEASUREMENT CAMPAIGN

According to [83], predefined discrete multiple bandwidths were utilised to perform 2D location estimation. Although an improved accuracy was observed, the study was limited in relation to a fixed bandwidth availability model. A realistic case would involve a CR device dynamically selecting multiple bandwidths based on availability to perform TOA positioning. Due to the unpredictable nature of spectrum occupancy, the bandwidth availability of the unoccupied spectrum would have to be modelled according to a specific type of pdf. This pdf would be derived based on the results obtained from a UHF spectrum occupancy measurement campaign conducted at the University of Pretoria campus. The objective was to determine the likelihood of available (unoccupied spectrum holes) or unavailable (occupied spectrum holes) bandwidths and thereafter apply the pdf model to the multiband TOA positioning system. The UHF bands consist primarily of TV bands, which according to the IEEE 802.22 WRAN standard aims to provide broadband access to rural areas through the use of certain CR functionality. Although the empirical measurements are limited to one area, the results provide a reasonable validation to the performance of the proposed multiband TOA positioning model.

5.4.1 Design Overview of Measurement Campaign

A measurement campaign with the objective of assessing the spectrum occupancy of the UHF band in a South African context was conducted over a six-week period. The overall measurement system was based on the energy detection spectrum sensing scheme. This method has been utilised in various spectral occupancy measurement campaigns [1–3, 84], due its low complexity and simplistic hardware implementation. The measurement readings were obtained over the whole UHF frequency band, i.e. 470-854 MHz. The spectrum occupancy measurements were conducted on the rooftop of the 15-storey Engineering I building, University of Pretoria, Hatfield campus, in a typical suburban area of Pretoria. Table 5.1 represents a summary of all the hardware components for the measurement system.

The key spectrum occupancy measurement system components consisted of an Ultra-

Table 5.1: Overview of hardware components utilised in the measurement system [85]

Hardware component	Specifications
Wideband Antenna	Super-M Ultra base antenna ranging from 25 MHz to 6 GHz with a maximum gain of 3 dBi
LNA	Low noise amplifier with bandwidth range from 50 MHz-3 GHz; low noise figure specified at 1.1 dB ; maximum gain of 13 dB
Power Supply	Regulated 5V DC power supply with a current capacity of 800 mA
Spectrum Analyser	N9010A Agilent EXA signal analyser with a 1.86 GHz Intel Celeron M processor, 3.26 GB RAM and a 20 GB of storage capacity
Air Conditioner	Custom built air conditioner for the cooling of the spectrum analyser
Scheduler PC	Windows XP PC with an Intel Core 2 Quad CPU at 2.33 GHz and 2GB of RAM
Remote Data Storage Server	PC with an Ubuntu operating system, Intel i3 Core CPU at 3.2 GHz, 4GB RAM and 5 TB of storage capacity

wideband antenna (ranging from 25 MHz and 6 GHz), Agilent spectrum analyser which was then connected to a PC, where sample data was remotely stored in a server accessible over the university's local area network.

In order to quantify the occupancy of the band in question, a measurement scheduler was designed to analyse the data over a 24-hour period for six weeks. Each measurement reading consisted of 1500 samples, where a sample consisted of an entire sweep of the band (384 points). The measurements were conducted at regular two-hour intervals with a resolution of 1 MHz for the UHF band. Approximately 170 million samples were collected over the whole course of the measurement campaign [85].

5.4.2 Spectrum Occupancy PDF of the UHF band

The raw measurements taken from the UHF measurement campaign were preprocessed and equalised in order to remove any outliers that might cause statistical inaccuracies. Figure 5.3 displays the mean received power profile of the UHF band over the whole duration of the measurement campaign.

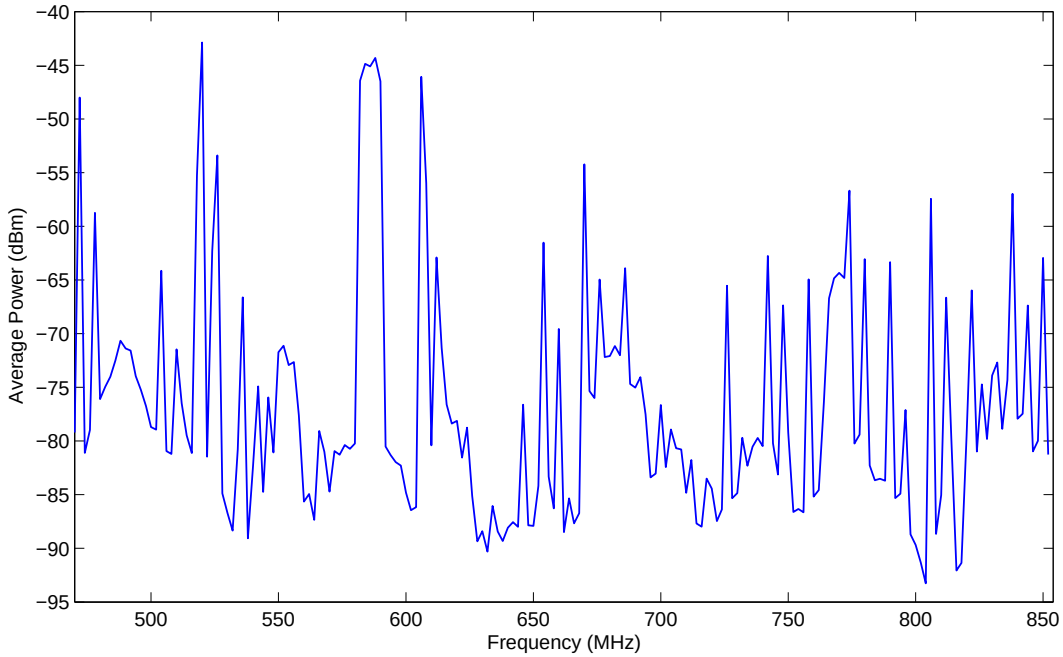

Figure 5.3: Mean received power profile of the UHF band over six weeks

The basis of this method is to infer the spectral occupancy based on the noise statistics of the measurement readings. The one problem that may arise is if the received signal strength is less than that of the noise floor, which may imply the detection of an unoccupied channel when in fact a signal is present. A histogram of all the sampled data over the whole measurement period for the UHF band was obtained and the probability as a function of the received signal strength was plotted, as illustrated in Figure 5.4.

According to the measurement results from Figure 5.4, the occupied and unoccupied (noisy) portions of the UHF band are clearly distinguishable. Analysis of the unoccupied spectrum

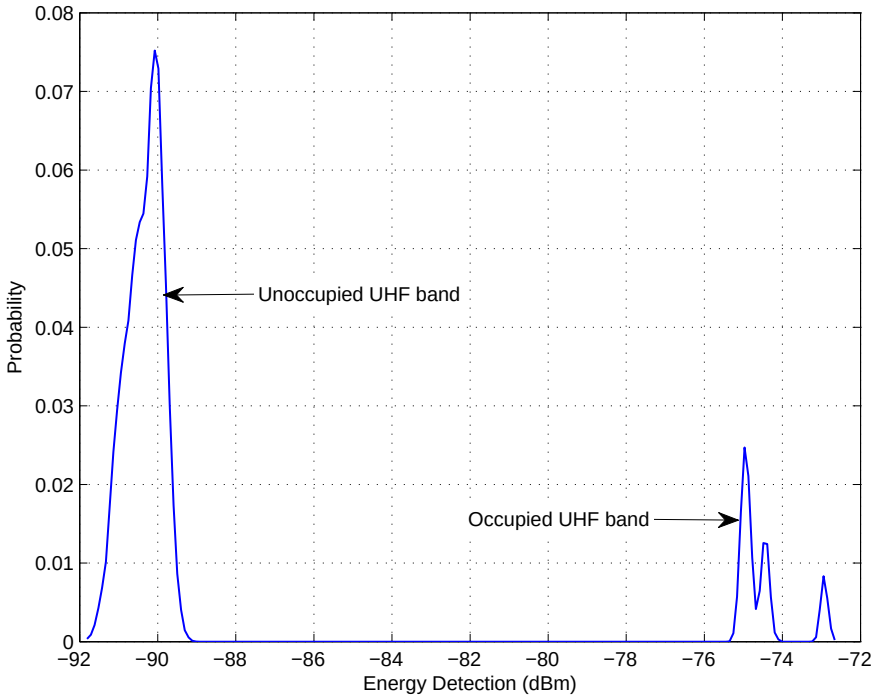

Figure 5.4: Probability density function of the received signal strength for the UHF band

for the UHF band reveals that the probability distribution is Gaussian with a mean (μ_{uhf}) of $-90.2\ dBm$ and a standard deviation given by $\sigma_{uhf} = 1.0139$.

The mean falls within the measured minimum system sensitivity, which was determined to be $-104.5\ dBm$ for the UHF band. The resulting probability distribution is used to model the dynamic bandwidth availability for the multiband TOA positioning model.

CHAPTER 6

RESULTS AND DISCUSSION

The performance evaluations of the proposed optimised CR positioning techniques in Chapters 4 and 5 are presented and analysed. Section 6.1 includes a comparative bandwidth efficiency plot between the SISO BD and SIMO BD model under three different generic environments, viz. rural, urban and suburban areas, which are based on the root mean square (RMS) delay spread. Section 6.2 compares the positional accuracy performance of the proposed multiband TOA positioning system with the conventional single band system for a fixed and dynamic bandwidth availability model. The dynamic bandwidth availability model is based on results taken from a UHF spectrum occupancy measurement campaign at the University of Pretoria.

6.1 BANDWIDTH EFFICIENT CPS

The performance of the bandwidth efficient cognitive positioning model was analysed using the LLS and TSML location estimation algorithms for three environmental scenarios. The first scenario is one in which LOS is a dominant component, as typically exhibited by a rural environment. The second and third scenarios are characterised by a NLOS dominant signal component, which is based on generalised RMS delay spreads for the aforementioned environments. The SNR (γ_s) was fixed at 10 dB while it was assumed that the number of transmitted symbols (G) was 10. The channel coefficients are modelled as random variables, depending on whether the scenario was LOS or NLOS.

The error induced by the NLOS component can be modelled as either deterministic or based on a specific probability distribution. In this investigation, the NLOS error was characterised as a random variable having an exponential distribution [86]:

$$g(\tau) = \begin{cases} \frac{1}{\tau_{rms}} \exp -\frac{\tau}{\tau_{rms}}, & \tau > 0 \\ 0 & otherwise, \end{cases} \tag{6.1}$$

where the decay parameters are given by the inverse of the delay spread $\left(\frac{1}{\tau_{rms}}\right)$. The delay spread (τ_{rms}) is represented as:

$$\tau_{rms} = L_0 r^{\rho} \psi, \tag{6.2}$$

where L_0 is the median value of τ_{rms} at 1 km, r is the distance between the base station and the MT, ρ is a power-law exponent factor that lies between 0.5 and 1 and ψ is a log-normal random variable characterised by a standard deviation of 4 dB for the two environments. This particular NLOS statistical error model is suitable for characterising various types of propagation environments, since it has been validated through numerous measurement results and its applicability can extend to scenarios involving mobile user positioning [86]. Table 6.1 is an overview of the key parameters utilised in the bandwidth efficient CPS simulation model.

Table 6.1: Simulation Parameters

Scenario	Delay spread (τ_{rms})	ρ	Channel coefficients (α)
Rural	0.1 μs	0.5	Rician
Urban	0.4 μs	0.5	Rayleigh
Suburban	0.3 μs	0.5	Rayleigh

In order to evaluate the performance of the proposed SIMO BD model, a comparison of the bandwidth efficiency with respect to the positional root RMSE was drawn against a conventional SISO system over a predefined bandwidth interval ranging from 1 MHz to 20 MHz.

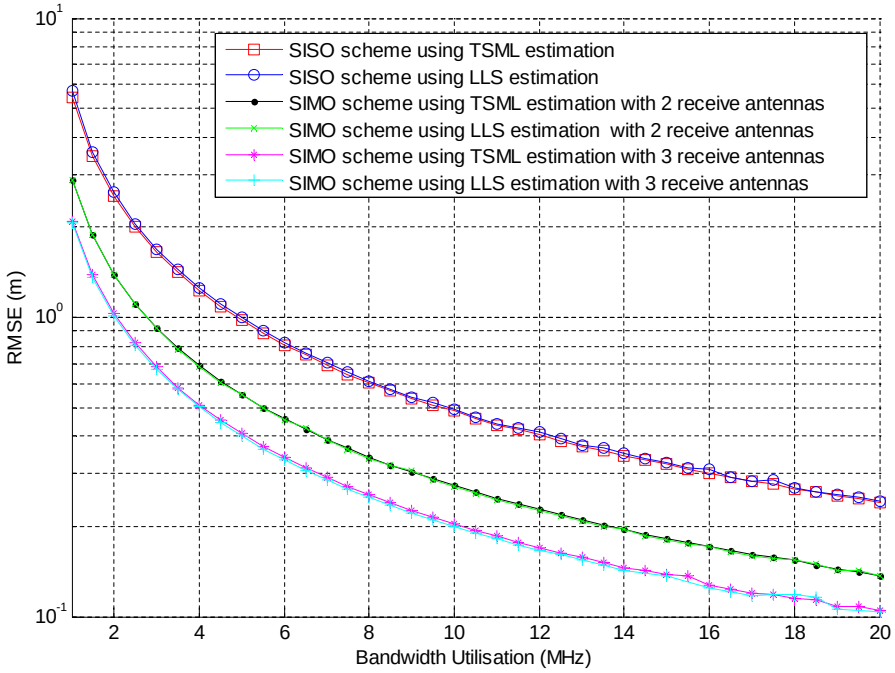

Figure 6.1: RMSE of the positional accuracy of the SISO and SIMO systems in a typical rural environment

The 1×2 and 1×3 SIMO BD positioning model was analysed using the LLS and TSML estimation technique at a fixed SNR of 10 dB. Figures 6.1, 6.2 and 6.3 represent the MT's 2D positioning RMSE with respect to the utilized bandwidth in a generalised rural, urban and suburban scenario, respectively. Accordingly all three aforementioned figures indicate that diversity in multiple antenna positioning systems plays an important role in improving bandwidth efficiency in relation to TOA positioning.

The following conclusions regarding the proposed SIMO BD model can be made [87]:

- In the case of all three environmental models a significant performance advantage in terms of positional accuracy of the SIMO positioning scheme can be attained at lower bandwidth intervals from 1 MHz to 8 MHz. An average RMSE reduction of 82% between the SISO and 1×3 SIMO case can be noted for all three scenarios at 1 MHz. This can enable improved dynamic spectrum access for positioning applications in CR, more particularly in cases where there is a shortage of large discrete bandwidths,

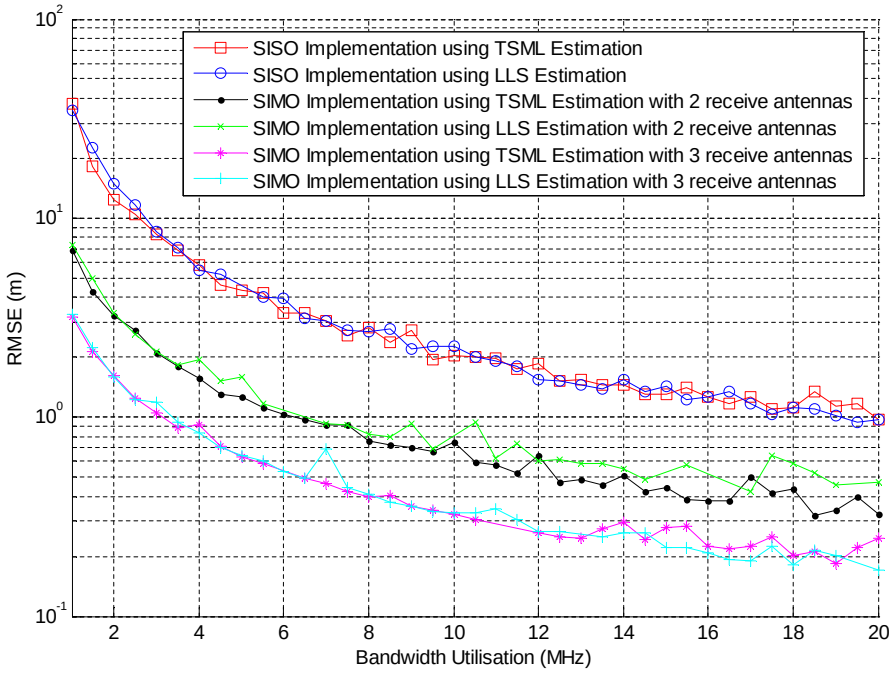

Figure 6.2: RMSE of the positional accuracy of the SISO and SIMO systems in a typical urban environment

depending on the time interval or location.

- It was observed that for bandwidths beyond 20 MHz, the SIMO positional RMSE for both the 1×2 and 1×3 scheme converged at an average RMSE of 0.1 m for the rural case and 0.2 m for the urban and suburban case. This indicates that a minimal change in positional accuracy is gained as the bandwidth is increased.

- Furthermore, it has been determined that the utilisation of more than three receive antennas (1×5 and 1×8 case) produced a minimal differential change of approximately 10% in the positional RMSE for bandwidths greater than 20 MHz when compared to the 1×3 case for all three scenarios. The performance evaluations therefore show that the 1×3 case was deemed to be the optimal SIMO scheme in terms of achieving the most significant improvement in bandwidth efficiency for the CPS.

- The TSML and LLS estimation techniques for all three scenarios display similar per-

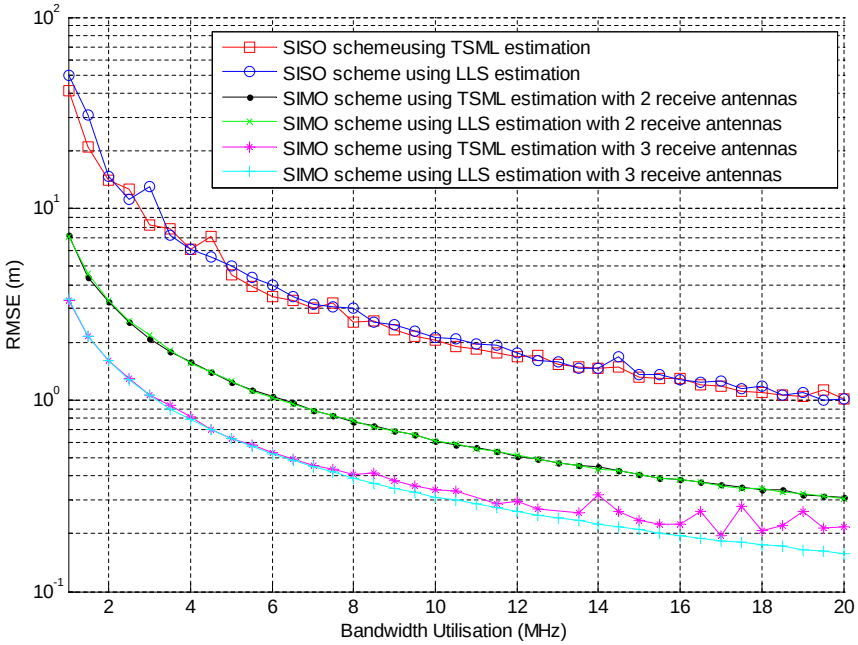

Figure 6.3: RMSE of the positional accuracy of the SISO and SIMO systems in a typical suburban environment

formance with respect to the specific antenna scheme.

6.2 MULTIBAND TOA POSITIONING TECHNIQUE

6.2.1 Fixed Bandwidth Availability Model

The RMSE positional accuracy of the single band and multiband systems are compared in order to quantify the improvement in terms of positional accuracy for a fixed (predefined) bandwidth availability model using three different LTE dispersed bandwidths (3, 5 and 10 MHz). It is envisioned that CR positioning can exploit various bandwidths of different magnitudes by switching between various technologies (e.g. WiMax, LTE, WCDMA and WiFi have various operating channel bandwidths), depending on the availability at any given instant in time. Figure 6.4 represents the MT's RMSE of the location estimate as a function of the SNR using the TSML location estimation technique for a scenario where the dominant signal component is LOS. A decrease in RMSE can be observed when estimating the MT's

location using two and three bands. This is due to the fact that each band is characterised by a different time delay and channel fading coefficient and can be optimally combined to yield an improved estimate. At lower SNRs the improvement in accuracy is much more significant, while at higher SNRs the location estimates tend to converge according to the number of bands utilised to perform TOA.

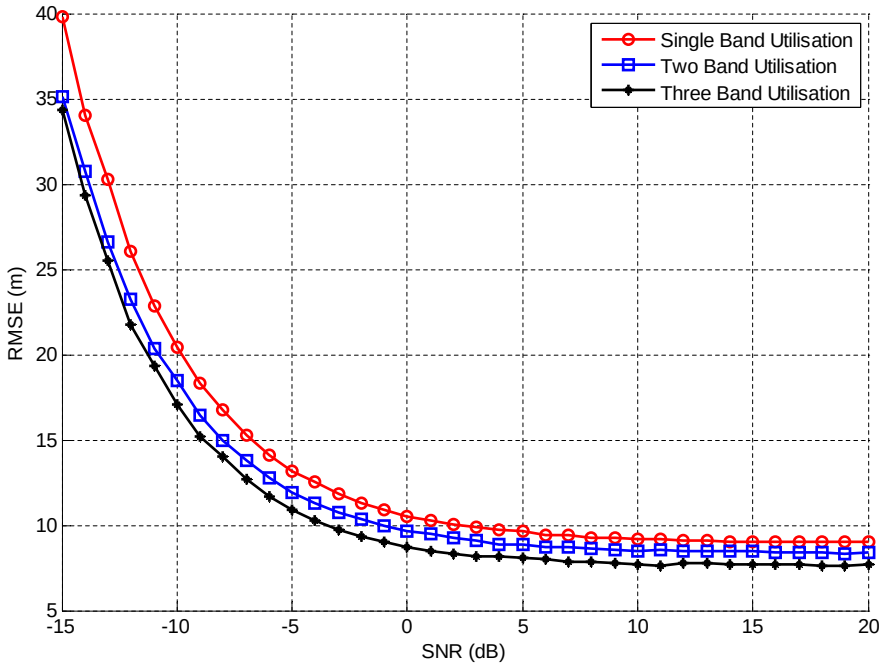

Figure 6.4: RMSE of the location estimate for rural scenarios using 3 MHz, 5 MHz and 10 MHz bandwidths.

Figure 6.5 further illustrates the effect of the average combining estimation technique on the RMSE error as the number of bands are increased. These results are compared for three different fixed SNR values. For this particular scenario four different bands were chosen, each with a bandwidth defined by:

$$\hat{\beta} = \{B_1, B_2, B_3, B_4\} \tag{6.3}$$

where $B_1 = 3\,MHz$, $B_2 = 5\,MHz$, $B_3 = 10\,MHz$ and $B_4 = 15\,MHz$. For the case of single band utilisation, the RMSE error for each individual band was separately computed and then

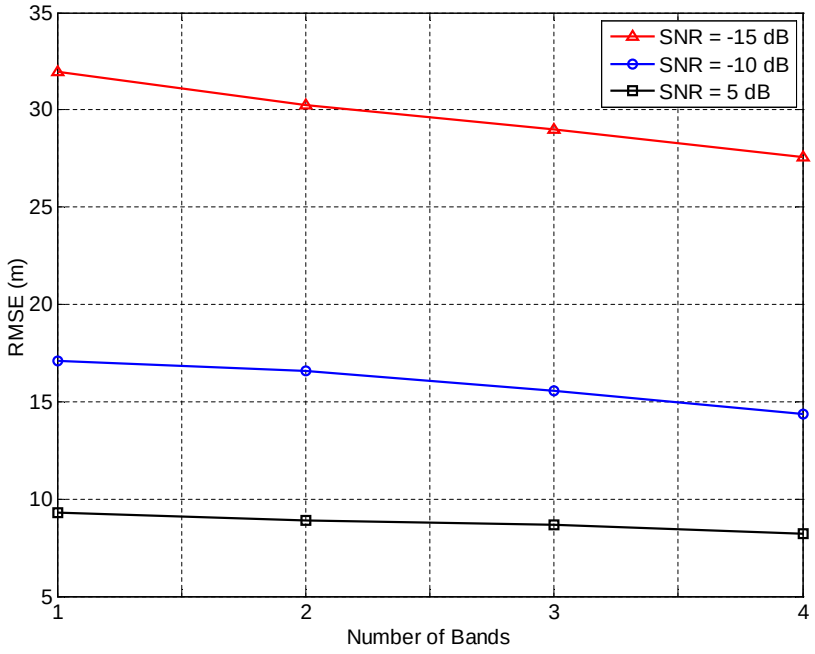

Figure 6.5: RMSE of the location estimate for rural scenarios using different SNRs (-15 dB, -10 dB and 5 dB).

this error averaged over all four bands. The overall positioning accuracy for each of the four bands was computed by taking the mean RMSE error over all possible k band permutations for a set defined by T total bandwidths, which can be generally represented as:

$$\begin{pmatrix} T \\ k \end{pmatrix} = \frac{T!}{(T-k)!k!}, \tag{6.4}$$

where ! represents a factorial expression. Therefore, in the case of $k = 2$ bands, the RMSE errors for all unique possible two band permutations, e.g.

$$\hat{\beta}_2 = [\{B_1, B_2\}, \{B_1, B_3\}, \{B_1, B_4\}, \{B_2, B_3\}, ...] \tag{6.5}$$

were obtained and then averaged over all T bands. The error computation also applies to the case where $k = 3$ and $k = 4$ bands. An decrease in the RMSE error can be observed for each band when comparing Figures 6.4 and 6.5. This is mainly to the fact that an additional larger band of 15 MHz has been introduced which significantly lowers the overall average.

A minimal change in accuracy can be observed, which tends to be the case as the SNR is increased (e.g. 5 dB).

6.2.2 UHF Bandwidth Availability Model

In order to simulate dynamic bandwidth availability, five different bandwidths were randomly generated from a predefined set (between 1 MHz and 20 MHz) according to a Gaussian distribution as determined for an unoccupied UHF spectrum in Figure 5.4. A priori information regarding the channel coefficients were assumed to be Rician-distributed with $K = 2\ dB$ (K-factor). Figures 6.6, 6.7 and 6.8 display the performance of the proposed technique in relation to the NLS, LLS and TSML algorithms respectively. Five discrete bandwidths were considered in this scenario, as opposed to Section 6.2.1, where only three bandwidths were considered at a given instant.

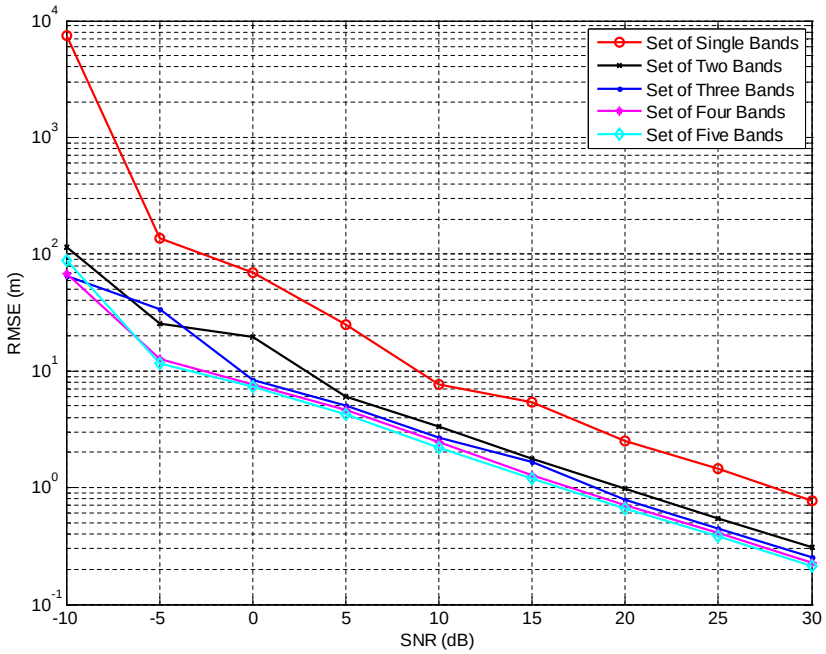

Figure 6.6: RMSE performance for the NLS algorithm (Rician fading, K= 2 dB)

According to Figures 6.6, 6.7 and 6.8, an improvement in location accuracy can be observed when performing multiband TOA estimation for all three different types of estimation algorithms. This is due to the fact that each band is characterised by a different time delay

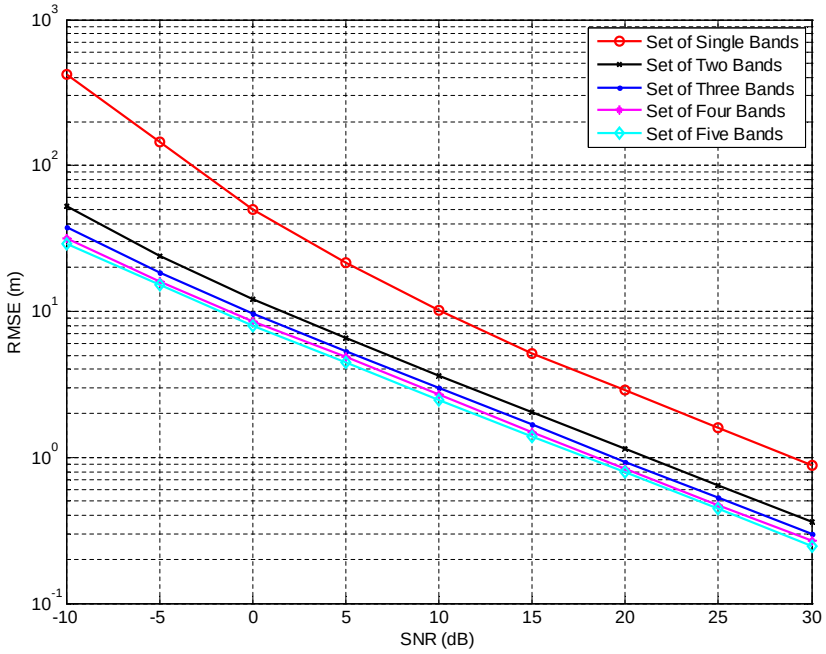

Figure 6.7: RMSE performance for the LLS algorithm (Rician fading, K= 2 dB)

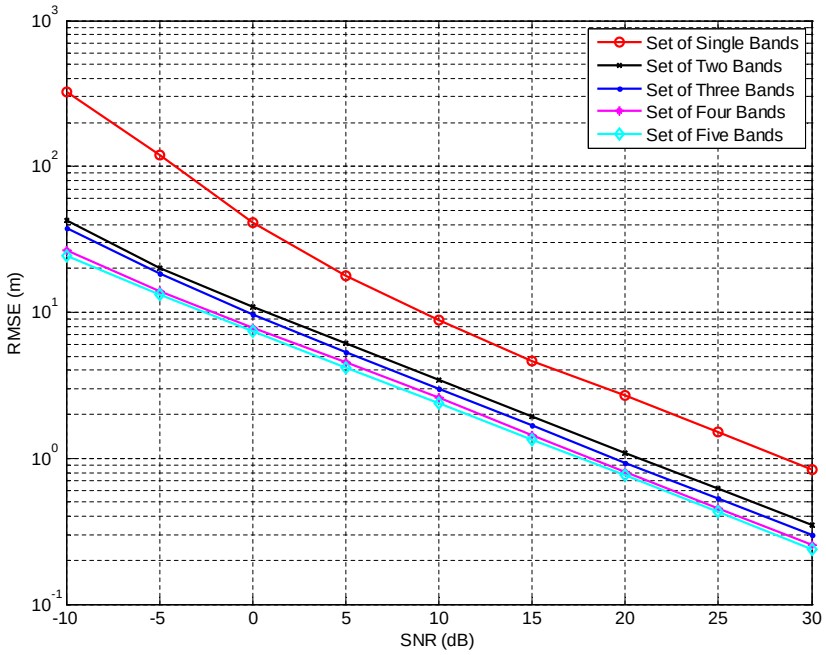

Figure 6.8: RMSE performance for the TSML algorithm (Rician fading, K= 2 dB)

and channel fading coefficient and therefore each band can be exploited to yield an optimal estimate. Tables 6.2, 6.3 and 6.4 show the different percentages in RMSE improvement for the multiple discrete bandwidths at SNRs of -10, -5 and 0 dB, respectively. The RMSE improvements for the NLS technique in Table 6.2, are quite high because of the large distance estimation error at -10 dB for the single band case. Furthermore, it can also be noted that the NLS technique displays more variation at lower SNRs, as shown in Table 6.3, where the two band case performs better than the three band case.

Table 6.2: Percentage RMSE improvement over single band systems at $SNR = -10\,dB$

	NLS (%)	LLS (%)	TSML (%)
Two bands	98	87	87
Three bands	99	91	88
Four bands	99	92	91
Five bands	99	93	93

Table 6.3: Percentage RMSE improvement over single band systems at $SNR = -5\,dB$

	NLS (%)	LLS (%)	TSML (%)
Two bands	81	84	83
Three bands	75	87	85
Four bands	91	89	88
Five bands	92	90	89

Figures 6.6, 6.7 and 6.8 show that there is a significant RMSE positional accuracy improvement at lower SNRs. The proposed multiband TOA positioning technique can therefore be exploited in low SNR conditions to achieve an improved localisation accuracy. Tables 6.3 and 6.4 also show that there is a 1% performance improvement between utilising four and five discrete bandwidths for TOA positioning which is a minimal improvement. Table 6.5 shows the comparative performance between the three location estimation algorithms at three different SNRs for the double band case.

The TSML algorithm displays the best performance at lower SNRs. It can be observed that

Table 6.4: Percentage RMSE improvement over single band systems at $SNR = 0\,dB$

	NLS (%)	LLS (%)	TSML (%)
Two bands	72	76	74
Three bands	88	81	77
Four bands	89	83	81
Five bands	90	84	82

Table 6.5: Comparative algorithmic performance in terms of RMSE for two bands

	NLS (m)	LLS (m)	TSML (m)
-10 dB	115.5	52.59	42.76
-5 dB	25.30	23.82	20.15
20 dB	0.97	1.14	1.1

the more complex NLS algorithm performs slightly better than the LLS and TSML algorithm at higher SNRs. Table 6.6 shows the differential change in the RMSE of the positional accuracy between the single and double band case in order to quantify the improvement in accuracy.

Table 6.6: Differential change of the RMSE for the double band case

	NLS (m)	LLS (m)	TSML (m)
-10 dB	7309.5	367.41	283.44
-5 dB	112.42	122.18	99.75
0 dB	49.63	37.75	41.15
10 dB	6.47	4.29	5.41
20 dB	1.52	1.76	1.59

According to Table 6.6, there is a significant decrease in RMSE for the double band case at -10 dB and -5 dB, indicating a large improvement in positional accuracy. As a result the proposed multiband positioning technique is suitable for performing CR-based localisation

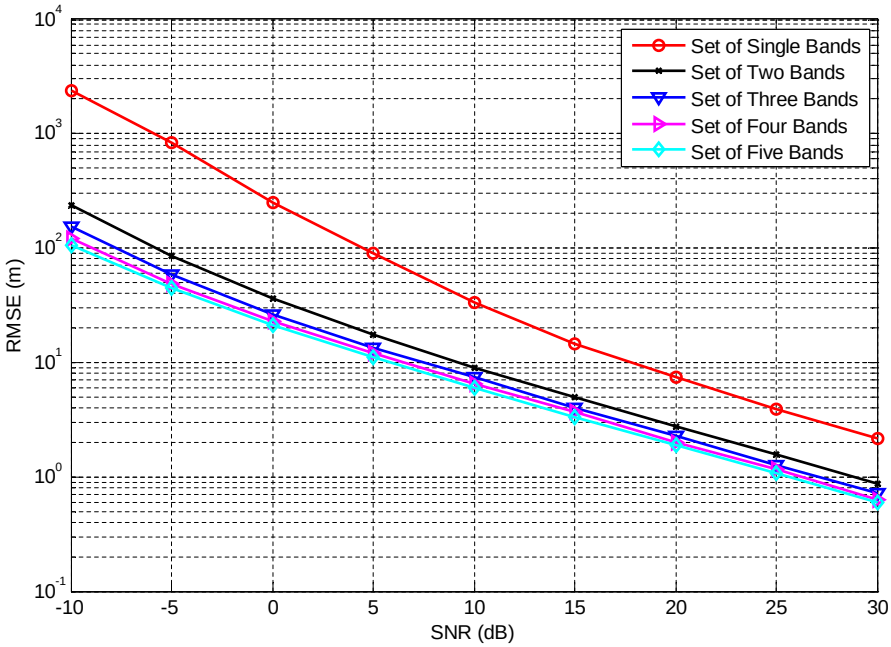

Figure 6.9: RMSE performance for the LLS algorithm (Rayleigh fading, K= 0 dB)

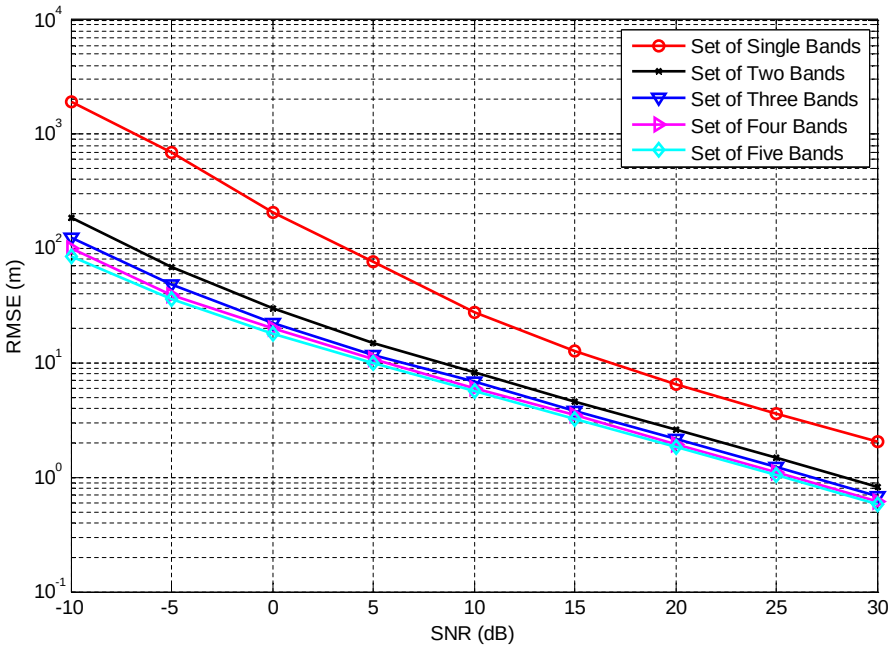

Figure 6.10: RMSE performance for the TSML algorithm (Rayleigh fading, K= 0 dB)

in scenarios where high SNRs of the signal are limited by the inherent constraint imposed by the surrounding environmental conditions.

The channel fading coefficients also affect the localisation accuracy of the multiband TOA positioning technique. Similar plots (refer to Figures 6.9 and 6.10) are presented for a K-factor of 0 dB (Rayleigh fading) for the LLS and TSML algorithms, as these estimation algorithms display good stability over the whole range of analysed SNR values. The overall RMSE error is much higher, which is as expected from a pdf that characterises NLOS behaviour.

CHAPTER 7

CONCLUSION

This study has investigated the optimisation of adaptive localisation techniques, specifically related to TOA ranging, in the context of CR. It has been discussed that the development of these techniques can lead to efficient and accurate location awareness in CR, thus offering the opportunity to enhance various CR tasks using positional information.

7.1 SUMMARY OF RESEARCH FINDINGS

Chapter 2 included a review about the principles of existing ranging techniques employed in mobile positioning. It has been shown that the time-based ranging schemes enable adaptivity in positioning due to the signal bandwidth playing an important role in the accuracy of a positioning system. Existing positioning systems such GPS, MIMO and WLAN can play a significant role in catering for both indoor and outdoor CR localisation. The role of environment and location awareness in the overall CR architecture has been outlined, together with a brief discussion on the relevance of geo-location in the IEEE 802.22 standard (providing broadband access over TV white spaces).

A detailed look at the different non-linear and linear location estimation algorithms utilised to perform location estimation has been provided in Chapter 3. It has been shown that Newton-Raphson and Gauss-Newton achieve the fastest convergence of the 2D position estimate for both the ML and NLS estimation algorithms. The linear estimation algorithms offer a more stable solution and are less complex to implement when compared to the

non-linear estimation algorithms. As a result, the linear estimation algorithms have been implemented in the proposed optimised positioning models.

A bandwidth efficient CPS model is proposed in Chapter 4. A detailed CRLB derivation of the bandwidth-accuracy relationship for the SIMO BD model has been developed. The EDSM component, which is an important component of the CPS, makes use of underlay and overlay spectrum access techniques to select the required bandwidth for A-TOA positioning. Chapter 5 follows on from the CRLB derivations in Chapter 4 to develop a multiband positioning technique based on the TOA ranging technique. The multiband system model is outlined, followed by the proposal of the combination estimation technique that exploits multiple time delays from each transmitted signal to improve the positional accuracy of an MT. An overview of the UHF spectrum occupancy measurement campaign utilised to model dynamic bandwidth availability is given. Based on the measurement results, it was possible to develop a pdf of the unoccupied spectrum and thereafter validate the performance of the multiband TOA positioning technique in a practical scenario.

Chapter 6 contains the performance evaluations of the proposed optimised positioning models in Chapter 4 and 5 under different scenarios and using different location estimation algorithms. The comparative bandwidth efficiency of both SISO and SIMO BD models have been analysed for three generic environmental models: rural, urban and suburban. Furthermore, in each scenario each of the antennas schemes (1×1, 1×2 and 1×3) was implemented using the TSML and LLS location estimation algorithm. The 1×2 and 1×3 SIMO schemes showed an improvement in bandwidth efficiency in relation to the RMSE positioning error of each environmental model, although the urban and suburban scenarios showed greater improvement. The results highlight the advantage of using multiple antennas and hence the role of spatial diversity, not only for communications but for CR positioning as well.

The second part of the chapter provides the RMSE performance of the multiband TOA positioning technique using a fixed (predefined) and dynamic bandwidth availability model based on spectrum occupancy measurements taken in the UHF band. In both cases, the results show the advantage of exploiting multiple discrete bandwidths in an opportunistic

manner at the CR receiver to improve positioning accuracy, although the latter case reflected an improved CR scenario. It was observed from the spectrum occupancy measurement results that the unoccupied portion of the UHF band followed a Gaussian distribution. As a result it was possible to model the dynamic bandwidth availability accordingly to perform multiband TOA estimation.

7.2 SUGGESTIONS FOR FUTURE WORK

Although current work has focused on conceptual models regarding location awareness in CR, little work has been done with regard to the analysis and actual implementation of these models within a suitable framework. The following avenues of additional research have been identified pertaining to this study:

- The performance of the multiband TOA positioning technique can be analysed using a suitable channel occupancy prediction model to investigate the benefits of positional accuracy in relation to an optimised bandwidth selection process.

- NLOS errors can vary, depending on the type of terrain and environment. Therefore it is suggested that a few additional NLOS deterministic and random models be investigated in relation to both the bandwidth efficient model as well as the multiband TOA positioning technique.

- Both models investigated in Chapters 4 and 5 considered a single-path received signal as the basis of the analysis. However, in practice TOA ranging signals are inevitably affected by multipath signal components, which can cause an undesired significant decrease in the positioning accuracy. The study was limited to the first arriving path of a TOA signal (single-path case), due to the complexity of the CRLB derivations in relation to the SIMO and multiband analysis. For a more realistic scenario, the performance of the proposed CR positioning models can be studied with the effects of multipath included.

- Since TOA is a time-based localisation scheme, it is susceptible to synchronisation

errors. In this particular study perfect synchronisation between the transmitter and receiver was assumed and hence no synchronisation errors were included. Future work in this area can take into account the effects of synchronisation errors on the RMSE positional accuracy.

REFERENCES

[1] M. Lopez-Benitez, F. Casadevall, R. Hachemani, and J. Palicot, "Spectral occupation measurements and blind standard recognition sensor for cognitive radio networks," in *Proc. 4th Intl. CrownCom Conf.*, Hannover, Germany, Aug. 2009, pp. 1–9.

[2] R. I. C. Chang, G. B. Rowe, and K. W. Sowerby, "A quantitative analysis of spectral occupancy measurements for cognitive radio," in *Proc. 65th IEEE Vehic. Technol. Conf. (VTC)*, Dublin, Ireland, May 2007, pp. 3016–3020.

[3] M. Wellens, J. Wu, and P. Mahonen, "Evaluation of spectrum occupancy in indoor and outdoor scenario in the context of cognitive radio," in *Proc. 2nd Intl. CrownCom Conf.*, vol. 4, Jun. 2006, pp. 1658–1663.

[4] Spectrum Efficiency Working Group, "FCC Spectrum Policy Task Force," Federal Communications Commission, Tech. Rep. TR 02-155, Nov. 2002.

[5] K. Qaraqe, H. Celebi, A. Gorcin, A. El-Saigh, H. Arslan, and M. Alouini, "Empirical results for wideband multidimensional spectrum usage," in *20th IEEE Intl. Symp. on PIMRC, 2009*, Sept. 2009, pp. 1262–1266.

[6] M. Islam *et al.*, "Spectrum survey in Singapore: Occupancy measurements and analysis," in *Proc. 3rd Intl. Conf. on CrownCom, 2008*, May 2008, pp. 1–7.

[7] J. Proakis and M. Salehi, *Digital Communications*, 5th ed. McGraw-Hill, 2008.

[8] P. Cook and W. Bonser, "Architectural overview of the SPEAKeasy system," *IEEE J.*

Sel. Areas Commun., vol. 17, no. 4, pp. 650–661, Apr. 1999.

[9] M. Dillinger, K. Madani, and N. Alonistioti, *Software Defined Radio: Architectures. Systems and Functions*, 1st ed. Wiley, New York, 2003.

[10] J. Mitola, "Cognitive Radio: An Integrated Agent Architecture for Software Defined Radio," Doctor of Technology, Royal Institute of Technology (KTH), Stockholm, Sweden, May 2000.

[11] J. Mitola and G. Q. Maguire, "Cognitive radio: Making software radios more personal," *IEEE Personal Communications*, vol. 6, no. 4, pp. 13–18, Aug. 1999.

[12] S. Haykin, "Cognitive radio: Brain-empowered wireless communications," *IEEE J. Sel. Areas Commun.*, vol. 23, no. 2, pp. 201–220, Feb. 2005.

[13] I. Akyildiz, W.-Y. Lee, M. Vuran, and S. Mohanty, "A survey on spectrum management in cognitive radio networks," *IEEE Commun. Mag.*, vol. 46, no. 4, pp. 40–48, Apr. 2008.

[14] B. Wang, Y. Wu, and K. J. R. Liu, "Game theory for cognitive radio networks: An overview," *Comput. Netw.*, vol. 54, no. 14, pp. 2537–2561, Oct. 2010.

[15] H. Arslan, *Cognitive Radio, Software Defined Radio and Adaptive Wireless Systems*, 1st ed. Springer, 2007.

[16] B. Fette, *Cognitive Radio Technology*, 1st ed. Elsevier-Newnes, 2006.

[17] X. Li, "RSS-based location estimation with unknown pathloss model," *IEEE Trans. on Wireless Commun.*, vol. 5, no. 12, pp. 3626–3633, Dec. 2006.

[18] T. S. Rappaport, *Wireless Communication Principles and Practice*, 2nd ed. Prentice-Hall, 2002.

[19] R. Zekavat and R. M. Buehrer, *Handbook of Position Location: Theory, Practice, and*

Advances. John Wiley and Sons, New Jersey, 2011.

[20] T. S. Rappaport, J. H. Reed, and B. Woerner, "Position location using wireless communications on highways of the future," *IEEE Commun. Mag.*, pp. 33–41, Oct. 1996.

[21] S. Gezici, Z. Tian, G. B. Giannakis, H. Kobayashi, A. F. Molisch, H. V. Poor, and Z. Sahinoglu, "Localization via Ultra-wideband radios," *IEEE Signal Process. Mag.*, vol. 22, no. 4, pp. 70–84, Jul. 2005.

[22] Z. Jafarian, H. Mirsalehi, M. Ahadi-Akhlaghi, and H. Keshavarz, "A neural network-based mobile positioning with hierarchical structure," in *Proc. 57th IEEE Veh. Technol. Conf. (VTC) 2003*, vol. 3, Apr. 2003, pp. 2003–2007.

[23] G. Sun, J. Chen, W. Guo, and K. Liu, "Signal processing techniques in network-aided positioning: A survey on the state-of-the-art positioning designs," *IEEE Signal Process. Mag.*, vol. 22, no. 4, pp. 12–23, Jul. 2005.

[24] S. Gleason and D. Gebre-egziabher, *GNSS Applications and Methods*, 1st ed. Artech House, 2009.

[25] J. Benedicto, S. E. Dinwiddy, G. Gatti, R. Lucas, and M. Lugert, "GALILEO: Satellite system design and technology developments," European Space Agency, Tech. Rep., Nov. 2000.

[26] G. Xu, *GPS Theory, Algorithms and Applications*, 2nd ed. Springer, 2007.

[27] K. Papakonstantinou and D. Slock, "Direct location estimation for MIMO systems in multipath environments," in *Proc. IEEE Globecom*, New Orleans, USA, Dec. 2008, pp. 1–5.

[28] P. Grover, R. Agarwal, and A. Chaturvedi, "Geolocation using transmit and receive diversity," in *Proc. IEEE Globecom Conf.*, vol. 6, December 2004, pp. 3681–3684.

[29] T. Yabu and S. Hara, "Impact of MIMO techniques on TOA-based location estimation,"

in *Proc. IEEE 70th Veh. Technol. Conf. (VTC)*, Anchorage, USA, Sept. 2009, pp. 1–5.

[30] S. Bizjajeva, T. Ryden, and O. Edvors, "Mobile positioning in MIMO systems using particle filtering," in *Proc. IEEE 66th Veh. Technol. Conf. (VTC)*, Baltmore, MD, Oct. 2007, pp. 1–5.

[31] J. Li, J. Conan, and S. Pierre, "Mobile terminal location for MIMO communication systems," *IEEE Trans. on Antennas Propag.*, vol. 55, no. 8, pp. 2417–2420, Aug. 2007.

[32] A. Hatami and K. Pahlavan, "A comparative performance evaluation of RSS-based positioning algorithms used in WLAN networks," in *Proc. IEEE Wireless Commun. and Networking Conf. (WCNC), 2005*, vol. 4, Mar. 2005, pp. 2331–2337.

[33] H. Wang, H. Zhou, L. Zhu, Q. He, and Z. Tian, "Analysis and research on indoor positioning method based on IEEE 802.11," in *Proc. Int. Conf. on Wireless Commun., Networking and Mobile Computing, (WiCom) 2007*, Sept. 2007, pp. 2181–2183.

[34] K. Kao, I. Liao, and J. Lyu, "An indoor location-based service using access points as signal strength data collectors," in *Proc. Int. Conf. on Indoor Positioning and Indoor Navigation (IPIN), 2010*, Sept. 2010, pp. 1–6.

[35] H. Reddy, M. G. Chandra, P. Balamuralidhar, S. Harihara, K. Bhattacharya, and E. Joseph, "An improved time-of-arrival estimation for WLAN-based local positioning," in *Proc. Int. Conf. on Commun. Systems Software and Middleware, (COMSWARE) 2007*, Jan. 2007, pp. 1–5.

[36] F. Izquierdo, M. Ciurana, F. Barcelo, J. Paradells, and E. Zola, "Performance evaluation of a TOA-based trilateration method to locate terminals in WLAN," in *Proc. Int. Symp. on Wireless Pervasive Computing, 2006*, Jan. 2006, pp. 1–6.

[37] S. A. Golden and S. S. Bateman, "Sensor measurements for Wi-Fi location with emphasis on time-of-arrival ranging," *IEEE Trans. on Mobile Comput.*, vol. 6, no. 10, pp. 1185–1198, Oct. 2007.

[38] N. Patwari, A. O. Hero, M. Perkins, N. S. Correal, and R. J. O'Dea, "Relative location estimation in wireless sensor networks," *IEEE Trans. on Signal Process.*, vol. 51, no. 8, pp. 2137–2148, Aug. 2003.

[39] M. Ciurana, D. Giustiniano, A. Neira, F. Barcelo-Arroyo, and I. Martin-Escalona, "Performance stability of software ToA-based ranging in WLAN," in *Int. Conf. on Indoor Positioning and Indoor Navigation (IPIN), 2010*, Sept. 2010, pp. 1–8.

[40] H. Celebi and H. Arslan, "Enabling location and environment awareness in cognitive radios," *Comp. Commun.*, vol. 31, no. 4, pp. 1114–1125, Jan. 2008.

[41] H. Arslan and H. Celebi, "Utilization of location information in cognitive wireless networks," *IEEE Wireless Commun. Mag.*, vol. 14, no. 4, pp. 6–13, Aug. 2007.

[42] H. Celebi, I. Guvenc, S. Gezici, and H. Arslan, "Cognitive-radio systems for spectrum, location, and environmental awareness," *IEEE Antennas Propag. Mag.*, vol. 52, no. 4, pp. 41–61, Aug. 2010.

[43] S. Yarkan and H. Arslan, "Exploiting location awareness toward improved wireless system design in cognitive radio," *IEEE Commun. Mag.*, vol. 46, no. 1, pp. 128–136, Jan. 2008.

[44] C. Stevenson, G. Chouinard, Z. Lei, W. Hu, S. Shellhammer, and W. Caldwell, "IEEE 802.22: The first cognitive radio wireless regional area network standard," *IEEE Commun. Mag.*, vol. 47, no. 1, pp. 130–138, Jan. 2009.

[45] H. Celebi and H. Arslan, "Cognitive Positioning Systems," *IEEE Trans. on Wireless Commun.*, vol. 6, no. 12, pp. 4475–4483, Dec. 2007.

[46] H. Celebi, K. A. Qaraque, and H. Arslan, "Performance analysis of TOA range accuracy adaptation for cognitive radio systems," in *Proc. IEEE 70th Veh. Technol. Conf. (VTC)*, Anchorage, USA, Septemeber 2009, pp. 1–4.

[47] I. Guvenc and C. Chong, "A survey on TOA based wireless localization and NLOS

mitigation techniques," *IEEE Commun. Surveys Tuts*, vol. 11, no. 3, pp. 107–124, Aug. 2009.

[48] I. J. Myung, "Tutorial on maximum likelihood estimation," *Journal of Mathematical Psychology*, vol. 47, no. 1, pp. 90–100, Feb. 2003.

[49] H. V. Poor, *An Introduction to Signal Detection and Estimation*, 2nd ed. Springer, 1994.

[50] S. M. Kay, *Fundamentals of Statistical Signal Processing, Volume 1: Estimation Theory*, 1st ed. Addison Wesley Longman, 2001.

[51] K. W. Cheung, H. C. So, W. K. Ma, and Y. T. Chan, "Least square algorithms for time-of-arrival-based mobile location," *IEEE Trans. on Signal Process.*, vol. 52, no. 4, pp. 1121–1128, Apr. 2004.

[52] F. K. W. Chan, H. So, J. Zheng, and K. Lui, "Best linear unbiased estimator approach for time-of-arrival based localisation," *IET Signal Processing*, vol. 2, no. 2, pp. 156–162, Jan. 2008.

[53] Y. T. Chan and K. C. Ho, "A simple and efficient estimator for hyperbolic location," *IEEE Trans. on Signal Process.*, vol. 42, no. 8, pp. 1905–1915, Aug. 1994.

[54] S. Yarkan and H. Arslan, "Identification of LOS and NLOS for wireless transmission," in *Proc. 2nd Intl. Conf. CrownCom*, Mykonos Islands, Jun. 2006, pp. 1–5.

[55] J. Borras, P.Hatrack, and N. Mandayam, "Decision theoretic framework for NLOS identification," in *Proc. IEEE 57th Veh. Technol. Conf. (VTC)*, vol. 2, Ottawa, May 1998, pp. 1583–1587.

[56] F. Benedetto, G. Giunta, A. Toscano, and L. Vegni, "Dynamic LOS/NLOS statistical discrimination of wireless mobile channels," in *Proc. 65th IEEE Veh. Technol. Conf. (VTC)*, vol. 2, Dublin, Apr. 1998, pp. 3071–3075.

[57] K. Yu and Y. J. Guo, "Statistical NLOS identification based on AOA, TOA and signal strength," *IEEE Trans. on Veh. Technol.*, vol. 58, no. 1, pp. 274–286, Jan. 2009.

[58] H. Miao, K. Yu, and M. J. Juntti, "Positioning for NLOS propagation: Algorithm derivations and Cramer-Rao bounds," *IEEE Trans. on Veh. Technol.*, vol. 56, no. 5, pp. 2568–2580, Sept. 2007.

[59] S. Venkatesh and R. M. Buehrer, "Non-line-of-sight identification in ultra-wideband systems based on received signal statistics," *IET Microwave Antennas and Propagation*, vol. 6, no. 1, pp. 1120–1130, Dec. 2007.

[60] S. Al-Jazzar, J. Caffery, and H.-R. You, "Scattering-model-based methods for TOA location in NLOS environments," *IEEE Trans. on Veh. Technol.*, vol. 56, no. 2, pp. 583–593, Dec. 2007.

[61] J. S. Al-Jazzar and J. C. Caffery, "New algorithms for NLOS identification," in *IST Mobile and Wireless Communication Summit*, Jun. 2003, pp. 1–5.

[62] A. A. Pack, L. Herman, M. Hoffmann-Kuhnt, and B. Branstetter, "The object behind the echo: dolphins (Tursiops truncatus) perceive object globally through echolocation," *Behavioural Processes*, vol. 1-2, no. 58, pp. 1–26, Oct. 2002.

[63] M. Wahlberg *et al.*, "Source parameters of echolocation clicks from wild bottlenose dolphins (Tursiops aduncus and Tursiops truncatus," *J. Acoust. Soc. Am.*, vol. 130, no. 4, pp. 2263–2274, Oct. 2011.

[64] M. Obrist, "Flexible bat echolocation: the influence of individual, habitat and conspecifics on signal sonar design," *Behav. Ecol. Sociobiol.*, vol. 36, no. 3, pp. 207–219, Jan. 1995.

[65] L. Jakobsen and A. Surlykke, "Vespertilionid bats control the width of their biosonar sound beam dynamically during prey pursuit," in *Proc. Natl. Acad. Sci. USA*, vol. 107, no. 31, Aug. 2010, pp. 13 930–13 935.

[66] J. Jarvis, K. Bohn, J. Tressler, and M. Smotherman, "A mechanism for antiphonal echolocation by free-tailed bats," *Animal Behaviour*, vol. 79, no. 4, pp. 787–796, Apr. 2010.

[67] H. Celebi and H. Arslan, "Adaptive positioning systems for cognitive radios," in *Proc. 2nd IEEE Int. Symp. on DySPAN, 2007*, Apr. 2007, pp. 78–84.

[68] Y. Xie, B. Armbruster, and Y. Ye, "Dynamic spectrum management with the competitive market model," *IEEE Trans. on Sig. Process.*, vol. 58, no. 4, pp. 2442–2446, Apr. 2010.

[69] D. Niyato and E. Hossain, "Competitive spectrum sharing in cognitive radio networks: A dynamic game approach," *IEEE Trans. on Wireless Commun.*, vol. 7, no. 7, pp. 2651–2660, Jul. 2008.

[70] L. Chen, S. Iellamo, M. Coupechoux, and P. Godlewski, "An auction framework for spectrum allocation with interference constraint in cognitive radio networks," in *Proc. IEEE INFOCOM, 2010*, Mar. 2010, pp. 78–84.

[71] H.-B. Chang, K.-C. Chen, N. Prasad, and C.-W. Su, "Auction based spectrum management of cognitive radio networks," in *Proc. 69th IEEE Veh. Techn. Conf.,(VTC), 2009*, Apr. 2009, pp. 1–5.

[72] B. Atakan and O. Akan, "BIOlogically-inspired spectrum sharing in cognitive radio networks," in *IEEE Wireless Commun. and Networking Conf.,(WCNC), 2007*, Mar. 2007, pp. 43–48.

[73] B. Bastami and E. Saberinia, "Optimal transmission time of secondary user in an overlay cognitive radio system," in *Proc. 6th Intl. Conf. on Inform. Techn.: New Gen. (ITNG), 2009*, Apr. 2009, pp. 1269–1274.

[74] V. A. Bohara, S. H. Ting, Y. Han, and A. Pandharipande, "Interference-free overlay cognitive radio network based on cooperative space time coding," in *Proc. 5th Intl.*

Conf. CrownCon, 2010, Jun. 2010, pp. 1–5.

[75] M. K. Kiskani and B. H. Khalaj, "Novel power control algorithms for underlay cognitive radio networks," in *Proc. 21st Intl. Conf. on Sys. Eng. (ICSEng), 2011*, Aug. 2011, pp. 206–211.

[76] R. Menon, R. M. Buehrer, and J. H. Reed, "Outage probability based comparison of underlay and overlay spectrum sharing techniques," in *Proc. 1st Intl. Symp. DySPAN, 2005*, Baltimore, Nov. 2005, pp. 101–109.

[77] J. Oh and W. Choi, "A hybrid cognitive radio system: A combination of underlay and overlay approaches," in *Proc. 72nd IEEE Veh. Technol. Conf. Fall (VTC), 2010*, Sept. 2010, pp. 1 –5.

[78] Y. Qi, H. Kobayashi, and H. Suda, "On time-of-arrival positioning in a multipath environment," *IEEE Trans. on Veh. Technol.*, vol. 55, no. 5, pp. 1516–1526, Sept. 2006.

[79] L. Mailaender, "Comparing geo-location bounds for TOA, TDOA and round trip TOA," in *Proc.18th IEEE Int. Symp. PIMRC*, Athens, Sept. 2007, pp. 1–5.

[80] S. Gezici, H. Celebi, H. V. Poor, and H. Arslan, "Fundamental limits on time delay estimation in dispersed spectrum cognitive radio systems," *IEEE Trans. on Wireless Commun.*, vol. 8, no. 1, pp. 78–83, Jan. 2009.

[81] F. Kocak, H. Celebi, S. Gezici, K. A. Qaraqe, H. Arslan, and H. V. Poor, "Time delay estimation in dispersed spectrum cognitive radio systems," *Eurasip Journal on Advances in Signal Processing*, vol. 2010, pp. 1–10, 2010.

[82] B. Farhang-Boroujeny and R. Kempter, "Multicarrier communication techniques for spectrum sensing and communication in cognitive radios," *IEEE Commun. Mag.*, vol. 46, no. 4, pp. 80–85, Apr. 2008.

[83] R. R. Thomas, B. Zayen, R. Knopp, and B. T. Maharaj, "Multiband TOA positioning technique for cognitive radio systems," in *22nd PIMRC Workshop on Cognitive Radio*

and Networking: Solutions and Challenges Ahead, Toronto, Canada, Sept. 2011, pp. 2315–2319.

[84] Y. Chan, H. C. Hang, and P. Ching, "Exact and approximate maximum likelihood localization algorithms," *IEEE Trans. on Veh. Techn.*, vol. 55, no. 1, pp. 10–16, Jan. 2006.

[85] S. D. Barnes, "Cognitive Radio Performance Optimisation Through Spectrum Availability Prediction," Master's thesis, University of Pretoria, 2012.

[86] P. C. Chen, "A non-line-of-sight error mitigation algorithm in location estimation," in *Proc. IEEE WCNC*, New Orleans, Sept. 1999, pp. 316–320.

[87] R. R. Thomas and B. T. Maharaj, "Towards a bandwidth efficient cognitive positioning system," *IET Electronics Letters*, vol. 48, no. 12, pp. 787–788, June 2012.

APPENDIX A

FISHER INFORMATION MATRIX OF A DISCRETE RECEIVED SIGNAL

Let the continuous waveform given by eq. (4.6) be sampled (using the Nyquist Sampling Theorem) at every $T_{samp} = \frac{1}{2f_B}$ seconds. The observed data is given by [50]:

$$r_l(kT_{samp}) = \alpha_l s(kT_{samp} - \tau_o) + n_l(kT_{samp}), \qquad k = 0, 1, ..., K-1.$$

Let $r_l[k]$ and $n_l[k]$ be the sampled sequences, then the discrete model is given by:

$$r_l[k] = \alpha_l s(kT_{samp} - \tau_o) + n_l[k]. \tag{A.1}$$

Since the signal is non-zero over the interval $\tau_o \leq t \leq \tau_o + N_{sym}T_s$, then eq. (A.1) becomes:

$$r_l[k] = \begin{cases} n_l[k] & 0 \leq k \leq k_o - 1 \\ \alpha_l s(kT_{samp} - \tau_o) + n_l[k] & k_o \leq k \leq k_o + M - 1 \\ n_l[k] & k_o + M \leq k \leq k_o + K - 1. \end{cases} \tag{A.2}$$

The total number of samples of the signal are given by M and the sample delay is given

as $k_o = \frac{\tau_o}{T_{samp}}$. Applying eq. (4.13), the Fisher information element (I_{11}) is calculated as follows:

$$\begin{aligned} I_{\tau\tau} &= \sum_{l=1}^{N} \frac{1}{\sigma_l^2} \sum_{k=0}^{K-1} \frac{\partial s[k;\theta]}{\partial \tau_o} \frac{\partial s[k;\theta]}{\partial \tau_o}, \\ &= \sum_{l=1}^{N} \frac{|\alpha_l|^2}{\sigma_l^2} G \sum_{k=k_o}^{k_o+M-1} \left| \frac{\partial s(kT_{samp} - \tau_o)}{\partial \tau_o} \right|^2, \\ &= \sum_{l=1}^{N} \frac{|\alpha_l|^2}{\sigma_l^2} G \sum_{k=k_o}^{k_o+M-1} \left| \frac{ds(t)}{dt} \, |_{t=kT_{samp}-\tau_o} \right|^2, \\ &= \sum_{l=1}^{N} \frac{|\alpha_l|^2}{\sigma_l^2} G \sum_{k=0}^{M-1} \left| \frac{ds(t)}{dt} \, |_{t=kT_{samp}} \right|^2, \qquad \tau_o = k_o T_{samp}. \end{aligned} \tag{A.3}$$

Assuming T_{samp} is sufficiently small, it can be approximated as a sum of an integral:

$$I_{\tau\tau} = \sum_{l=1}^{N} \frac{|\alpha_l|^2}{\sigma_l^2 T_{samp}} G \int_0^{T_s} \left| \frac{ds(t)}{dt} \right|^2 dt.$$

Let $\hat{\varepsilon} = G \int_0^{T_s} \left| \frac{ds(t)}{dt} \right|^2 dt$ which is the signal energy of the derivative of $s(t)$. Therefore:

$$I_{\tau\tau} = \hat{\varepsilon} \sum_{l=1}^{N} \frac{|\alpha_l|^2}{\sigma_l^2 T_{samp}}. \tag{A.4}$$

The column vectors, $\mathbf{I}_{\tau\alpha}$and $\mathbf{I}_{\alpha\tau}$are orthogonal and therefore:

$$\mathbf{I}_{\tau\alpha} = \frac{1}{[\sigma_1^2, ..., \sigma_l^2]} G \sum_{k=0}^{K-1} \frac{\partial s[k;\theta]}{\partial \tau_o} \frac{\partial s[k;\theta]}{\partial \alpha_l},$$

$$\mathbf{I}_{\tau\alpha} = \frac{1}{[\sigma_1^2, ..., \sigma_l^2]} G \sum_{k=k_o}^{k_o+M-1} \left| \frac{\partial \left([|\alpha_1|, .., |\alpha_l|] s(kT_{samp} - \tau_o) \right)}{\partial \tau_o} \right| \left| \frac{\partial \left([|\alpha_1|, .., |\alpha_l|] s(kT_{samp} - \tau_o) \right)}{\partial \alpha_l} \right|,$$

$$= \left[\frac{|\alpha_1|}{\sigma_1^2}, ..., \frac{|\alpha_l|}{\sigma_l^2} \right] \sum_{k=0}^{M-1} - \left| \frac{ds(t)}{dt} \right| |s(t)|_{t=kT_{samp}},$$

$$= -\left[\frac{|\alpha_1|}{\sigma_1^2},...,\frac{|\alpha_l|}{\sigma_l^2}\right]\frac{1}{T_{samp}}\int_0^{T_s}\left|\frac{ds(t)}{dt}\right||s(t)|\,dt.$$

Let $\tilde{\varepsilon} = G\int_0^{T_s}\left(\frac{ds(t)}{dt}\right)(s(t))\,dt$ represent the product between the derivative of the signal energy and the actual energy of the signal. Therefore:

$$\mathbf{I}_{\tau\alpha} = \mathbf{I}_{\alpha\tau} = -\tilde{\varepsilon}\left[\frac{|\alpha_1|}{T_{samp}\sigma_1^2},...,\frac{|\alpha_l|}{T_{samp}\sigma_l^2}\right]. \tag{A.5}$$

Lastly, since $\mathbf{I}_{\alpha\alpha}$ is also an orthogonal matrix:

$$\begin{aligned}\mathbf{I}_{\alpha\alpha} &= G\sum_{k=0}^{M-1}|s(t)|\,|s(t)|\,|_{t=kT_{samp}}\times diag\left[\frac{1}{\sigma_1^2},...,\frac{1}{\sigma_N^2}\right],\\ &= \frac{1}{T_{samp}}G\int_0^{T_s}|s(t)|\,|s(t)|\,dt\times diag\left[\frac{1}{\sigma_1^2},...,\frac{1}{\sigma_N^2}\right],\end{aligned}$$

where $diag\{...\}$ represents a diagonal matrix and since $\varepsilon = G\int_0^{T_s}|s(t)|^2\,dt$, the final Fisher matrix element is given as:

$$\mathbf{I}_{\alpha\alpha} = \frac{\varepsilon}{T_{samp}}\times diag\left[\frac{1}{\sigma_1^2},...,\frac{1}{\sigma_l^2}\right]. \tag{A.6}$$